Mitochondrial and cell cycle functions of SLIMP

Albert Antolin Fontes

UNIVERSITAT DE BARCELONA

UNIVERSITAT DE BARCELONA
FACULTAT DE FARMÀCIA I CIÈNCIES DE L'ALIMENTACIÓ

Programa de doctorat en Biomedicina

INSTITUTE FOR RESEARCH IN BIOMEDICINE

MITOCHONDRIAL AND CELL CYCLE FUNCTIONS OF SLIMP

Memòria presentada per **Albert Antolin Fontes** per optar al títol de doctor per la Universitat de Barcelona

Lluís Ribas de Pouplana	Albert Antolin Fontes	Antonio Zorzano Olarte
Thesis director	PhD candidate	Tutor

Albert Antolin Fontes
2018

"It is the long history of humankind that those
who learned to collaborate have prevailed"

Charles Darwin

TABLE OF CONTENTS

SUMMARY

The mitochondrial Seryl-tRNA Synthetase (SerRS2) is a member of the class II tRNA synthetase family. The mature enzyme catalyses the ligation of serine to $tRNA^{Ser}$ in mitochondria. During the process of constructing a model for human disorders caused by mitochondrial tRNA aminoacylation deficiencies in *Drosophila melanogaster*, a previously uncharacterized paralogue of SerRS2 named Seryl-tRNA synthetase-Like Insect Mitochondrial Protein (SLIMP) was identified. SLIMP is a new type of aminoacyl tRNA synthetase-like protein that has acquired an essential function in insects. This fast evolving paralogue is a mitochondrial RNA-binding protein which lacks tRNA aminoacylation activity. It has been previously demonstrated that mitochondrial SLIMP interacts with its homologue SerRS2 and also with LON protease. We confirmed these interactions and we described the function of SLIMP by depleting its protein levels in *Drosophila melanogaster* S2 cells, which led to severe defects in mitochondrial function and cell cycle arrest. We found that SLIMP simultaneously acts as a regulator of DNA replication and translation in the mitochondria and, as regulator of cell cycle progression. We show that SLIMP activates mitochondrial protein synthesis through its interaction with SerRS2 and regulates mitochondrial DNA levels by stimulating TFAM digestion by the protease LON. SLIMP was previously reported to be required for correct cell cycle progression. We showed that the depletion of a non-mitochondrial pool of SLIMP causes cell cycle arrest in G2 and the activation of E2F-related and G2/M check-point genes. Our results indicate that SLIMP activity provides an important protein for the communication between mitochondrial anabolism and cell cycle regulation.

RESUM

La Seril-ARNt Sintetasa mitocondrial (SerRS2) es membre de la família de ARNt sintetases de classe II. Aquest enzim es responsable de la lligació de l'aminoàcid serina al corresponent $ARNt^{Ser}$ a la mitocòndria. En el procés de desenvolupament d'un model de malalties mitocondrials causades per deficiències en l'aminoacilació de ARNt en *Drosophila melanogaster,* es descobrí una proteïna paràleg de SerRS2 no caracteritzada fins el moment, anomenada Seril-ARNt sintetasa-Like Insect Mitochondrial Protein (SLIMP). SLIMP representa una nova classe de proteïna semblant a les ARNt sintetases que ha adquirit funcions essencials en insectes. Aquest paràleg ha evolucionat en poc temps i constitueix una proteïna amb unió a ARN però sense capacitat d'aminoacilació. Prèviament s'havia caracteritzat que SLIMP interacciona amb el seu homòleg SerRS2 i també amb la proteasa mitocondrial LON. Ara hem confirmat aquestes interaccions i hem descrit les funcions de SLIMP, caracteritzant l'efecte de la depleció dels seus nivells proteics en cèl·lules S2 de *Drosophila melanogaster*, que comportà severs defectes mitocondrials i un arrest del cicle cel·lular. Hem definit que SLIMP actua simultàniament com un regulador de la replicació del ADN i la traducció a la mitocòndria i, com a regulador de la progressió del cicle cel·lular. SLIMP activa la síntesis proteica mitocondrial gràcies a la interacció amb SerRS2, i a més regula els nivells de ADN mitocondrial, estimulant la degradació de TFAM per la proteasa LON. Anteriorment, es descrigué que SLIMP és necessari per la correcta progressió del cicle cel·lular. Hem trobat que la depleció d'una isoforma no mitocondrial de SLIMP arresta el cicle cel·lular en la fase G2 i activa la transcripció de gens relacionats amb E2F i amb el punt de control de G2/M. Aquests resultats indiquen la important tasca de SLIMP per la comunicació entre l'anabolisme mitocondrial i la regulació del cicle cel·lular.

ABBREVIATIONS

A – Ala – alanine
aa – amino acid
AAA^+ – LON ATPase domain
ARS – Aminoacyl tRNA synthetase
ATP – adenosine triphosphate
BirA – Biotin ligase
BrdU – Bromodeoxyuridine
BSA – Bovine serum albumin
C – Cys – cysteine
cDNA – complementary DNA
$CuSO_4$ – Copper sulfate
D – Asp – aspartic acid
DAPI – 4',6-diamidino-2-phenylindole
DHE – Dihidroehtidium
DNA – Deoxyribonucleic acid
dNTP – deoxyribonucleoside triphosphate
DTT - Dithiothreitol
E – Glu – glutamic acid
ECL – Enhanced chemiluminescent
ETC – Electron Transport Chain
F – Phe – phenylalanine
FBS – Fetal bovine serum
FCCP – Carbonyl cyanide-4-(trifluoromethoxy)phenylhydrazone
FDR – False discovery rate
FSC – Forward scatter
G – Gly – glycine
GFP – green fluorescent protein
GO – Gene Ontology
H – His – histidine
H2Av – Histone H2 variant
H3P – Phosphorylated histone H3
HU – hydroxyurea
I – Ile – isoleucine
IPTG – isopropyl b-D-1-thiogalactopyranoside
IR – irradiated
K – Lys – lysine
L – Leu – leucine

M – Met – methionine
MCM – Minichormosome maintenance
mRNA – messenger RNA
MSP – Mitochondrial Signal Peptide
mtDNA – mitochondrial DNA
N –Asn – asparagine
ns – not significant
OCR – Oxygen consumption rate
ORC – Origin of replication complex
OXPHOS – oxidative phosphorilation
P – Pro – proline
PBS – Phosphate buffered saline
PD – LON proteolytic domain
PI – Propidium iodide
PLB – Protein loading buffer
PVDF – Polyvinylidene difluoride
Q – Gln – glutamine
R – Arg – arginine
RNA – Ribonucleic acid
RNAi – Interference RNA
ROS – Reactive Oxygen Species
rRNA – Ribosomal RNA
RT-qPCR – Real time quantitative polymerase chain reaction
S – Ser – serine
S2 – Schneider 2 Drosophila cells
SARS2 – Homo sapiens mitochondrial Seryl-tRNA Synthetase
SBD – LON substrate binding domain
SDS-PAGE – Sodium dodecyl sulfate–polyacrylamide gel electrophoresis
SerRS2 – Drosophila melanogaster mitochondrial Seryl-tRNA Synthetase
shRNA – Short hairpin RNA
SLIMP – Seryl-tRNA synthetase Like Insect Mitochondrial Protein
SSC – Side scatter
T – Thr – threonine
tRNA – transfer RNA
U – Sec – selenocysteine
V – Val – valine
VDAC – Voltage dependent anion channel
W – Trp – tryptophan
WT – wild type
Y – Tyr – tyrosine

INTRODUCTION

All cellular life forms share the same fundamental scheme of genome replication and expression. Genes are composed by deoxyribonucleic acid (DNA) that define the biology structure and maintain the integration of cellular function. It was proposed by Francis H. C. Crick that the coded genetic information hard-wired into DNA is transcribed into individual transportable cassettes, composed of messenger ribonucleic acid (mRNA); each mRNA cassette contains the program for synthesis of a particular protein (or small number of proteins) (Crick, 1958). Moreover, he already postulated that the information from the DNA could be transferred again into DNA, or transferred to RNA and finally into protein.

The introduction of this thesis is divided in four main parts. First, a general overview on the central biology dogma, starting from the DNA replication, briefly introducing transcription and finally focussing on eukaryotic protein translation. In the second part, mitochondria are introduced, with special attention on mitochondrial DNA replication and transcription, mitochondrial translation and protein quality control. A special emphasis is given to aminoacyl tRNA synthetases, and more specifically to the seryl-tRNA synthetases and the Seryl-tRNA synthetase Like Insect Mitochondrial Protein (SLIMP). Finally, an introduction to cell cycle and cell cycle control is given.

DNA replication

Before every cell divide, the genome has to be completely and accurately replicate to maintain the integrity of genetic information across generations.

DNA replication initiates from thousands of origins of replication that direct the assembly of a large group of protein complexes to the sites that ultimately allow for DNA unwinding and the establishment of two bidirectional replication forks. DNA ahead of the fork is progressively unwound generating single-stranded DNA that serves as a template for the synthesis of new DNA (Figure 1) (Bleichert et al., 2017). Replication initiation requires that the origins of replication are bound by the origin recognition complex (ORC) (composed of the six proteins ORC 1–6). The replication initiation factor cell division cycle 6 (Cdc6) is then recruited to the origin to form a complex with ORC. ORC and Cdc6 work cooperatively to recruit the initiation factor Cdt1 or Double Parked (DUP) in *Drosophila*, and the Minichromosome Maintenance (MCM 2–7) replicative helicase complex. Two hexamers of the MCM2–7 complex are loaded onto origin DNA in an inactive state before the onset of S phase (Crevel et al., 2005; Parker et al., 2017). Under the regulation of two kinases, the S phase cyclin-dependent kinase and Dbf4-dependent kinase, the MCM2–7 complex is joined by CDC45 and the Go-Ichi-Ni-San (GINS) complex (Ilves et al., 2010). Together, the CDC45/MCM2–7/GINS (CMG) complex forms the functional replicative helicase (Georgescu et al., 2017). As two MCM2–7 hexamers are loaded onto a single origin of replication, two CMG complexes establish the independent, bidirectional replication forks after origin activation. The leading strand is synthesized continuously by DNA polymerase ε (Pol ε), whereas the lagging strand is composed of Okazaki fragments and is synthesized by Pol δ (Lujan et al., 2016). Proliferating cell nuclear antigen (PCNA) is a ring composed of three identical subunits that, once loaded, acts as a sliding clamp, tethering the replicative DNA polymerase onto the DNA template during DNA synthesis (Jonsson and Hubscher, 1997; Perkins and Diffley, 1998). After copying most of the replicon, forks come too close to each other and cause the formation of

supercoils in the unreplicated DNA, leading to the onset of convergence. During convergence, which lasts until forks encounter each other, topological stress is relieved by the formation of pre-catenanes (Postow et al., 2001). Converging CMGs bypass each other and keep translocating until they pass over the single stranded DNA (ssDNA)–double-stranded DNA (dsDNA) junction of the downstream Okazaki fragment, presumably by translocating along dsDNA. This allows leading strands to be extended to the downstream Okazaki fragments. The final Okazaki fragment is then processed by de novo recruitment of DNA polymerase δ (Pol δ) and by 3′ flap processing by flap endonuclease 1 (FEN1) (Balakrishnan and Bambara, 2013; Waga and Stillman, 1998).

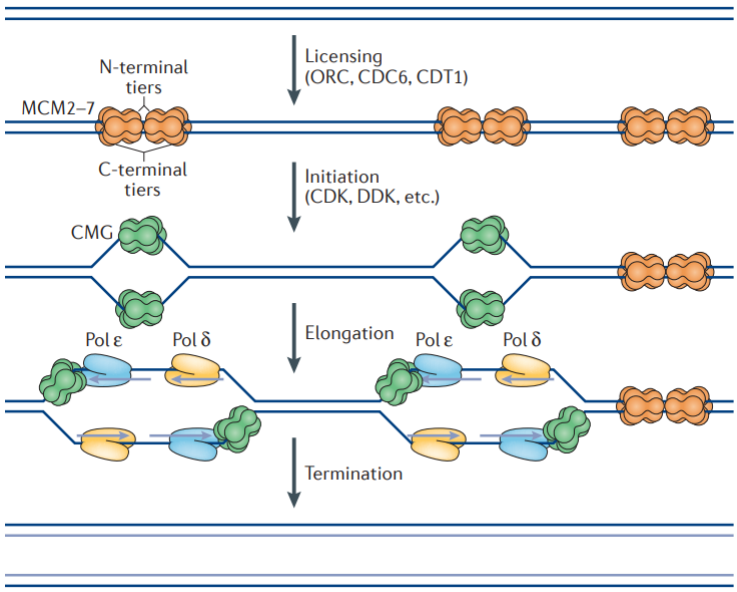

Figure 1| DNA replication. Licensing of replication origins is restricted to the G1 phase of the cell cycle and results from the sequential loading of pre-replication complex (pre-RC) proteins on all potential origins in the genome. First, the ORC recruitment is followed by the binding of Cdc6 and CDT1. Loading of the MCM helicase complex is the last step of the licensing. Origin activation involves the formation of a pre-initiation complex (pre-IC)

and activation of the MCM helicase complex by DBF4-dependent kinase (DDK) and cyclin-dependent kinases (CDKs) at the G1–S phase transition. Helicase activation induces the recruitment of other proteins (PCNA and DNA polymerases) that convert the pre-IC into two functional replication forks that move in opposite directions from the activated origin Adapted from: (Dewar and Walter, 2017).

Once CMG encircles dsDNA, it undergoes polyubiquitylation on its MCM7 subunit by SCFDIA2 (Skp, Cullin, F-box-containing complex associated with DIA2) or CRL2LRR1 (Cullin RING ligase 2 associated with LRR1). Finally, the ubiquitylated MCM7 is extracted from chromatin by the ATPase p97 and the catenanes are removed (Dewar et al., 2015; Dewar and Walter, 2017; Fragkos et al., 2015).

Transcription

Gene expression is the process whereby genes, encoded by DNA, express their inherited information usually in the form of proteins. Transcription represents the first step in gene expression. Transcription of the eukaryotic genome is carried out by nuclear RNA polymerase I (Pol I), Pol II and Pol III. Pol I transcribes the ribosomal RNAs (rRNAs) precursor and Pol III transcribes small non-coding RNAs as transfer RNAs (tRNAs). Pol II is the responsible of the transcription of protein-coding genes. For transcription initiation, Pol II assembles with the general transcription factors TFIIB, TFIID, TFIIE, TFIIF and TFIIH, which are collectively known as the general transcription factors, at promoter DNA to form the pre-initiation complex (PIC). The general transcription factors cooperate with Pol II to

bind and open promoter DNA, and to initiate RNA synthesis and stimulate the escape of Pol II from the promoter. TFIID contains the TATA box-binding protein (TBP) and several TBP-associated factors (TAFs). Whereas TBP is required for transcription from all promoters, the TAFs have promoter-specific functions (Lodish, 2000; Luse, 2014; Nikolov and Burley, 1997).

It has been described that Pol II–TFIIF complex binds to an already formed TFIIB–TBP–DNA promoter complex, resulting in the formation of a core initiation complex. The core initiation complex is conserved in the Pol I and Pol III transcription systems, which also use TBP and contain proteins with homologies to TFIIB and TFIIF. Then, the core initiation complex binds to TFIIE and TFIIH to form a complete PIC that contains closed, double-stranded promoter DNA. In the presence of nucleoside triphosphates, a central DNA region is melted leading to a 'transcription bubble' and the formation of the open promoter complex. In the open promoter complex, the DNA template strand passes near the Pol II active site and can programme DNA-templated RNA chain synthesis (Lodish, 2000; Sainsbury et al., 2015). The mechanistic details of termination remain unclear. Prevailing models for termination of mRNA-coding genes propose either that Pol II is released following an allosteric change in the elongation complex, or that the elongation complex is dismantled following degradation of the nascent transcript by a 5'–3' exoribonuclease (Porrua and Libri, 2015).

Eukaryotic translation

Translation is the process by which the information contained in the nucleotide sequence of an mRNA molecule is used to synthetize a protein. Eukaryotic translation process can be divided in four different phases (Figure 2) (Jackson et al., 2010; Sonenberg and Hinnebusch, 2009). First, methionyl initiator tRNA (Met-tRNA$_i$), GTP and eukaryotic initiator factor 2 (eIF2) are assembled in the eIF2-GTP-Met-tRNA$_i$ ternary complex (Sokabe and Fraser, 2014). This complex is then bound to the P site of the small ribosomal subunit (40S) generating the 43S complex. All nuclear transcribed mRNAs from eukaryotes contain an m7GpppN sequence on the 5' end that is recognized by eIF4F to be delivered to the ribosome. The structures found in the mRNA 5' untranslated region (5' UTR) are unwind by eIF4F and, in conjunction with other eIFs and the poly(A) binding protein (bound to the 3'-poly(A) tail), load the mRNA onto the 43S complex in an ATP consuming mechanism (Ramakrishnan, 2002).

The 43S complex begins to scan the mRNA in the 5' to 3' direction, until it localizes the AUG initiation codon (Hinnebusch, 2014; Kozak, 1986; Pestova and Kolupaeva, 2002). Finally, base pairing occurs between this initiation codon and the Met-tRNA$_i$, triggering GTP hydrolysis by eIF2 and generating the 48S complex. eIF2-GDP releases the Met-tRNA$_i$ into the P site of the 40S subunit and then dissociates. At the same time, eIF5B-GTP binds to the complex and facilitates the joining of the large (60S) ribosomal subunit. eIF5B is then released and peptide chain elongation begins (Fringer et al., 2007).

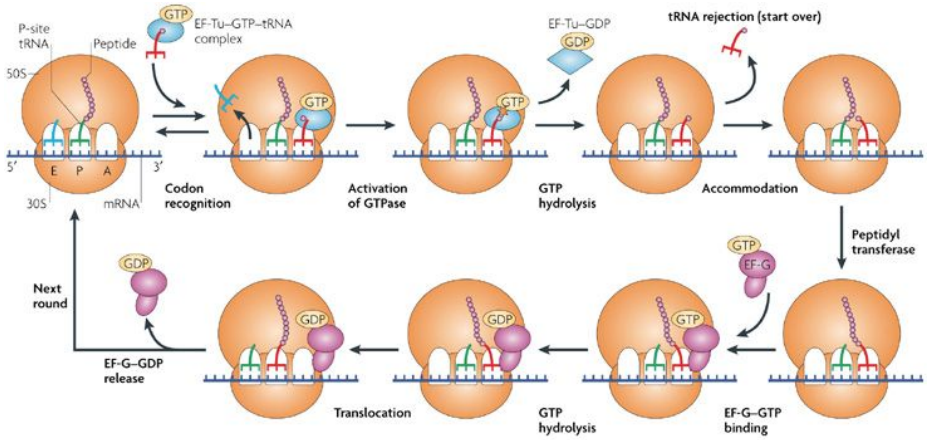

Figure 2| An overview of ribosomal structure and mRNA translation. mRNA translation is initiated with the binding of Met-tRNA$_i$ to the P site. An incoming tRNA is delivered to the A site in complex with elongation factor (EF)-Tu–GTP. Correct codon–anticodon pairing activates the GTPase centre of the ribosome causing the release of the aminoacyl end of the tRNA from EF-Tu. Binding of tRNA also induces conformational changes in rRNA that optimally orientates the peptidyl-tRNA and aminoacyl-tRNA for the peptidyl-transferase reaction to occur, which involves the transfer of the peptide chain onto the A-site tRNA. The ribosome shifts in the 3' mRNA direction so that it can decode the next mRNA codon. Translocation of the tRNAs and mRNA is facilitated by binding of the GTPase EF-G that causes the movement of the deacylated tRNA at the P site to the E site and the peptidyl-tRNA at the A site to move to the P site. The ribosome is then ready for the next round of elongation. The deacylated tRNA in the E site is released on binding of the next aa-tRNA to the A site. Elongation ends when a stop codon is reached, which initiates the termination reaction that releases the polypeptide. Adapted from: (Steitz, 2008).

During the elongation step, a new aminoacyl-tRNA (aa-tRNA) is carried to the A site of the ribosome complexed with eukaryotic elongator factor 1A (eEF1A) and GTP. The correct codon-anticodon base pairing activates eEF1A GTPase activity releasing the new aa-tRNA into the A site. The ribosomal peptidyl transferase center (PTC) catalyses the formation of a peptide bond between the methionine of Met-tRNA$_i$ in the case of the first

elongation cycle or the incoming amino acid in the growing peptide. The result is a deacylated tRNA with its acceptor end in the E (exit) site (of the 60S subunit) but with its anticodon still at the P site (of the 40S subunit), and a peptidyl-tRNA with the acceptor end at the P site (of the 60S subunit) but the anticodon end still at the A site (of the 40S subunit). The translocation of three positions of the mRNA, the concomitant positioning of the deacylated tRNA completely in the E site, and the peptidyl-tRNA completely in the P site is achieved by eEF2. The release of the deacylated tRNA from the E site has been postulated to be performed by an intrinsic eEF3-like activity (Hernández and Jagus, 2016). The protein elongation cycle is repeated until a stop codon is encountered, when the process of termination is triggered (Lodish, 2000; Steitz, 2008).

In response to any of the three eukaryotic stop codons UAA, UAG or UGA in the A site, eukaryotic releasing factor 1 (eRF1) promotes, with the help of eRF3, the hydrolysis of the ester bond linking the polypeptide chain to the tRNA on the P site and, therefore, the release of the completed polypeptide from the ribosome (Preis et al., 2014). At the end of the termination stage, the ribosome is left on the mRNA with a deacylated tRNA, presumably in intermediate state with the acceptor end in the E site of the 60S subunit and the anticodon end in the P site of the 40S subunit (Jackson et al., 2012).

The ribosome recycling process is the less known of the four stages and, contrary to prokaryotes, no ribosome recycling factors (RRF) have been found in eukaryotes. Instead, eIF3 has been proposed as the principal factor that promotes recycling of the ribosomes after termination, splitting the ribosomes into tRNA bound 60S subunits and mRNA bound 40S subunits (Pisarev et al., 2007). eIF1 mediates the release of the tRNA from the P site,

and eIF3j ensures the dissociation of the mRNA (Pisarev et al., 2007). This way, ribosomes can participate in translation of another mRNA(Dever and Green, 2012).

Mitochondria

Mitochondria are cellular organelles that produce cellular energy through oxidative phosphorylation. They have been described to carry out other functions including a portion of urea cycle, heme biosynthesis or to play a role in apoptosis. They were named from the Greek words, *mítos* meaning "thread" and *khondros,* meaning "granule" (Benda, 1898). According to the endosymbiont hypothesis initially proposed by Ivan Wallin (Wallin, 1926) and popularized by Lynn Margulis, mitochondria evolved from a bacterial progenitor via symbiosis within an essentially eukaryotic host cell. Mitochondria are of unquestioned bacterial ancestry, originated from within the bacterial phylum α-proteobacteria that rapidly lost or transferred most of the genomic material to the nuclear genome (Cooper, 2018; Pagliarini and Rutter, 2013).

Mitochondrial internal structure was already visualized with high-resolution electron-microscopy in the early fifty's (Palade, 1952; Sjostrand, 1953). They are dynamic organelles that undergo fusion and fission processes and are generally viewed as round or oblong-shaped organelles surrounded by two membranes that divide the mitochondrial matrix and the intermembrane space (Figure 3). The outer membrane is a phospholipidic bilayer that outlines the overall shape and separates the mitochondrial inside with the rest of the

cell by restricting the passage to small molecules. The inner membrane is highly invaginated forming a structure called mitochondrial *cristae*. It harbours the oxidative phosphorylation (OXPHOS) complexes that generates most of the ATP used by aerobic cells. This membrane is a tight diffusion barrier to ions and molecules that need highly specific carriers or transport proteins to get through. This produces an electrochemical membrane potential that is required for the activity of the electron transport chain (ETC) proteins (Figure 4).

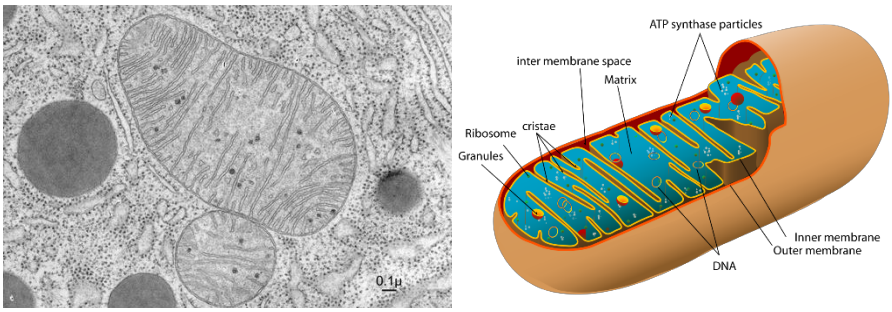

Figure 3| Mitochondrial structure. The left panel shows an electron microscopy image illustrating two mitochondria and showing two very different shaped organelles. The right figure shows the mitochondrial structure, the outer and inner membranes with the intermembrane space between them, and the mitochondrial matrix inside. The inner membrane creates folded structures called *cristae* and contains the electron transport chain.

The mitochondrial ATP production relies on the ETC that is composed of the respiratory chain complexes I-IV that transfer electrons until they finally reduce oxygen to form water. NADH and FADH2 generated in the glycolysis, citric acid cycle or fatty acid oxidation donate electrons to the ETC. The electrochemical gradient generated by Complexes I, III and IV drives the production of ATP from ADP and inorganic phosphate by the mitochondrial F_1F_0-ATP synthase (Complex V). Additionally, mobile

electron carriers coenzyme Q (CoQ) and cytochrome c move electrons between protein complexes. The consumption of oxygen in respiration is a measurable parameter that reflects mitochondrial function (Cooper, 2018; Hatefi, 1985).

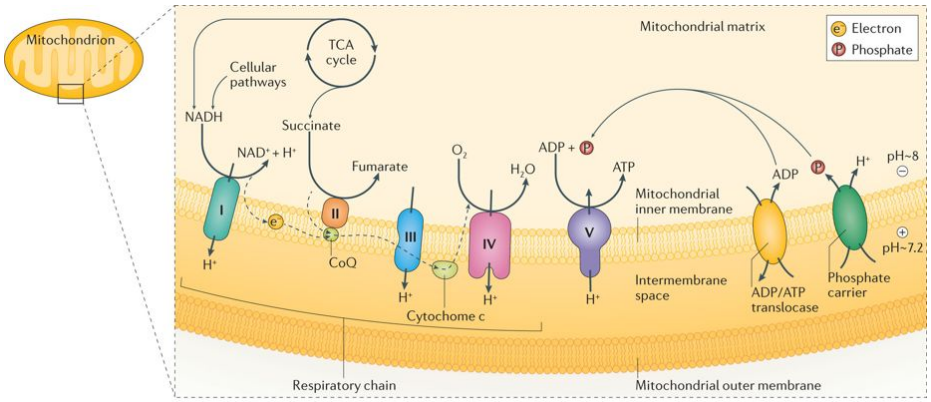

Figure 4| Schematic representation of oxidative phosphorylation. The respiratory pathway includes complexes I–IV of the respiratory chain and complex V, an ATP synthase.

Mitochondrial DNA

Most animal mitochondria have their own genome of about 16,000 base pairs of DNA encoding for 2 rRNAs, 22 tRNAs and 13 open reading frames encoding for proteins of the ETC complexes that include seven subunits of Complex I (NADH:ubiqionone oxidoreductase), one subunit from complex III (ubiquinone: cytochrome c oxidoreductase), three subunits from complex IV (cytochrome c: oxygen oxidoreductase) and 2 subunits of complex V (ATP synthase). Complex II is the only one entirely encoded in the nuclear genome. However, most of the proteins present in mitochondria are encoded by nuclear genes, synthesized in the cytosol and imported into the organelle.

OXPHOS complexes formation requires a coordinated expression of genes by nuclear and mitochondrial DNA (mtDNA) (Chandel, 2014; Couvillion et al., 2016; Kotiadis et al., 2014). The signal peptide hypothesis predicted that some proteins encode specific peptide sequences that determine their localization (Blobel and Dobberstein, 1975).

It has been shown that most of the nuclear encoded proteins that localize to the mitochondria contain a mitochondrial signal peptide (MSP), usually localized in the N-terminal part, that addresses them to the organelle. The MSP is recognized by the TOM complex in the mitochondrial outer membrane and the protein is internalised in the mitochondrial inner membrane by the TIM complex. Then the MSP is often cleaved by the mitochondrial processing peptidase (MPP), allowing proper protein folding (Bauer et al., 2000; Nielsen et al., 1997). However, it was recently described that proteins that have a MSP can also localize to the nucleus and, in some cases, act as direct signals from mitochondria to regulate nuclear events (Monaghan and Whitmarsh, 2015). Therefore, it is of extreme importance that this communication between mitochondria and nuclei is properly regulated in order to avoid changes in metabolism and proteostasis (Quiros et al., 2016).

Mitochondrial DNA expression and maintenance

Mitochondrial DNA expression and maintenance also depends on the import of hundreds of nuclear-encoded proteins that control genome maintenance, replication, transcription, RNA maturation and mitochondrial translation. The two strands of mtDNA differ in base composition, with the guanine-rich heavy strand (H-strand) and the cytosine-rich light strand (L-strand).

mtDNA genes lack introns and the only non-coding region contains the promoters for mitochondrial transcription and the origin of replication. In *Drosophila*, this region contains 90-96% deoxyadenylate and thymidylate residues (A+T rich region). This region is called "control region" and contains a dedicated promoter for the transcription of each mtDNA strand, the light-strand promoter (LSP) and the heavy-strand promoter (HSP), as well as sequences to control mtDNA replication (Garesse and Kaguni, 2005).

Transcription by mitochondria RNA polymerase (POLRMT) is initiated at the LSP or the HSP and produces polycistronic transcripts that encompass all of the coding information on each strand (Gaspari et al., 2004). Primary transcripts are further processed to release individual RNA molecules. The 5' ends of tRNAs are cleaved by ribonuclease P (RNase P), whereas the 3' ends are processed by RNase Z (ELAC2) (Dubrovsky et al., 2004; Hartmann et al., 2009). This model where mRNAs, tRNA and rRNAs are transcribed as a polycistronic transcript was named the tRNA punctuation model (Ojala et al., 1981; Sanchez et al., 2011). Addition of the CCA end completes maturation of the tRNA 3' site by the tRNA-nucleotidyl transferase. The other RNAs are constitutively adenylated, with one to ten adenine residues and 50-60 nt long poly(A) tails added to the 3' terminus of rRNAs and mRNAs respectively (Figure 5) (Bobrowicz et al., 2008; Wydro et al., 2010).

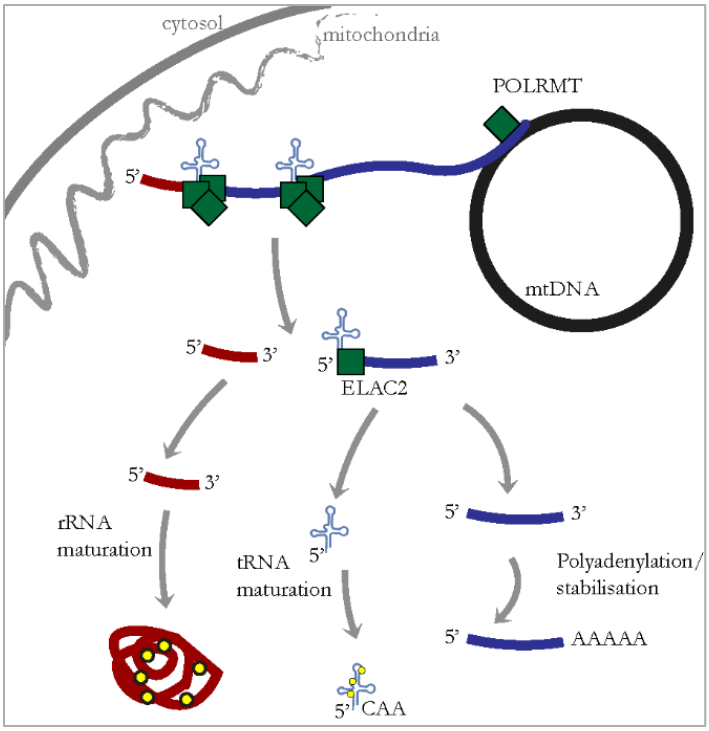

Figure 5| mtDNA transcription and RNA maturation. Each strand of mtDNA is transcribed as a long polycistronic transcript that is further processed to release the individual mRNAs, tRNAs, and rRNAs. The mitochondrial RNase P consists of three subunits (MRPP1–MRPP3) and cleaves the primary transcript at the 5' end of tRNAs. The tRNAs are released by cleavage at their 3' ends by RNase Z (ELAC2). Yellow dots indicate RNA modifications. Adapted from: (Hallberg and Larsson, 2014).

In addition to POLRMT, the mitochondrial transcription machinery is also composed by the mitochondrial transcription factor A (TFAM), the mitochondrial transcription factor B1 and B2 (TFB1 and TFB2M), as well the mitochondrial termination factor (mTERF1 or mTTP in *Drosophila*). TFAM is the major component of the mitochondrial nucleoid and contains two "high mobility groups" (HMG) box domain family that allow it to bind, unwind and bend DNA without sequence specificity (Matsushima et al., 2010; Shi et al., 2012). Moreover it binds to the mitochondrial promoters and

creates a stable U-turn in DNA (Rubio-Cosials et al., 2011). This bend may be needed to enhance the interaction with TFB2M to increase the rate of transcription initiation at the LSP (Ngo et al., 2011). TFB2M was first discovered as a homologous protein to the yeast transcription factor mtTFB and it transiently interacts with POLRMT forming part of the catalytic site in the initiation of transcription (Sologub et al., 2009). In the initiation complex TFB2M directly interacts with the priming substrate. TFB2M and the homologous protein TFB1M are similar in sequence to the rRNA methyltransferases. TFB1M likely represents the ancestral methyltransferase, whereas TFB2M is the result of a gene duplication that has evolved into a mitochondrial transcription factor. While TFB2M has been described to be required for efficient mitochondrial transcription and for maintenance of mtDNA, TFB1M showed no important role in none of the processes (Matsushima et al., 2005; Matsushima et al., 2004).

After initiation of RNA synthesis and promoter escape by POLRMT, the initiation factors are released, and the elongation factor is recruited. Mitochondrial transcription elongation factor (TEFM) was described as a critical protein for mitochondrial transcription (Posse et al., 2015). It interacts with the C-terminal part of POLRMT and stimulates the interaction with an elongation-like DNA:RNA template. TEFM helps the polymerase to transcribe longer stretches of RNA and to bypass regions generating highly structured RNA (Minczuk et al., 2011). In the absence of TEFM, POLRMT prematurely terminates at a conserved G-quadruplex-forming sequence downstream of the LSP producing short transcripts that are thought to serve as primers for replication of the heavy strand of mtDNA (Hillen et al., 2017; Wanrooij et al., 2010).

At the end of each transcription cycle, POLRMT ceases RNA synthesis and dissociates from mtDNA. mTERF1 binds to the termination site within the

gene encoding for $tRNA^{Leu}$ in the LSP. In contrast, the termination mechanism of the HSP remains unknown, and has been suggested to also involve an obstruction protein that binds near the 3' end of the 7S DNA. In *Drosophila*, mTTF has been described to bind two mtDNA sequence elements located at the boundary of clusters of genes transcribed in opposite direction (ND3/ND5 and Cyt B/ND1). It has been described that in the mTTF binding sites the mtDNA replication is paused, suggesting that it could be coordinating conflicts between the replisome and transcription processes (Barshad et al., 2018; Roberti et al., 2006).

Mitochondrial DNA replication

Similar to the mitochondrial transcription machinery, mtDNA replication factors are related to the replication machineries found in bacteriophages. The DNA polymerase-γ (POLγ) is the only mitochondrial replicative polymerase. It is unable to use double-strand (dsDNA) as a template and requires TWINKLE, the DNA helicase that travels together with POLγ at the replication fork and catalyses nucleotide triphosphate-dependent unwinding of the mtDNA duplex in the 5' to 3' direction (Ciesielski et al., 2016).

Mitochondrial DNA replication occurs continuously on both strands without Okazaki fragments formed. To coordinate DNA synthesis of the two strands, mtDNA contains a dedicated origin of DNA replication on each strand, the heavy-strand origin (O_H) and the light-strand origin (O_L). Replication is initiated at the O_H and POLγ proceeds to produce a new H-strand. The first phase of DNA replication does not involved simultaneous synthesis of the complementary L-strand. Mitochondrial single-strand DNA binding protein

(mtSSB) stimulates TWINKLE's helicase activity and stabilizes the long stretches of single-stranded DNA (ssDNA) formed at the replication fork. Once the replication machinery has synthesized two-thirds of the mtDNA, the replication at the O_L starts and becomes single-stranded folding into a stem-loop. Then, mtSSB is displaced from this region allowing POLRMT to initiate primer synthesis, and POLγ to synthesise the L-strand.

Although *Drosophila* mitochondrial genome closely resembles the vertebrate overall structure (Figure 6), it presents a different gene order. Sequence analysis in several *Drosophila* species has detected the presence of three conserved elements in the A+T region (I, II and a stretch of deocythymidylate residues) that may be involved in mtDNA replication and transcription (Garesse and Kaguni, 2005). The mtDNA replication mechanism in *Drosophila* is less understood and it has been demonstrated that most DNA molecules are replicated with concomitant synthesis of both strands, initiating unidirectionally within control region and pausing frequently in specific regions. The strand-asynchronous model was also found in a limited number of mtDNA molecules (Ciesielski et al., 2016; Joers and Jacobs, 2013).

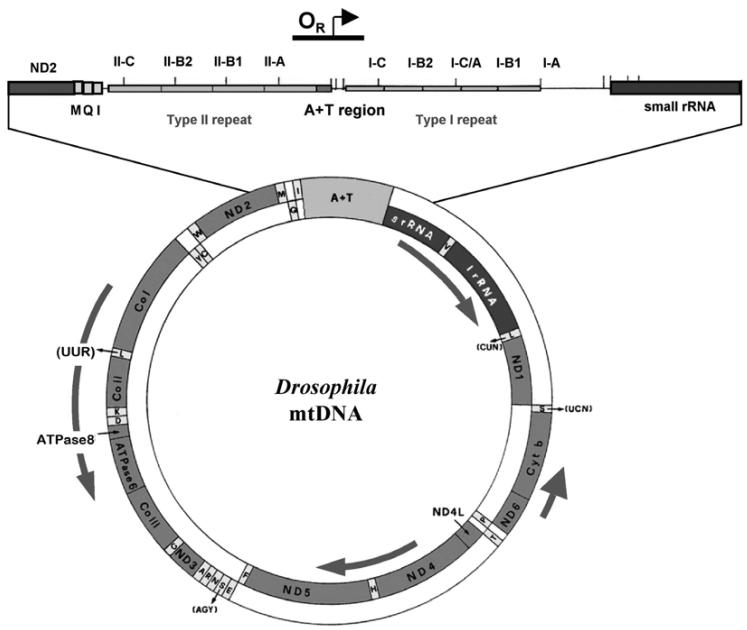

Figure 6| *Drosophila melanogaster* mitochondrial DNA genome. The mtDNA gene order and distribution on both strands is different in *Drosophila* than in vertebrates and encodes 13 polypeptides, 22 tRNAs and two rRNAs. ND, NADH dehydrogenase; Cytb, cytochrome b; Co, cytochrome oxidase; ATPase, ATP synthase; s and l rRNAs, small and large ribosomal RNAs. The 22 tRNAs are denoted according to the single letter amino acid code. A + T-rich control region is shown in detail with the type I and II repeats. The region containing the origin of replication (O_R) is depicted with the arrow indicating the direction of synthesis of the leading strand. Adapted from: (Garesse and Kaguni, 2005).

Mitochondrial translation

Similar to the cytosolic or bacterial ribosomes, mitochondrial translation is a multistep process that requires several factors for initiation, elongation, termination, and recycling. Mitochondria contain a distinct set of ribosomes (mitoribosomes) which sediment as 55S particles and consist of 28S small subunits and 39S large subunits with two rRNA species, 12S in the small

subunit (SSU) and 16S in the large subunit (LSU) (Christian and Spremulli, 2012; Pietromonaco et al., 1991).

The initiation process requires two initiation factors (IFs), mtIF2 and mtIF3. First, mtIF3 binds the SSU and dissociates the monosome to release the LSU. The SSU together with mtIF3 interacts with mtIF2, mRNA and the tRNA that carries formylated methionine ($tRNA^{FM}$) (Gaur et al., 2008). The initiation complex is then formed, and $tRNA^{FM}$ is bound to the start codon of the open reading frame (ORF) of the mRNA. Then, mtIF2 hydrolyses its GTP and both initiation factors are released when LSU binds to start translation. In the elongation phase, the mitochondrial elongation factor Tu (mtEFTu) in complex with GTP and the aminoacylated tRNA, enters the A site of the mitoribosome (Burnett et al., 2014). Base pairing of the tRNA anticodon with the codon contained in the mRNA leads to the conversion of GTP to GDP and the release of mtEFTu. The peptide chain of the tRNA present at the P site is transferred to the newly entered aminoacylated tRNA of the A site, where the ribosome catalyses the peptide bond formation leading to the elongation of the peptide chain. Binding of the elongation factor G1 (mtEFG1) catalyses the translocation of the tRNA with the peptide chain from the A site to the P site and moves the deacylated tRNA from the P to the E site. Finally, at the end of the ORF, the stop codon recognizes the non-aminoacylated tRNA and translation termination factors interact with it to release the nascent peptide chain from the ribosome (Figure 7) (Chrzanowska-Lightowlers et al., 2011; Hallberg and Larsson, 2014).

Mitochondrial genetic codes often differ from the universal code. In *Drosophila* the AGG codon is absent, the cytosolic stop codon UGA is decoded as tryptophan and the cytosolic isoleucine AUA codon is decoded as methionine (Jukes and Osawa, 1993).

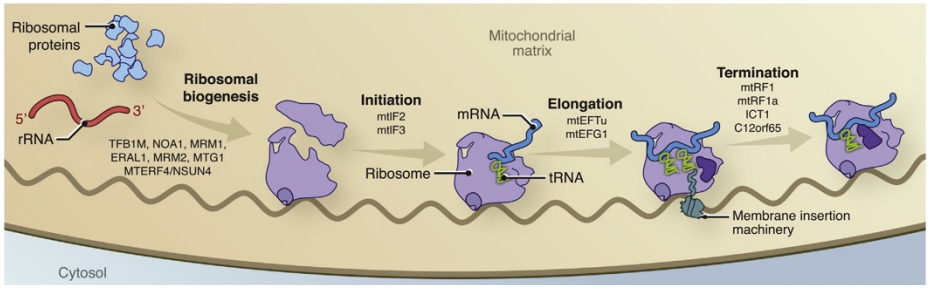

Figure 7| Mitoribosomes biogenesis and the mitochondrial translation cycle. The biogenesis of the mitoribosome requires that the 12S and 16S rRNAs are modified and assembled along with the ribosomal proteins. The translation cycle requires several factors for initiation, elongation, and termination depicted in the diagram. The membrane anchoring of the mitoribosome facilitates the insertion of newly synthesized proteins into the inner mitochondrial membrane. Adapted from: (Hallberg and Larsson, 2014).

Mitochondrial protein folding and degradation

As previously mentioned, mitochondria lack large part of the required genetic information and most mitochondrial proteins are synthesized in the cytosol and imported into the organelle, where polypeptides must fold and assemble into active proteins. It is well known that under pathological conditions, mitochondrial proteins become misfolded or damaged and need to be repaired with the help of chaperones. Eventually these damaged proteins are removed by specific proteases. The protein quality control mechanisms in the mitochondria is necessary for the correct mitochondrial function and structural integrity (Gustafsson et al., 2016; Hallberg and Larsson, 2014).

There are surveillance pathways in the mitochondria that oppose and reverse this damage, including the AAA^+ proteases family (Figure 8). LON protease belongs to the family of ATP-dependent serine proteases and it has been associated with diverse cellular activities. LON has been described as the

major protease in the mitochondria (Pinti et al., 2015; Pinti et al., 2016) where it presents a highly conserved homooligomeric, ring-shape structure (Park et al., 2006; Stahlberg et al., 1999).

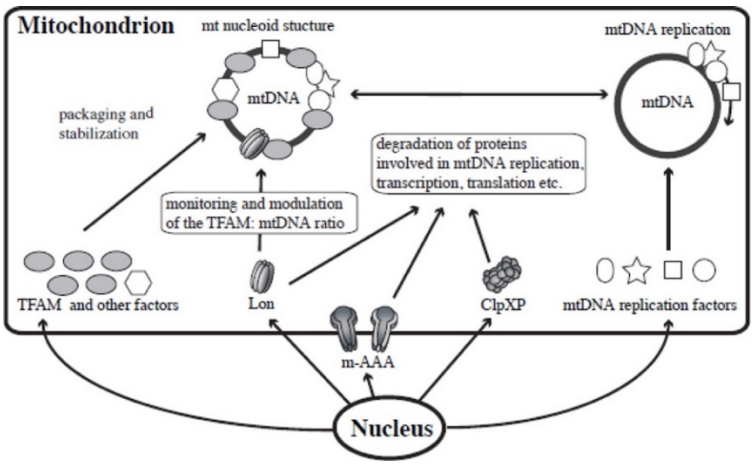

Figure 8| Mitochondrial protein quality control. The diagram shows that three nuclear encoded AAA+ proteases in the mitochondrial matrix regulate mitochondrial protein levels to sustain proper mtDNA functions, and to degrade oxidatively modified or misfold proteins. Adapted from: (Matsushima and Kaguni, 2012).

It has been described that LON possesses three different activities, serving as a chaperone, as a DNA-binding protein and as a protease (Pinti et al., 2015; Pinti et al., 2016). LON is responsible for the protein quality control in the mitochondria by degrading oxidatively modified or misfolded proteins before aggregation (Bezawork-Geleta et al., 2015; Bota and Davies, 2002).

LON is composed by three domains, the N-terminal domain, central AAA+ ATPase domain, and the C-terminal protease domain (Figure 9). The N-terminal domain is involved in protein substrate binding. The AAA+ domain contributes to ATP binding and hydrolysis and the C-terminal protease domain contains a serine and lysine dyad in the active site.

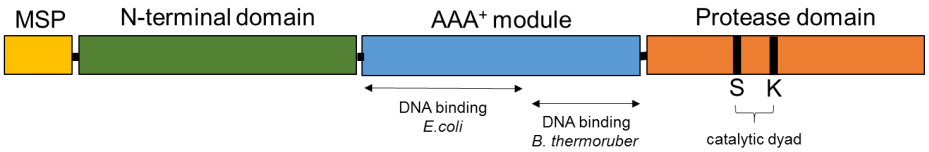

Figure 9| LON protease domains. LON comprises the mitochondrial signal peptide and three protein domains, an N-terminal domain or mitochondrial signal peptide (MSP), the central AAA+ ATPase domain, and a C-terminal protease domain. The DNA-binding domains in *E.coli* and *B.thermoruber* LON reside in different regions within the AAA+ module. The C-terminal protease domain contains a serine and lysine from the catalytic dyad.

LON has been shown to be a component of mitochondrial nucleoids, which are complexes of protein and DNA required for the package of mtDNA (Alam et al., 2003; Bogenhagen, 2012). LON is responsible for the selective degradation of TFAM, when multiple serine residues in the two high mobility groups are phosphorylated by protein kinase A (Lu et al., 2013). In *Drosophila,* LON stabilizes TFAM:mtDNA ratio, playing a crucial role in mtDNA replication and transcription. LON depletion has been described to increase TFAM and mtDNA levels, while overexpression causes the reduction of both components. Therefore, through the degradation of TFAM, *Drosophila* LON represses the replication of mtDNA (Matsushima et al., 2010).

Moreover, it has recently been shown in *Drosophila* that LON depletion confers shortened lifespan, locomotor impairment, and respiratory defects specific to respiratory chain complexes that contain mitochondrially encoded subunits. These defects appeared to result from severely reduced mitochondrial translation derived from sequestration of mitochondrially encoded transcripts in highly dense ribonucleoparticles (Pareek et al., 2018).

Aminoacyl tRNA synthetases

Aminoacyl tRNA synthetases (ARSs) constitute an ancient family of enzymes that catalyze aminoacylation reactions by attaching amino acids to cognate tRNAs. The need of aminoacyl tRNA synthetases to mediate the translation of the genetic code was first suggested by Crick in 1958 as part of his adaptor hypothesis of protein assembly (Crick, 1958). ARSs are autonomous and self-sufficient enzymes that typically do not require additional protein cofactors for their canonical function.

The aminoacylation reaction is a 2-step process (Figure 10). In the first step, the amino acid is activated by ATP to generate an aminoacyl-adenylate intermediate. In the second step, the activated amino acid is transferred to the 3' end of the tRNA bearing the appropriate anticodon triplet that recognizes the corresponding codon in the mRNA. The aminoacylated tRNA is then delivered to the ribosome for nascent polypeptide synthesis. Because ARSs recognize specific amino acids and the corresponding tRNAs, they translate the genetic code into amino acids (Giege et al., 1998). ARSs are thus fundamental components of the protein synthesis process in all cells of all species in the three primary kingdoms of life (Ibba and Soll, 2000).

There are 20 standard amino acids, and for each of them cells are expected to express at least one ARS. ARS can be classified in two classes, class I ARSs contain a characteristic Rossman fold catalytic domain and usually function as monomeric or dimeric proteins, while class II ARSs contain three conserved motifs and are usually dimeric or tetrameric. ARSs may also be classified according to their subcellular sites of action: cytoplasmic, mitochondrial, or both cytoplasmic and mitochondrial. Eukaryotic ARSs play a broad array of regulatory roles in cell biology and tissue development. In

terms of tRNA aminoacylation, the vast majority of ARSs are autonomous and self-sufficient enzymes that do not require additional protein cofactors for their function (Carter, 2017; Ribas de Pouplana and Schimmel, 2001).

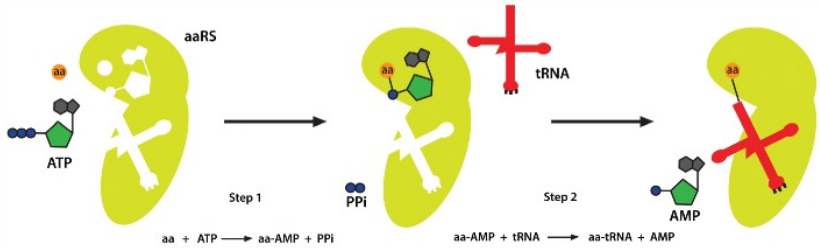

Figure 10| Aminoacyl-tRNA synthetase catalyzes a two-step aminoacylation reaction. In the first step, the ARS activates the substrate amino acid. By consuming an ATP, it forms an aa-AMP intermediate. In the second step, the aa-AMP is transferred to the acceptor end of the cognate tRNA, generating an aa-tRNA that can be delivered to ribosomes for protein synthesis. aa, amino acid; aaRS, aminoacyl-tRNA synthetase; PPi, pyrophosphate. Adapted from: (Lu et al., 2015).

Structurally, ARS represent evolutionary hot points that readily incorporate new domains to acquire non-canonical regulatory functions (Guo and Schimmel, 2013; Yao et al., 2014). ARS-like proteins are homologous molecules with specific domains of ARS that may carry functions related to the aminoacylation of tRNA or carry out additional biological functions. Also, proteins structurally associated with ARS may also dissociate to control diverse signalling pathways (Park et al., 2008). ARS have been linked with autoimmune disorders, cancers and neurological disorders highlighting the non-translational functions of these proteins (Figure 11) (Guo and Schimmel, 2013).

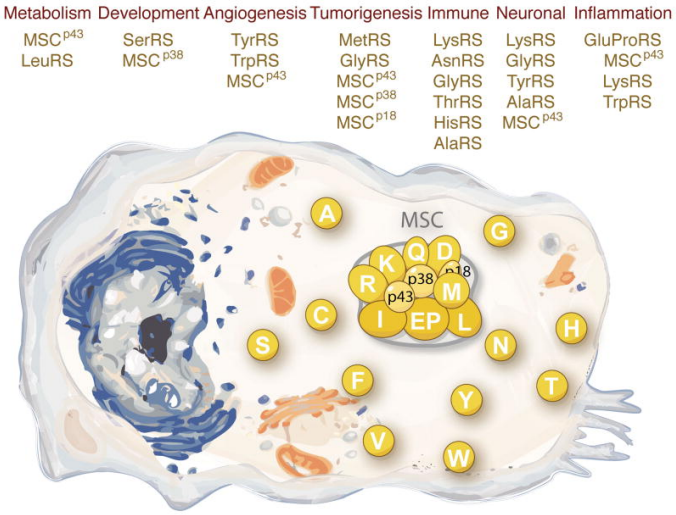

Figure 11| The non-translational functions of ARSs. ARSs are commonly in a free form in the cytoplasm, but also as part of a high molecular weight multi-tRNA synthetase complex (MSC), which includes 3 scaffold proteins designated as MSCp43, MSCp38, and MSCp18. These proteins not only are an essential part of the translation apparatus, but also have a numerous cytoplasmic, nuclear and extra-cellular functions. Synthetases are designated by single letters, using the standard abbreviations for amino acids. Adapted from: (Guo and Schimmel, 2013).

The Seryl-tRNA Synthetase

SerRSs are homodimeric enzymes that belong to the class IIa of ARS. The structure of the SerRS monomer comprises an active site domain and an N-terminal domain that folds into a long coiled-coil structure (Cusack et al., 1990) that recognizes the long variable arm of $tRNA^{Ser}$. In metazoans, SerRS are among the few enzymes that remain duplicated in the cell; one isoform acts in the cytosol, and the second functions in the mitochondria, where it needs to recognize the highly diverged structures of mitochondrial $tRNA^{Ser}$. However, the three-dimensional structure of mitochondrial SerRS from *Bos*

taurus reveals a similar structure to cytosolic enzymes, including a coiled-coil motif at its N terminus (Chimnaronk et al., 2005). In addition, it has been reported that SerRS plays a role during the development of zebrafish (Amsterdam et al., 2004; Fukui et al., 2009; Herzog et al., 2009).

The mitochondrial seryl-tRNA synthetase (SerRS2) is the enzyme in charge of loading $tRNA^{Ser}$ with serine in the mitochondria. It has been described a homozygous founder mutation in the human mitochondrial seryl-tRNA synthetase (SARS2) that was highly prevalent among inhabitants of a Palestinian village, with an uncharacterized multisystem fatal mitochondrial cytopathy, which was named HUPRA syndrome (hyperuricemia, pulmonary hypertension, renal failure in infancy, and alkalosis) (Belostotsky et al., 2011). Moreover, it was also described that an insertion in the mitochondrial $tRNA^{Ser}$ resulted in a reduction in serylation efficiency, a moderate mitochondrial dysfunction, morphological alterations and lactate elevation that cause sensorineural hearing loss (Cardaioli et al., 2006; Toompuu et al., 2002). Also, mutations in $tRNA^{Ser}$ related to multisystem disease with cataracts and deafness, retinal degeneration, myopathy and epilepsy cause defects in mitochondrial function, abnormal mitochondrial morphology and proliferation, and those involved in MELAS/MERRF diseases result in a group of features, such as pleomorphic mitochondria, increment in lactate, decrease in respiratory chain activity and increase in mitochondrial density (Hutchin et al., 2001; Swalwell et al., 2008; Tiranti et al., 1995; Zheng et al., 2012).

In our laboratory, we generated a *Drosophila melanogaster* model for human mitochondrial disease caused by mitochondrial aminoacylation restriction through the depletion of SerRS2. The model has been first characterized at the molecular level, showing a decrease in SerRS2 expression and function, with a reduction in $tRNA^{Ser}$ aminoacylation. SerRS2 depletion compromised

viability, longevity, motility and tissue development. At the cellular level, SerRS2 silencing affected mitochondrial morphology, biogenesis and function, and induced lactic acidosis and reactive oxygen species (ROS) accumulation (Guitart et al., 2013).

Initial characterization of SLIMP

During the investigation of the function of *Drosophila* mitochondrial seryl-tRNA synthetase SerRS2 (Guitart et al., 2013), our laboratory discovered SLIMP (CG31133), a paralog of this protein that retains a typical SerRS structure but has lost all tRNA aminoacylation activity (Figure 12). The first characterisation of SLIMP was performed *in vivo* by studying SLIMP and SerRS2 depletion in *Drosophila melanogaster*.

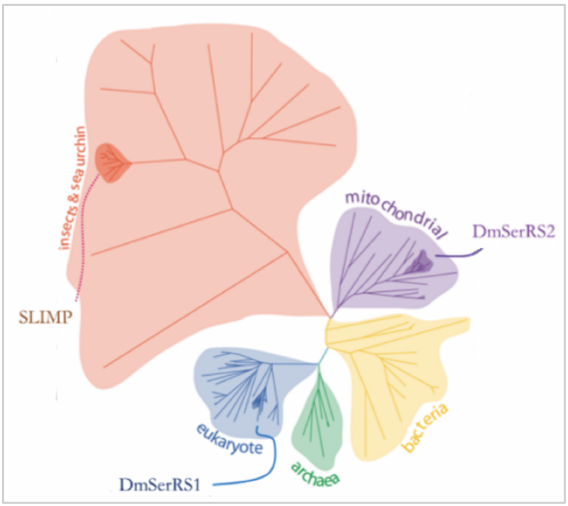

Figure 12|Phylogenetic analysis of SLIMP and SerRS and its presence in different insect species. The distance tree indicates that the SLIMP clade evolved faster than SerRS. All the SLIMP proteins cluster together, sharing the same ancestor as a mitochondrial SerRS. *Drosophila melanogaster* cytosolic and mitochondrial SerRS are represented as DmSerRS1 and DmSerRS2 respectively. Adapted from: (Guitart et al., 2010).

SLIMP was described to interact with its homologous protein SerRS2 and by this interaction they stabilize each other. Analysis of this complex by size exclusion chromatography and Multi Angle Light Scattering (MALS) unequivocally showed that SerRS2 and SLIMP form a αβ heterodimer in solution. SLIMP was also found to be interacting with LON protease, in mass spectrometry assays confirmed by immunoprecipitation. Moreover, it was described that LON is not degrading SLIMP, assessed by immunoblot in LON-overexpressing cells. Furthermore, an *in silico* analysis of the three-dimensional model of SLIMP indicated that six of the eleven amino acids responsible for the recognition of the seryl-adenylate in *Bos taurus* mitochondrial SerRS (BtSRS2) are not conserved in SLIMP (Figure 13). The mutated residues are physically incompatible with the interactions established between serine, ATP and SerRS. In contrast, these positions are perfectly conserved in the canonical SerRS2.

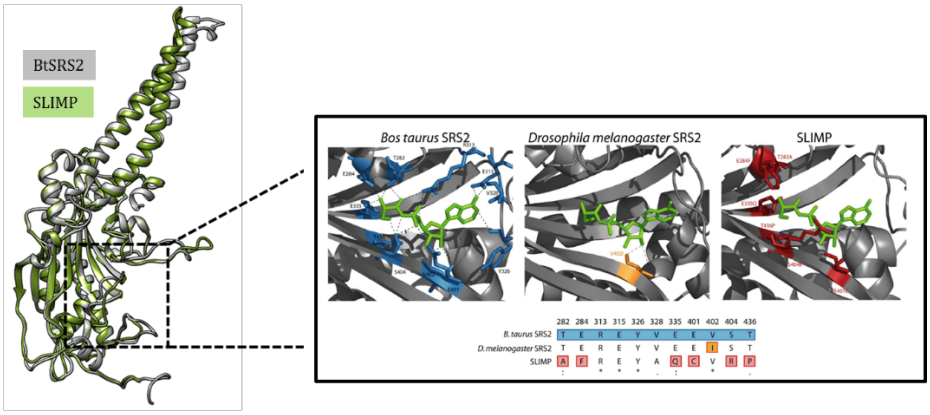

Figure 13|SLIMP structural analyses. The model of SLIMP (in green) with the BtSRS2 (in grey). *B.taurus* and *D.melanogaster* mitochondrial SerRS structure is shown with the seryl-adenylate in green. The residues that contact the intermediate are depicted in blue, and the non-conserved residues that would disrupt the interaction between SerRS substrates in SLIMP are shown in red. Adapted from: (Guitart et al., 2010).

Moreover, pure SLIMP protein had no detectable $tRNA^{Ser}$ aminoacylation activity (Figure 14), and it is not able to bind any of the initial substrates required for the serylation of tRNA by SerRS (any amino acids or ATP). SLIMP depletion severely affects mitochondrial function, increases mitochondrial DNA (mtDNA) levels, and is lethal at any stage of development. Although SLIMP mRNA has been detected at all the stages of development, it was described to be synthesized at late embryonic stages and remains present throughout the rest of the cycle (Guitart et al., 2010).

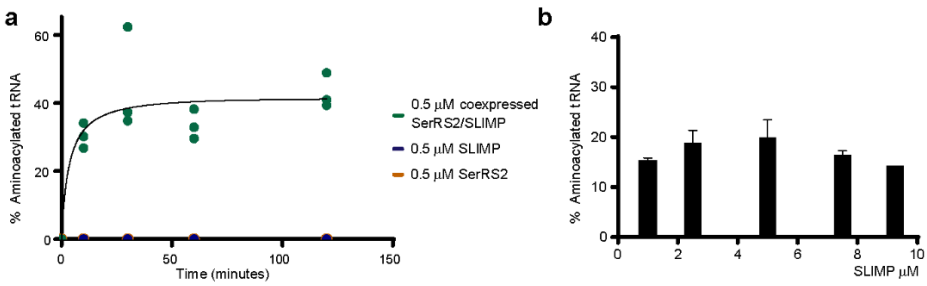

Figure 14| Mitochondrial $tRNA^{Ser}_{GCU}$ aminoacylation assays. (a) Activity percentage of the purified SLIMP-SerRS2 complex is shown in green. SLIMP or SerRS2 purified alone are not able to aminoacylate $tRNA^{Ser}$. (b) Aminoacylation assays were performed for a total reaction time of 60 minutes with increasing SLIMP concentrations. Data represent mean values ± s.e.m of three independent experiments.

Two independent genetic screens in *Drosophila melanogaster* have identified SLIMP as an important factor for cell cycle progression (Ambrus et al., 2009; Liang et al., 2014). SLIMP depletion compensated for the inactivation of the dE2F pathway, allowing cell cycle progression from G1 to S phase in the absence of dE2F1 and SLIMP acted as a repressor of a subset of E2F target genes through a mechanism independent of the RB-E2F pathway (Benevolenskaya and Frolov, 2015). Furthermore, a functional genomic

analysis of the periodic transcriptome in *Drosophila melanogaster* wing imaginal disks and S2 cells identified SLIMP as factor required for successful cell cycle progression, and reported that it displays a highly periodic expression profile (Liang et al., 2014).

Cell cycle

The prototypical eukaryotic cell cycle is divided into four phases. In the gap 1 (G1) phase, cells typically grow and may enter the synthesis (S) phase, where the nuclear DNA is replicated. Next, cells progress to gap 2 (G2) phase, the second interphase in cell cycle before mitosis (M) starts, where sister chromatids are separated and distributed to the newly forming daughter cells. Cytokinesis follows mitosis and completes the cell division program with the formation of two daughter cells separated by a plasma membrane (Cooper, 2018).

At key transitions during eukaryotic cell cycle progression, signalling pathways monitor the successful completion of upstream events prior to proceeding to the next phase. These regulatory pathways are referred to as cell cycle checkpoints (Hartwell and Weinert, 1989). The major checkpoints are at entry into S phase (G1–S checkpoint) or mitosis (G2–M check- point), and the spindle checkpoint that controls progression into anaphase. Therefore, cells can arrest at cell cycle checkpoints temporarily to allow for cellular damage to be repaired, the dissipation of an exogenous cellular stress signal, or the availability of essential growth factors, hormones, and nutrients. Checkpoint signalling may also result in activation of pathways leading to

programmed cell death if cellular damage cannot be properly repaired (Pietenpol and Stewart, 2002).

The general view of cell cycle regulation is that Cdk4 and Cdk6 together with D-type cyclins promote the transition in early G1 or from G0, a resting phase in which cells are in a quiescent state, into phase by initiating phosphorylation of the retinoblastoma (Rb) family proteins and releasing the transcription of early E2F target genes (including Cyclin E (CycE) and Cyclin A (CycA)) from their repression by Rb proteins (Bertoli et al., 2013). Then, Cdk2 controls entry into and progression through S phase in complex with CycE and CycA by completing the phosphorylation of Rb proteins, leading to further activation of E2F target genes and culminating in the initiation of S phase. Cdk1, in conjunction with CycA and Cyclin B (CycB), then controls the entry and progression through M phase. Exit from mitosis requires degradation of mitotic A- and B-type cyclins by the anaphase promoting complex (APC) (Figure 15) (Harashima et al., 2013).

The E2F/DP heterodimeric transcription factors (referred to as E2F) are best known for their ability to regulate the G1-to-S transition. The transcriptional activity of E2F is inhibited by the retinoblastoma protein (pRB), which blocks S-phase entry and, in response to anti-proliferative signals, promotes cell-cycle exit. *Drosophila* is particularly advantageous to study this mechanism due to high conservation yet relative simplicity of the RB pathway. Unlike the large mammalian E2F and DP gene families, there are only two E2F genes, *dE2f1* and *dE2f2*, and one DP gene, *dDP*, in *Drosophila* genome. Both dE2F1 and dE2F2 heterodimerize with dDP and require dDP to bind to DNA. Inactivation of *dDP* had been described to produce the same phenotype that the loss of both *dE2f1* and *dE2f2*. Interestingly, in flies, loss of E2F control is permissive for most of animal

development since *dDP* single mutant or *dE2f1 dE2f2* double mutants develop normally throughout embryonic and larval stages. Therefore, the phenotype of *dDP* mutant larva reflects the results of E2F inactivation without unwanted consequences of developmental defects (Ambrus et al., 2013; Benevolenskaya and Frolov, 2015; Blais and Dynlacht, 2004; van den Heuvel and Dyson, 2008).

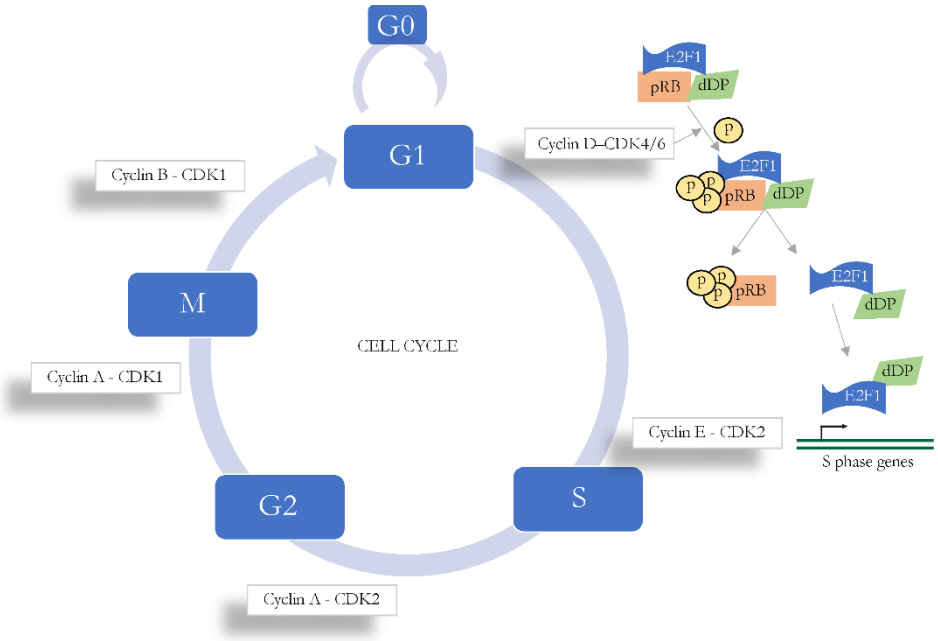

Figure 15| Overview of the eukaryotic cell cycle. The eukaryotic cell cycle consists of four phases; G1, S, G2, and M. Progression through the cell cycle is tightly controlled. E2F activation through the phosphorylation of pRB is depicted. Adapted from (Bagga and Bouchard, 2014).

Furthermore, it is known that cell cycle regulation varies between different species, but also exists a wide diversity of cell cycle programs within one species such as *Drosophila*. These are typically associated with specific developmental stages or physiological conditions, like the embryonic cell cycles that are often very fast and can skip one or both gap phases (Edgar and Lehner, 1996).

OBJECTIVES

The main goal of this thesis is to further expand the knowledge on the biological roles of SLIMP in *Drosophila melanogaster*.

Detailed objectives:

1. Define the subcellular localization and SLIMP protein environment.
2. Characterize SLIMP function in mitochondrial translation.
3. Describe the effect of SLIMP in mitochondrial homeostasis.
4. Characterize the interaction of SLIMP and LON protease.
5. Define the role of SLIMP in cell cycle progression.

MATERIALS AND METHODS

Experimental model and cell line

Drosophila melanogaster Schneider 2 cells (S2 cells) (ATCC CRL-1963) were maintained at 25ºC in Schneider's *Drosophila* medium (Gibco) supplemented with 10% fetal bovine serum (FBS) and 50 μg/ml penicillin and streptomycin. S2 cells were transfected using Effectene (Qiagen) and stable cell cultures were selected by adding 200 μg/ml hygromycin B (Gibco) to the media, and/or 2.5 μg/ml puromycin (InvivoGen) as indicated in each experiment. S2 cells were induced by the addition of 400 μM $CuSO_4$ to the media for eight days or the indicated period of time in each experiment in order to overexpress the cloned proteins or the RNAi.

For visualization and imaging, Elipse TD2-FL microscope was used with the NIS-elements BR software (Nikon).

A HeLa and Hek293T human cell lines were maintained at 37ºC in DMEM (Gibco) supplemented with 10% FBS and 50 μg/ml penicillin and streptomycin.

Cells were counted using Countess Automated Cell Counter (Invitrogen), with Trypan Blue solution 0.4% (Thermo).

Generation of expression constructs, cloning and protein purification

For expression of SLIMP RNAi, SerRS2 RNAi, LON RNAi, SLIMP-FLAG and LON WT, 1μg of the respective pMK33 based vectors (Flybase: FBmc0003027) were transfected. pMK33 empty vector was transfected as a control. SLIMP with a different codon usage (SLIMPr) was designed and ordered with GeneArt – Thermo, digested with XhoI and SpeI restriction enzymes (New England Biolab) according to manufacturer's protocol and cloned into pMK33 (for transient expression) or pMT-puro (for stable

expression) vectors (Addgene) as indicated in each experiment. SLIMPr without the mitochondrial signal peptide (ΔN-SLIMPr) was amplified by PCR, digested with the same enzymes and ligated into the vectors. Ligation reactions were performed with equimolar PCR product and vector at 16ºC overnight, following manufacturer's instructions (T4 ligase – Fermentas). Oligonucleotides are listed in Table 1.

Plasmid preparation was performed with Minipreps according manufacturer's protocols (NZYTech). Six ml of *E. coli* cultures grown overnight with the appropriate selection antibiotic were used. Larger quantities of plasmid were obtained using the PureLink HiPure Plasmid Filter Maxiprep Kit (Invitrogen) according to manufacturer's protocol with 250 ml of *E. coli* culture grown overnight with the appropriate selection antibiotic.

For the identification of SLIMP protein interactors with BioID, SLIMP-BirA*-FLAG or BirA*-FLAG were PCR amplified and cloned into pMK33 plasmid in collaboration with Philip Knobel (Travis Stracker Lab), transfected and expressed in *Drosophila melanogaster* S2 cells as indicated in the BioID section below.

ΔN-SLIMP C-terminal HIS and ΔN-LON C-terminal Flag tagged or its separate domains, and ΔN-SerRS2 and ΔN-LON C-terminal Flag tagged, were cloned into pET-duet expression vectors (Merck: 71146-3) as a bicistronic product. ΔN-SLIMP or ΔN-SerRS2 were PCR amplified, digested with EcoRI and NotI enzymes (New England Biolab) and ligated with the pET-duet empty vector. Then, PCR amplified ΔN-LON or each separate subdomain were digested with NdeI and AvrII restriction enzymes and ligated with the pET-duet vector containing either SLIMP or SerRS2.

Oligonucleotides are listed in Table 1. For protein expression, BL21 (DE3) cells (Nzythech) were transformed. The starter culture was diluted 1/100 in LB media at 37ºC for 2 hours, and 2.5h hours at 37ºC in 1mM isopropyl β-D-1-thiogalactopyranoside (IPTG). Cell pellet was resuspended in lysis buffer (PBS, 1X protease inhibitor cocktail, and 1μg/ml DNAseI (Merck: 260913)) and lysed using cell sonication (15 seconds on 15 seconds off for 5 minutes at 3% - Branson sonifier SFX550). The lysate was centrifuged at 24,000g for 1 hour at 4ºC. The enzymes were purified using anti-FLAGM2-conjugated magnetic Dynabeads (Invitrogen) according to manufacturer's protocol with some minor modifications. Shortly, 20 packed gel beads per sample were equilibrated twice in TBS buffer (50 mM Tris-HCL, 150 mM NaCl, pH 7.4) and in the sample buffer, before incubating the sample for one hour at 4ºC in a rotating wheel. Beads were then washed, and the elution was performed in Protein Loading Buffer (PLB – 100mM Tris-HCl pH 6.8, 4% SDS, 0.1% bromophenol blue, 20% glycerol) at 60ºC for 5 min. The elution was analysed by SDS-PAGE and western blot.

For expression of SLIMP, SARS2, full length protein sequences fused to a Tandem Affinity Purification tag (TAP) were subcloned into the pLV vector (Lentiviral vector-CMV, SV40-Puromycin) for expression in HeLa cells. SARS2 and the TAP tag were PCR amplified from the laboratory available plasmids pDPV-9 and pDP-47 respectively. SARS2 PCR product was digested with XbaI and BamHI while TAP PCR product was digested with BamHI and SalI. pLV vector was digested with XbaI and SalI and ligated with the amplified genes. SLIMP-TAP was directly digested from the pDP-37 plasmid available in our laboratory, with XhoI and SalI enzymes, and ligated to the pLV multiple cloning site. HeLa cells were infected with lentivirus to produce stable cell lines expressing SLIMP-TAP, SARS2-TAP

or the TAP tag alone with the standard procedures. To produce the lentivirus, Hek293T cells were seeded in 10 cm plates to get 70% confluency the following day, when the medium was replaced, and cells were transfected with a mix of Envelope plasmid (pMD2G), the packaging plasmid (psPAX2) and our lentiviral plasmid of interest (pLV). The next day, the cell media was replaced, and the HeLa cells were seeded. Finally, the Hek293T medium was collected, filtered (0.45 μm) and added to the HeLa cells.
Stable cell lines produced in our laboratory for Federica Lombardi, with the shRNA for SARS2, and a scrambled non-targeting shRNA as a control were used to silence the gene (SARS2 shMISSION: TRCN0000045501, plKO.1 shSCR (Sigma)).

All plasmids were sequenced to confirm the presence of the correct inserted sequences in proper orientation and to ensure no additional mutations have been introduced to the plasmid during DNA manipulation. Sequencing reactions were performed by an external provider (GATC Biotech). Oligonucleotides used for sequencing are listed in Table 1.

Mitochondrial signal peptide identification

For mitochondrial signal peptide identification by mass spectrometry, samples were digested directly in polyacrylamide gel using three different enzymes for the three replicates: trypsin, Glu-C and Lys-C. Protein bands were reduced with DTT 10mM for 30 min at 56ºC and alkylated for 30 min in the dark with 55 mM iodoacetamide (IAM). Then, in-gel digestions were performed with trypsin (cleaves at lysin and arginine) and Lys-C (cleaves lysin) (0.1 μg/μL) in 50mM NH_4HCO_3 at 37ºC and Glu-C (cleaves at glutamic acids) (0.1 μg/μL) in 50mM NH_4HCO_3 at 25ºC overnight. The digestions were stopped by adding formic acid. Peptides were extracted with

100% acetonitrile (ACN) and completely evaporated. The bands were reconstituted in 15 μL 1% formic acid aqueous solution with 3% of ACN for MS analysis. Next, samples were loaded into strong cation exchange columns and peptides were eluted in 5% NH_4OH, 30% MeOH. Samples were evaporated to dry and reconstituted in 15 μL of 1% formic acid/3% ACN for MS analysis (performed by the mass spectrometry facility at IRB Barcelona).

LC-MS coupling was performed with the Advion Triversa Nanomate (Advion BioSciences, Ithaca, NY, USA) as the nano-electrospray ionization (nanoESI) source performing nanoelectrospray through chip technology. The Nanomate was attached to an Orbitrap Fusion Lumos™ Tribrid mass spectrometer and operated at a spray voltage of 1.6 kV and a delivery pressure of 0.5 psi in positive mode.

A database search was performed with Proteome Discoverer software v2.1 (Thermo) using Sequest HT search engine and contaminants database and protein SLIMP manually introduced. Search was run against targeted and decoy database to determine the false discovery rate (FDR). Search parameters included no enzyme, allowing for two missed cleavage sites, carbamidomethyl in cysteine as static modification; methionine oxidation and acetylation in N-terminal as dynamic modifications. Peptide mass tolerance was 10 ppm and the MS/MS tolerance was 0.6 Da. Peptides with a q-value lower than 0.1 and a FDR < 1% were considered as positive identifications with a high confidence level. Finally, the Percolator FDR node was used to estimate the number of falsely identified proteins among all the identified proteins.

For mitochondrial signal peptide prediction, three different online tools were used (Bannai et al., 2002; Fukasawa et al., 2015; Savojardo et al., 2015).

BioID analysis of proximity interactors

Stable S2 cell lines expressing BirA* or SLIMP-BirA* vector were created. Cell lines were seeded +/- 50 μM biotin (Panreac #143977), and 400 μM $CuSO_4$ during 24h. Cells were harvested, washed twice in PBS and lysed in modified RIPA buffer (150mM Tris-HCl pH 7.5, 150mM NaCl, 1mM EDTA, 1mM EGTA, 1% Triton X100, 0.1% SDS, protease inhibitor cocktail (Roche)) on ice.

Biotinylated proteins were isolated using streptavidin Dynabeads M-280 (Invitrogen) following manufacturer's instructions, washed three times in PBS and digested with trypsin directly in solution. LC-MS coupling was performed with the Advion Triversa Nanomate (Advion BioSciences, Ithaca, NY, USA) as the nanoESI source performing nanoelectrospray through chip technology. The Nanomate was attached to an Orbitrap Fusion Lumos™ Tribrid mass spectrometer and operated at a spray voltage of 1.6 kV and a delivery pressure of 0.5 psi in positive mode (performed by the mass spectrometry facility at IRB Barcelona).

For the quantitative analysis, contaminant identifications were removed and unique peptide spectrum matches of protein groups identified with Sequest HT were analyzed with SAINTexpress-spc v3.1(Teo et al., 2014). Control samples (BirA*) were compared to SLIMP-BirA* samples. High confidence interactors were defined with a SAINT score ≥ 0.7.

Gene Ontology analysis was performed selecting proteins with a fold change ≥ 1.5. A proportion test was used to compare the number of times each GO term in the list and the number of times each GO term appears in the whole proteome with a $p\ value < 0.01$.

Reverse transcription and quantitative real-time polymerase chain reaction (RT-qPCR)

Total RNA was extracted from cultured cells with TRIzol (Invitrogen). 500 ng of total RNA was retrotranscribed into cDNA using random primers (Reverse Transcription System, Promega-A3500) to perform quantitative real-time polymerase chain reactions (RT-qPCR) by means of Power SYBR Green and a StepOnePlus Real-time PCR System (Applied Biosystems) following manufacturer's instructions. Primers used are listed in Table 2. Standard curves were calculated for both primer pairs to ensure a high efficiency level. Fold expression changes were calculated using the 2-ΔΔCT method, where ΔΔCT is the sample ΔCT [CT average for target gene - CT average for the reference gene (Rp49)] - the control ΔCT [CT average for target gene - CT average for the reference gene (Rp49)]. The value obtained for control cells is represented as 1 and the other values are represented relative to it.

For mitochondrial DNA quantification, total DNA was extracted with TRIzol (Invitrogen) and was also quantified by real-time qPCR. Genomic DNA templates from S2 cells were amplified with primers designed to amplify the mitochondrial gene ATPase6, and the gene mRp110 used as a control for nuclear gene. Oligonucleotides are listed in Table 2.

Protein quantification and immunoblotting

Protein lysates were quantified by Pierce BCA Protein Assay Kit (Thermo Fisher Scientific) following manufacturer's instructions, and equal protein amounts were resolved on 10-12% polyacrylamide gels in Tris-glycine running buffer. Gels were transferred to polyvivylidene fluoride (PVDF)

membranes (Immobilon-P, Millipore) and blocked with 5% milk TBS-T for one hour at room temperature. Incubation with the appropriate dilution of the primary antibody was performed o/n at 4ºC and with secondary antibodies for 1h at room temperature. Antibody detection was performed by using enhanced chemiluminescent (ECL) system (Amersham), and exposure to X-ray film (Fujifilm) or captured by the Odyssey Infrared Imaging System (Li-Cor; Lincoln, NE). The antibodies used for proteins detection are listed in Table 3.

Immunofluorescence

For immunofluorescence experiments, cells were treated with 100 nm Mitotracker Red (Invitrogen-M7512) for 15 min, while coverslips were treated with 50 µl Concanavalin A (Sigma) at 0.5 mg/ml and placed into 12 wells plate. 500 µl of cells/well were rinsed once with PBS and incubated for 30 min in Schneider's media. Once the cells were attached to coverslips, culture media was aspirated and rinsed in PBS. To fix the cells, 300 µl 4% paraformaldehyde in PBS were added to each well and incubated for 15 min at room temperature. Cells were then rinsed in PBS, incubated for 20 min in permeabilization buffer (PBS, 0.3% Triton X100, 0.2% Bovine Serum Albumin (BSA)) and incubated with primary antibodies at 1:500 in the same buffer overnight at 4ºC. Cells were then washed three times in the permeabilization buffer and incubated with fluorophore-conjugated secondary antibody at 1:400 for 1 h at room temperature and protected from light. Cells were washed twice with 1 ml PBS-0.3% Triton X100 and twice in PBS. For nuclear staining, cells were incubated 5 min with 4',6-diamidino-2-phenylindole (DAPI) in PBS at 0.04 ng/µl and rinsed twice in PBS. Coverslips were mounted on slides in 5 µl Mowiol (Merck) and stored

overnight at room temperature before analysis. Images were acquired with Leica TCS SP5 MP confocal laser-scanning microscope and processed using Fiji software.

In vivo labelling of mitochondrial translation products

Cells were harvested at room temperature and washed twice with methionine-free Grace's insect medium (Gibco) supplemented with 10% FBS, 200 μg/ml emetine, and 100 μg/ml cycloheximide, to inhibit cytosolic translation. Control sample was treated with chloramphenicol (100 μg/ml) to also inhibit mitochondrial translation. Five minutes after cell resuspension, EasyTag L-35S-methionine (Perkin Elmer, NEG709A005MC) was added to a final concentration of 200 μCi/ml, and the cells were incubated for 3h at 25°C. After incubation, the cells were diluted with 2 volumes of Schneider Medium, and washed twice with PBS.

Cells were lysed in RIPA buffer. Total cellular protein (50 μg per lane) was separated by SDS-PAGE. Gels were transferred to polyvivylidene fluoride (PVDF) membranes (Immobilon-P, Millipore) at 250 mA for 90 minutes at 4ºC in transfer buffer. The membrane was dried 30 minutes at room temperature, exposed to a Storage Phosphor Screen (Molecular Dynamics) for 15 days, and imaged using a Typhoon 8600 Variable Mode Imager (Molecular Dynamics).

LON protease activity assay

Stable S2 cells expressing SLIMP, SerRS2 or LON RNAi, SLIMP or LON-overexpression and control (empty vector) were induced for eight days in $CuSO_4$, collected and washed with PBS. Cell pellet was resuspended in ice-

cold Cell Buffer (225 mM mannitol, 75 mM sucrose, 0.1 mM EGTA, 30 mM Tris-HCl, pH 7.4), and homogenized using a tight douncer (25 strokes). The homogenate was centrifuged at 300g for 5 minutes at 4ºC, the supernatant was collected in a new Eppendorf, and centrifuged at 6000g for 10 minutes at 4ºC. The mitochondrial pellet was washed twice in Wash Buffer (225 mM mannitol, 45 mM sucrose, 10 mM KCl, 10 mM Tris-HCl, 5 mM KH_2PO_4, pH 7.4), and the final pellet was resuspend in Reaction Buffer (50 mM HEPES pH 8,5 mM $Mg(OAc)_2$, 2 mM DTT, 5 mM imidazole) and quantified as indicated in protein quantification section.

Monitoring of the specific LON protease activity was performed as previously reported (Fishovitz et al., 2011). FRETN 89-98Abu was synthesised according to the published protocols (Fishovitz et al., 2011) by the Unit 3 of the CIBER in Bioengineering, Biomaterials & Nanomedicne (CIBER-BBN) at the Barcelona Scientific Park (PCB). Reactions were performed in black 96 well assay plates (Costar) in 200 µl Reaction Buffer, 1 mM ATP, 100 µM FRETN 89-98Abu, and 35 µg of isolated mitochondria. The fluorescent emission (420 nm) was monitored during 3 hours by Infinite plate reader (Tecan).

5-bromodeoxyuridine (BrdU) pulse-chase assay

S2 cells were incubated for one hour with 100 µM BrdU (BD Pharmingen #550891), and the excess BrdU was removed by two washes with PBS. Cells were resuspended in Schneider's *Drosophila* medium for 24 hours, aliquots were taken every two hours in 70% cold ethanol and stored at -20ºC until the day of the analysis. Cell aliquots were washed in PBS 0.5% BSA, and cell pellets were resuspended 2M HCl for 20 minutes at room temperature. Cells were washed again in PBS 0.5% BSA before resuspension in 0.1 M sodium borate (pH 8.5) for 2 minutes at room temperature. Another wash was

performed, and cells were incubated with an antibody against BrdU (FITC Mouse Anti- BrdU Set, BD Pharmingen) for 20 minutes.

Samples were analysed using a Gallios multi-colour flow cytometer instrument (Beckman Coulter, Inc, Fullerton, CA) set up with the 3-lasers 10 colours standard configuration. Excitation was done using a blue (488nm) laser. Forward scatter (FSC), side scatter (SSC), red (620/30nm) fluorescence emitted by propidium iodide (PI) and green fluorescence for FITC were collected. Aggregates were excluded gating single cells by their area vs. peak fluorescence signal. Proliferating cells were gated on a PI vs FITC dot plot according to its green fluorescence. Cell cycle was analysed using FlowJo Software (FlowJo).

Cell cycle analysis

Cells were collected, washed with PBS and fixed in 70% ice-cold ethanol for at least 2 h. Cells were permeabilized with PBS containing 0.25% Triton X100, and incubated at 37ºC for 30 minutes in PBS containing 40 μg/ml RNase A (Sigma) and 1 μg/ml PI (Sigma). Flow cytometry experiments were carried out using an Epics Cyan ADP flow cytometer (Beckman Coulter, Inc, U.S). The instrument was set up with the standard configuration. Excitation of the sample was done at 488nm. FSC, SSC and red (613/20 nm) fluorescence for PI were recorded. PI fluorescence was projected on a monoparametrical histogram. Aggregates were excluded gating single cells by their area vs. peak fluorescence signal. Time was used as a control of the stability of the instrument. Histograms were analysed using Multicycle Software (Phoenix).

Sorting of cell cycle populations was performed by flow cytometry using a FacsAria Fusion sorter (Beckton Dickinson, San Jose, California). Scatter parameters were obtained from a blue (488nm) laser; red (582/15) fluorescence from propidium iodide was used to exclude dead cells, and cell cycle from live cells stained with Vybrant® DyeCycle™ Violet Stain (Thermofisher) was obtained using a violet (405nm) laser for excitation and collecting the blue emission (450/50nm). For fixed and permeabilized cells, PI was used to define cell cycle. Red (613/20 nm) fluorescence was projected on a monoparametrical histogram. Single cells were gated according to the fluorescence area-peak signal.

For mitotic cells detection, cells were fixed in 70% ice-cold ethanol overnight, washed twice in PBS, and incubated in blocking solution (0.25% Triton X100, 0.5% BSA in PBS) for 15 minutes. Cells were washed in PBS 0.5% BSA prior to the incubation with the H3 antibody for 2h. Two additional PBS 0.5% BSA washes were performed. The secondary antibody Alexa-488 was incubated for 30 minutes at room temperature. Two washes were performed before cell cycle analysis with propidium iodide (as indicated above). Cell cycle was analysed using FlowJo Software (FlowJo).

For cell cycle recovery samples, SLIMP knockdown cells were transfected with a plasmid containing a gene coding for SLIMP with a different codon usage (SLIMPr), SLIMPr without the mitochondrial signal peptide (ΔN-SLIMPr), or the pMK33 empty vector; cotransfected with another vector encoding for Green Fluorescent Protein (GFP) with the actin promoter (gift from Dr. F. Azorín Lab). Flow cytometry experiments were carried out using a FacsAria Fusion sorter (Beckton Dickinson, San Jose, California). Scatter parameters were obtained from a blue (488nm) laser; green (530/30) fluorescence from GFP was collected from live cells. GFP positive and

negative cells were sorted and collected in ice-cold 70% ethanol. Cell cycle was analysed with propidium iodide as previously described.

For nucleosides incubation and cell cycle analysis, cells were plated, induced for seven days with $CuSO_4$ and divided in two different flasks for treated (Embryomax Nucleosides mix 100x (Merck)) or non-treated cells. Cells were incubated for 24 hours and collected in ethanol for cell cycle analysis.

Flow cytometry-based assays for ROS detection

To detect mitochondrial ROS production, cells were incubated at 25 °C for 30 min in 5μM MitoSox (Molecular Probes, M36008). To detect total cellular superoxide, cells were incubated in 5μM dihydroethidium (DHE) (Invitrogen) for 30 min at room temperature. Cells were then washed once with PBS and immediately analysed by flow cytometry. Data were collected with a Gallios flow cytometer using Kaluza for Gallios software (Beckman Coulter). For analysis, FSC, SSC and red (613/20 nm) fluorescence were recorded and the mean of all the events was collected. A negative control without MitoSox or DHE, as well as a positive control with cells treated with 50 μM antimycin were used to determine the gating strategy.

S2 and HeLa cell cycle synchronization

Induced S2 cells were seeded at 0.5 x 10^6 cells/ml, and next day, cells were synchronized in G1 cell cycle phase with 0.5 mM hydroxyurea (Sigma) for 24 h. Cells were rinsed three times in PBS and plated in a new flask. At the collection times, cells were centrifuged and stored in 70 % cold ethanol for cell cycle analysis.

For HeLa cell cycle synchronization, cells were plated at low confluency, washed with PBS and grown in the presence of 2 mM thymidine for 18 h. After the first block thymidine was removed, cells were washed and grown in fresh medium for 9 h to release cells from the block. The release was followed by the second block by the addition of 2 mM thymidine and cultivation for 17 h. Cells were rinsed twice in PBS and collected at each time point in 70% cold ethanol for cell cycle analysis.

Gene expression analysis

RNA from 25,000 cells was isolated using magnetic beads. cDNA synthesis, library preparation, and amplification were performed as previously described (Gonzalez-Roca et al., 2010). The cDNA generated by reverse transcription from each sample was added to an amplification mix and the cDNA:mix was divided in 3 equivalent parts for PCR amplification. A sample without RNA, sample "0", was included in the amplification experiment. Amplification was performed for 15 cycles. Subsequently, cDNA was purified with a PureLink Quick PCR Purification Kit (Invitrogen), and eluted in 40 µl. cDNA concentration was determined using the Nanodrop 1000 spectrophotometer. Samples were processed with WTA2 (Sigma) method, and hybridized with GeneChip *Drosophila* Genome 2.0 (Affymetrix).

Affymetrix arrays were normalized using RMA background correction and summarization (Irizarry et al., 2003) as implemented in the "affyPLM" package (Bolstad et al., 2004) from the R statistical framework (R Development Core Team, 2008). Annotations for the GeneChip Drosophila Genome 2.0 array were downloaded from Affymetrix. Computation of *p*-values was performed through moderated t-statistics by empirical Bayes shrinkage, as implemented in the limma package (Ritchie et al., 2015). The biological replicate was included in the model as covariate.

DNA damage

Cells were plated and kept at low confluency (<1 x 10^6 cells/ml) during induction. Two different plates were seeded from the same cell culture. One of the plates was used as a positive control and was irradiated for 10 min at 10 Gy by using X-Ray Smart 200 (YXLON). Cells were then collected and lysed in RIPA buffer for western blot analysis to detect Histone H2Av.

Cell viability test: WST-1

WST-1 provides an accurate assay to measure cell viability. The WST-1 assay protocol is based on the cleavage of the tetrazolium salt WST-1 to formazan by cellular mitochondrial dehydrogenases. Cells were seeded at a concentration of 1.2 x 10^4 cells/well in 100 µl Schneider's medium and incubated for 30 min at 25ºC. 10 µl of Cell Proliferation Reagent WST-1 was added to each well and incubated at 25ºC for 2 h. Absorbance was measured at 450 nm with a reference wavelength at 630 nm with BioTek ELx800 microplate reader.

Mitochondrial respiration calculation by Seahorse technology

Mitochondrial respiration was measured as previously reported (Meng et al., 2017) with minor modifications. At least 12 h before use, 200 µl of XF calibrant was added to each well of the 24 well utility plate and place at 25ºC. S2 cells were grown and induced to overexpress (SLIMP, SLIMPr or ΔN-SLIMPr) or deplete (SLIMP or SerRS2) for eight days, counted and diluted to 2x10^6 cells/ml in serum-free Schneider's *Drosophila* medium. 100 µl of diluted cells were plated in XF24 cell culture microplates previously coated

with concanavalin A. The microplate was then centrifuge at 200 g for 1 min without breaking system and incubated at 25ºC for 30 min. 500 µl of serum-free medium was added to each well and incubated 5 more minutes.
Oligomycin was used as the inhibitor of the ATP synthase, carbonyl cyanide-4-(trifluoromethoxy) phenylhydrazone (FCCP) as an uncoupling agent, and the combination of antimycin and rotenone to inhibit electron transport chain. During plate incubation, compounds (oligomycin at 5µM, FCCP at 20 µM and antimycin and rotenone at 50 µM) were loaded for calibration of the cartridge sensor and loaded into the Seahorse Analyser's tray. MitoStress assay was performed according to the manufacturer's protocol. Oligomycin concentration was set up by a calibration curve experiment.

Statistical analyses

Statistical analyses were performed using GraphPad Prism software version 6.0 (GraphPad Software). Data is shown as the mean ± standard deviation (SD). Two-tailed t-test was performed when comparing two groups with normal distribution. ANOVA test was used when comparing more than two groups, followed by a Dunnett multiple comparison.

Table 1: Oligonucleotides used for protein cloning. All the primers were ordered from Sigma.

Gene/target	Purpose	Forward (5'-3')	Reverse (5'-3')
SLIMP DCU	Cloning SLIMP with different codon usage into the pMK33 vector	CAGTCTCGAGATGTTGAGCCTG	TCCACGTTTAAACTTCAGGTAAAC
SLIMP ΔN-DCU	Cloning ΔN-SLIMP with different codon usage into the pMK33 vector	ATCGCTCGAGATGATCTCCGCGCTGTA	TCCACGTTTAAACTTCAGGTAAAC
SLIMP-HIS	Cloning SLIMP -HIS tagged into the pET-duet vector	TTAGAATTCATGGATAAAGCGAACGAAAACTATGTG	CTAGCGGCCGCTTAGTGGTGATGATGGTGATGGCTCGTGAAAAGG
LON-FLAG	Cloning LON-FLAG tagged into the pET-duet vector	TTTCATATGATGAAAGACGACAAGGATGCCAT	TTTGGTACCTTACTTGTCATCGTCGTCCTTGTAGTCCTCGCCTTCTTTTTTGA
LON-SBD-FLAG	Cloning substrate binding domain (SBD)-FLAG tagged into the pET-duet vector	TATCATATGAGCCGCAAGCGGGATGATTCC	TATGGTACCTTACTTGTCATCGTCATCCTTGTAGTCTTTTTCGATGCC
LON-AAA-FLAG	Cloning ATPase domain (AAA)-FLAG tagged into the pET-duet vector	TATCATATGAAAGACGACAAGGATGCCATTG	TATGGTACCTTACTTATCATCGTCATCCTTATAGTCCTCGCCTTCTTTTTTGAC
LON-PROT-FLAG	Cloning proteolytic domain (PROT)-FLAG tagged into the pET-duet vector	TTTCATATGATGCACTTTCCGGTTAACGCTGA	TTTGGTACCTTACTTGTCATCGTCGTCCTTGTAGTCCTCGCCTTCTTTTTTGA
SerRS2	Cloning SerRS2 into the pET-duet vector	CACACAGAATTCATTAAAGAGGAG	ATTGCGGCCGCAGCTTAGTGATGG
SARS2	Cloning human SARS2 into pLV vector	GTTCCTCTAGAAAGATGGCTG	AAAAGGATCCGCTTACAGCAGGCTGGCC

TAP tag	Cloning tap tag into plv vector	CATGGTCGACTAGAACTAGAGCTTCAG	AAAAGGATCCAGTATGGAAAAGAGAAGATGG
pMK33 sequencing	Vector MCS sequencing	TTGTGGTCAGCAGCAAAATC	CCCGGAGGATGAGATTTTCT
pMK33 sequencing	Vector MCS sequencing	CTGAAACATAAAATGAATGC	GGAAGACTGCAAACTTTTGG
pMT sequencing	Vector MCS sequencing	TGTAAAACGACGGCCAGT	CATCTCAGTGCAACTAAAG
pMT sequencing	Vector MCS sequencing	GTGGTTTGTCCAAACTCATC	TCCACGTTTAAACTTCAGGTAAAC
pET-duet sequencing	Vector MCS1 sequencing	ATGCGTCCGGCGTAGA	GATTATGCGGCCGTGTACAA
pET-duet sequencing	Vector MCS2 sequencing	TTGTACACGGCCGCATAATC	GCTAGTTATTGCTCAGCGG
pLV sequencing	Vector MCS sequencing	CTTTCCGCCTCAGAAGG	TTCCTGGCCACCGTCGG

Table 2: Oligonucleotides used for RT-qPCR. All the primers were ordered from Sigma.

Gene/target	Purpose	Forward (5'-3')	Reverse (5'3')
SLIMP	RT-qPCR	GGCGATAAAGCGAACGAAAAC	AAAAATTGCCGCTCTCCAAA
Rp49	RT-qPCR	TGCCCACCGGATTCAAGA	AAACGCGGTTCTGCATGAG
SerRS2	RT-qPCR	CCGTTCTGCGACCATTCAT	CAGCTTCGTCTCCGGTATCC
RBF	RT-qPCR	TAAATGGCGCAGCACATCCA	ACATGGATCGGCAGACAGAG
dE2F1	RT-qPCR	CATCCGTTGACCAACCAG	TTATATTCAGGCTGGGACTGC
dE2F2	RT-qPCR	GGAGCAGTGTCTGCCCTTAT	CTCACTGGTCCTGCTCACAC
dDP	RT-qPCR	GGACACGGATGCGGATGG	GTGCGGCTCCTGACTAACC
CyclinB	RT-qPCR	GTTTGGTCAGCGACTTCTTCG	CCGTTCCGCCCAAGGTC
ATPase6	RT-qPCR	CCCGCTATTCTTATACCTTTTATAGT	TGTCCAGCAATTATATTAGCAGTTA
p38c	RT-qPCR	GGAGTTCGTGAGAGTGGCAA	AGTGCCTCGTAGTCTCACCT
mRpl10	RT-qPCR	TCGAACAGGCGGTGAAGAA	TGCAATGATTGGAGTGGAACA

Table 3: Antibodies used for western blot analysis.

Antibody	Source	Cat. number
Anti-DmSLIMP	Ribas Lab	N/A
Anti-DmLON	Kaguni's Lab	N/A
Anti-DmSerRS2	Ribas Lab	N/A
Anti-FLAG	Sigma-Aldrich	Cat. #F3165
Anti-βATPase	Ribas Lab	N/A
Anti-VDAC/porin	Abcam	Cat. #ab14734
Anti-TFAM	Kaguni's Lab	N/A
Anti-His	Abcam	Cat. #ab18184
H2Av	Rockland	Cat. #600-401-914
Histone H3p	Merck	Cat. #06-570
Lamin A	DSHB	Cat. #ADL67.10
MCM5	Coteril's Lab	N/A
MCM2	Coteril's Lab	N/A
PCNA	Santa Cruz	Cat. #sc-56
ORC2	Coteril's Lab	N/A
ORC5	Coteril's Lab	N/A
Cdc6	Coteril's Lab	N/A
E2F1	Everest	Cat. #EB12261
Cyclin B	DSHB	Cat. #F2F4
Cyclin E	Santa Cruz	Cat. #d-300
Chicken HRP	Chemicon International	Cat. #AP194P
Mouse HRP	Amersham	Cat. #NA931
Rabbit HRP	Amersham	Cat. #NA934
Mouse Alexa 488	Invitrogen	Cat. #A21202
Rabbit Alexa 488	Invitrogen	Cat. #A11008

RESULTS

Chapter 1: SLIMP localization and cellular environment

In collaboration with: Alba Pons, Alba Serrano, Philip Knobel and Marina Gay.

1.1 SLIMP contains a mitochondrial signal peptide

The Seryl-tRNA-synthetase Like Insect Mitochondrial protein (SLIMP) was previously described as a mitochondrial localized protein (Guitart et al., 2010) and online mitochondrial signal peptide predictors indicated theoretical cleavage sites upon mitochondrial import (Figure 16). TPpred 2.0 (Savojardo et al., 2015) proposed a cleavage site between asparagine-21 and isoleucine-22 with a score of 0.65. MitoFates (Fukasawa et al., 2015) predicted the cleavage site after serine-19 with a score of 0.956 of presequence provability. Finally, iPSORT (Bannai et al., 2002) predicted that the mitochondrial signal peptide was larger, and the cleavage site was after aspartic acid 30.

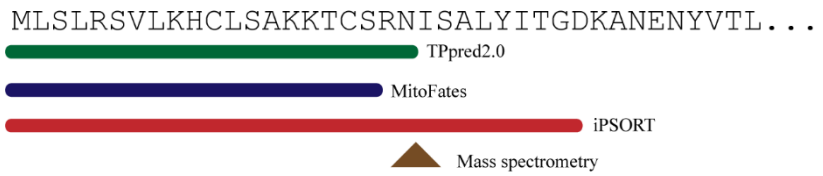

Figure 16| SLIMP mitochondrial signal peptide. Amino acid sequence of the N-terminal site of SLIMP, with the mitochondrial signal peptide predictions indicated below. TPpred2.0 prediction is shown in green, MitoFates calculation in blue and iPSORT in red. Mass spectrometry detected cleavage site is shown with an arrow in brown.

Mass spectrometry analysis allowed us to determine the exact sequence of the mitochondrial targeting peptide (Figure 16). We run crude S2 wild type cell extracts in an SDS-PAGE, purified the band section that corresponds to the SLIMP molecular weight (around the molecular weight marker of 48kDa – NZYTech protein marker II) and directly digest with the enzymes Glu-C, Lys-C or Trypsin. With these digestions we detected the N-terminal peptide starting from isoleucine-22, that is a not a cleavage site for any of the enzymes (Supplementary figure 1 and supplementary table 1). Thus, we assigned this cleavage site to the natural protease activity and we defined the mature mitochondrial sequence of SLIMP.

Immunofluorescence assays confirmed that endogenously expressed SLIMP is mostly co-localizing with mitochondria (Figure 17a). In order to ensure antibody specificity, we used SLIMP-depleted cells as a control (Figure 17b). Immunofluorescence in S2 cells overexpressing the full length SLIMP confirmed the mitochondrial co-localization (Figure 17c), while SLIMP without the mitochondrial signal peptide (ΔN-SLIMP) was overexpressed outside the organelle (Figure 17d). This result indicated that the N-terminal region of SLIMP represented the mitochondrial signal peptide and was necessary for the protein import.

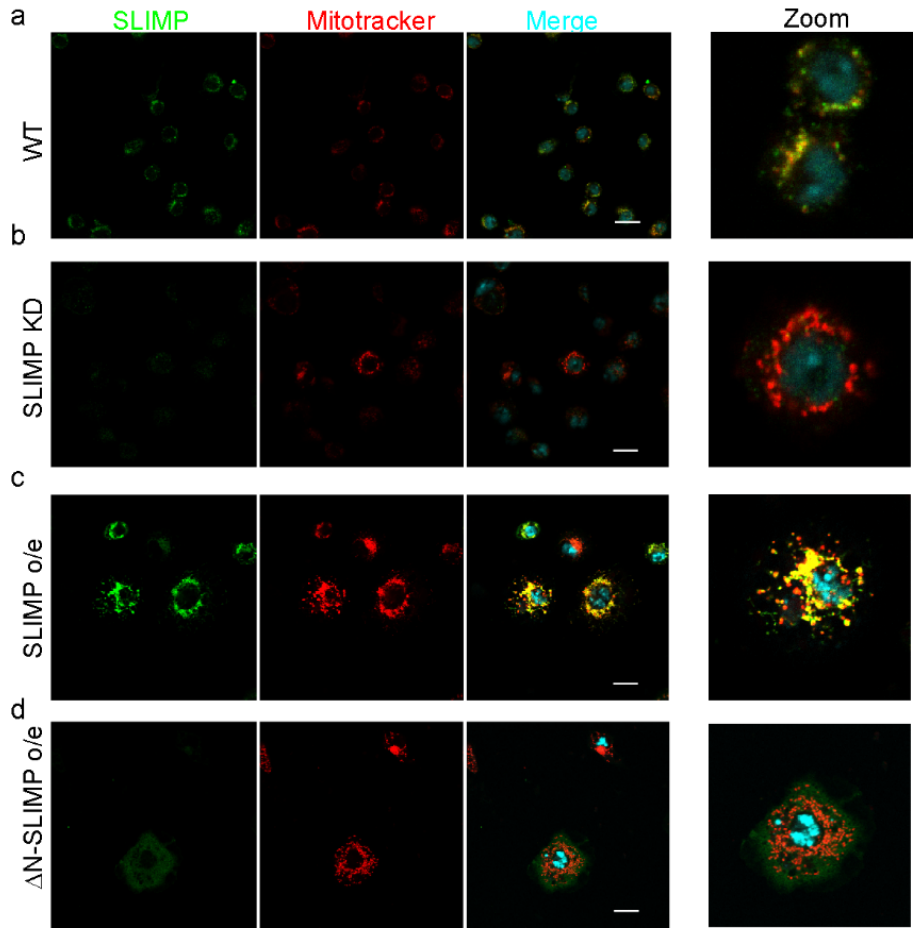

Figure 17| SLIMP cellular localization. Representative immunofluorescence analysis of (a) wild type (WT), (b) SLIMP-depleted (SLIMP KD), (c) SLIMP-overexpressed (SLIMP o/e) and (d) ΔN-SLIMP-overexpressed cells (ΔN-SLIMP o/e). SLIMP was detected with α-SLIMP antibody and Alexa Fluor-488 secondary antibody (in green). Mitochondria were detected using Mitotracker Red and nucleus was stained with DAPI. The merge of the different channels showed the green and red channels colocalization (in yellow), indicating that most of SLIMP (a, c) localized in the mitochondria, and SLIMP expressed without the signal peptide (d) was localized outside the mitochondria. Zoom to a single cell is shown and scale bar corresponds to 10 μm.

1.2 SLIMP is localized in the mitochondrial RNA granules

Considering that SLIMP has been described in our laboratory to be a mitochondrial protein and to interact with two mitochondrial proteins (SerRS2 and LON), we were next interested to address SLIMP cellular environment. Thus, we performed a BioID analysis by fusing the modified biotin ligase BirA* to the C-terminal site of SLIMP. Biotin gets incorporated into the SLIMP vicinity proteins through the action of BirA* and we analysed the streptavidin pulled-down proteins by mass spectrometry. First, we performed expression test that showed that the fusion protein was mainly expressed in mitochondria, while the BirA* alone expressed in control cells was distributed in all the cellular compartments (Figure 18).

BioID results confirmed previously defined SLIMP protein interactors, such as SerRS2 or LON protease (Figure 19). To identify the possible contaminants and quantitatively determine the significance of protein interactors, we analysed the results using SAINTexpress (Teo et al., 2014). SLIMP was shown to be the more significant detected protein compared to control cells, with a SAINT score of 1 and a fold change of 387.27. SerRS2 was also significantly increased in the SLIMP-BirA* pull-down with a SAINT score of 1 and a fold change of 47.27, and LON protease was detected with a score of 0.71 and a fold change of 10.64 (Supplementary table 2). Many of the proteins detected in the BioID were uncharacterised proteins in *Drosophila melanogaster*.

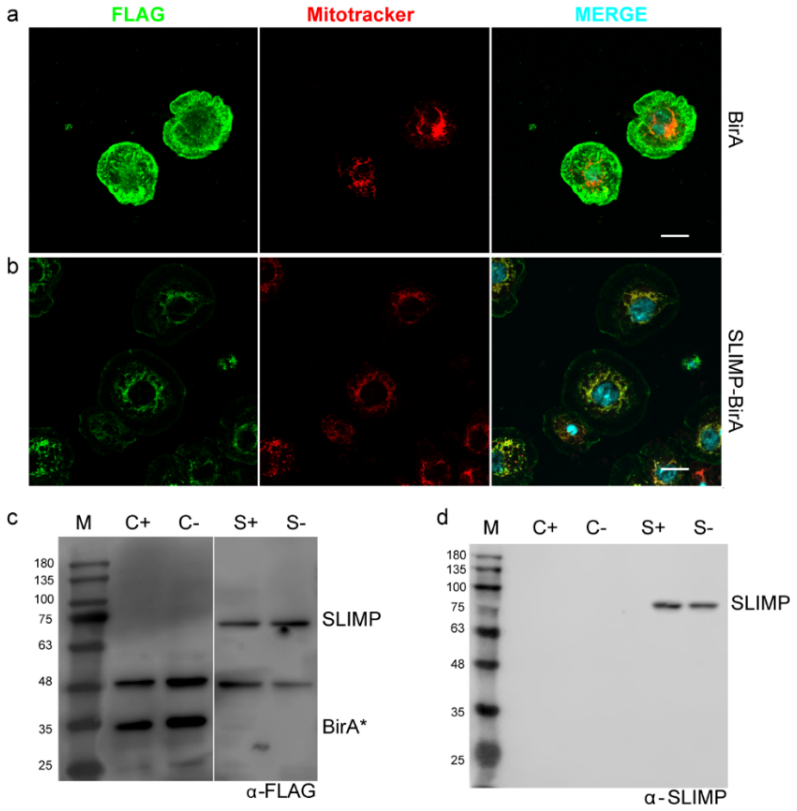

Figure 18| SLIMP-BirA* expression test. (a) Immunostaining of BirA* overexpressing S2 cells localised in all the cellular compartments. (b) SLIMP-BirA* overexpressing cells immunostaining. FLAG antibody was used to detect BirA* alone or fused to SLIMP, with a secondary Alexa Fluor-488 (in green). Mitochondria was visualized by the incubation with Mitotracker red (in red) and nucleus with DAPI (in blue). Scale bar 10 μm. (c) Expression test of control cells with the BirA* alone (C) and SLIMP-BirA* cells (S), incubated for 24h in $CuSO_4$ and with (+) or without (-) streptavidin, detected with FLAG antibody. (d) Western blot with the SLIMP antibody to identify SLIMP-overexpression.

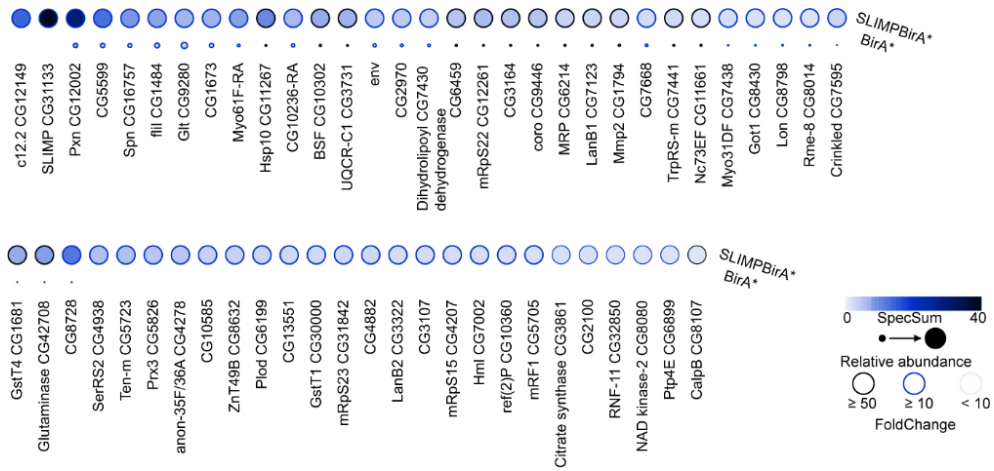

Figure 19| BioID results. Graphical representation of SLIMP-BirA* interactors list with a SAINT score >0.7. Average spectrum sum and fold change is represented.

To further understand the SLIMP interactome, we performed gene ontology analysis from each of the enriched proteins in the SLIMP-BirA* pull-down with a fold change ≥ 1.5. We identified mitochondrial proteins that belong to the mitochondrial translation apparatus (Figure 20), e.g. ribosomal proteins such as mRpS22/23/27 or mRpS15 (*bonsai*), as well as mRF1 translation release factor or aminoacyl tRNA synthetases such as SerRS2 or TrpRS2. We also identified mitochondrial matrix proteins like the dihydrolipoamide acetyltransferase component of pyruvate dehydrogenase complex, the ubiquinol-cytochrome c reductase core protein 1 (UQCR-C1) or one of the mitochondrial presequence protease (PITRM1). Altogether these results indicated that SLIMP resides in the vicinity of the ribosome granules in the mitochondrial matrix.

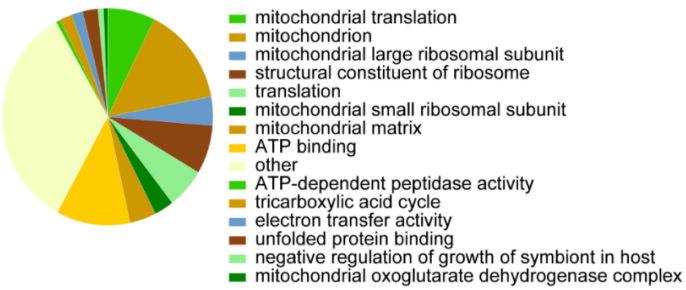

Figure 20| BioID gene ontology. Gene ontology categories of the proteins with a fold change ≥ 1.5 between control and SLIMP-BirA* samples. Mitochondrial translation and ribosomal granule categories are highly represented. The category named "other" corresponds to unfolded protein binding, negative regulation of growth of symbiont in host, mitochondrial oxoglutarate dehydrogenase complex, early endosome membrane, positive regulation of endocytosis, mitochondrion morphogenesis, GTP binding and NADH dehydrogenase activity.

Additionally, we analysed the cellular compartment of each of the higher ranked proteins (SAINT score ≥0.7) by manual annotation. Surprisingly not all the identified peptides were described as mitochondrial. We identified nuclear proteins such as zinc transporter 9 or NIF3L1, a transcriptional corepressor that was described to negatively regulate the expression of genes involved in neuronal differentiation (Figure 21) (Akiyama et al., 2003; Perez et al., 2017). We also detected proteins described as cytosolic, such as protein flightless-1 (Lee et al., 2004), myosin-6 (Jung et al., 2006; Vreugde et al., 2006), or the glutathion S-transferase (Saisawang et al., 2012). These results suggested that SLIMP might be also present outside mitochondria.

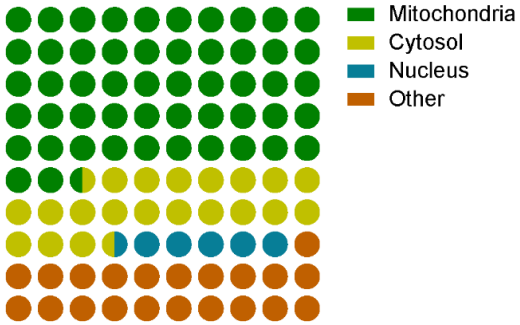

Figure 21| SLIMP proteins partners subcellular localization. Analysis of cellular localization of the proteins detected with a SAINT score ≥0.7. Mitochondrial proteins represented the 53 %. We also detected cytosolic (22 %) and nuclear (5 %) proteins. Other compartments represent membrane and extracellular proteins (20 %).

Chapter 2: Mitochondrial function of SLIMP/ SerRS2 heterodimer

In collaboration with: Joana Silva and Juan Pablo Muñoz.

2.1 Mitochondrial SLIMP and SerRS2 protein levels are interdependent

To evaluate whether overexpression of mitochondrial SLIMP or extramitochondrial SLIMP could rescue SerRS2 protein levels we design an SLIMP transcript with a different codon usage in the sequence recognised by the RNAi (SLIMPr). Then, we transfected and selected stable cell lines to express SLIMPr in SLIMP-depleted cells. We first checked protein levels by western blot and protein localization by immunocytochemistry. Protein expression analysis showed that SLIMP-FLAG levels were higher than SLIMPr, suggesting that the codon usage was affecting transcript stability or translation efficiency. SLIMP without mitochondrial signal peptide (ΔN-SLIMPr) was little expressed possibly due to a tightly regulated or less stable SLIMP outside the mitochondria (Figure 22).

Moreover, we confirmed previous results from our lab where it was shown that SLIMP and SerRS2 protein levels are interdependent. SerRS2 protein levels were increased in the SLIMP and in the recued SLIMPr overexpressing cells, while in SLIMP-depleted and the rescued ΔN-SLIMP-overexpressing cells, SerRS2 protein levels were not increased. These results confirmed that the heterodimer stability is taking place inside the mitochondria.

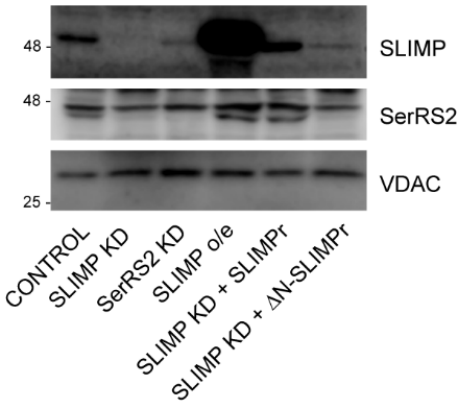

Figure 22| SLIMP and SerRS2 protein expression. Immunoblot analysis of SLIMP and SerRS2 protein levels. Representative western blot is shown. VDAC was used as a loading control. In SLIMP-depleted cells a decrease in SerRS2 levels is observed that could be rescued with the expression of SLIMP and SLIMPr but not with ΔN-SLIMPr in a SLIMP-depleted context.

We next performed immunocytochemistry analysis and observed that full length SLIMPr and ΔN-SLIMPr were expressed in SLIMP-depleted cells (Figure 23). The results confirmed that SLIMP expression was mostly mitochondrial for SLIMPr and non-mitochondrial in ΔN-SLIMPr cells.

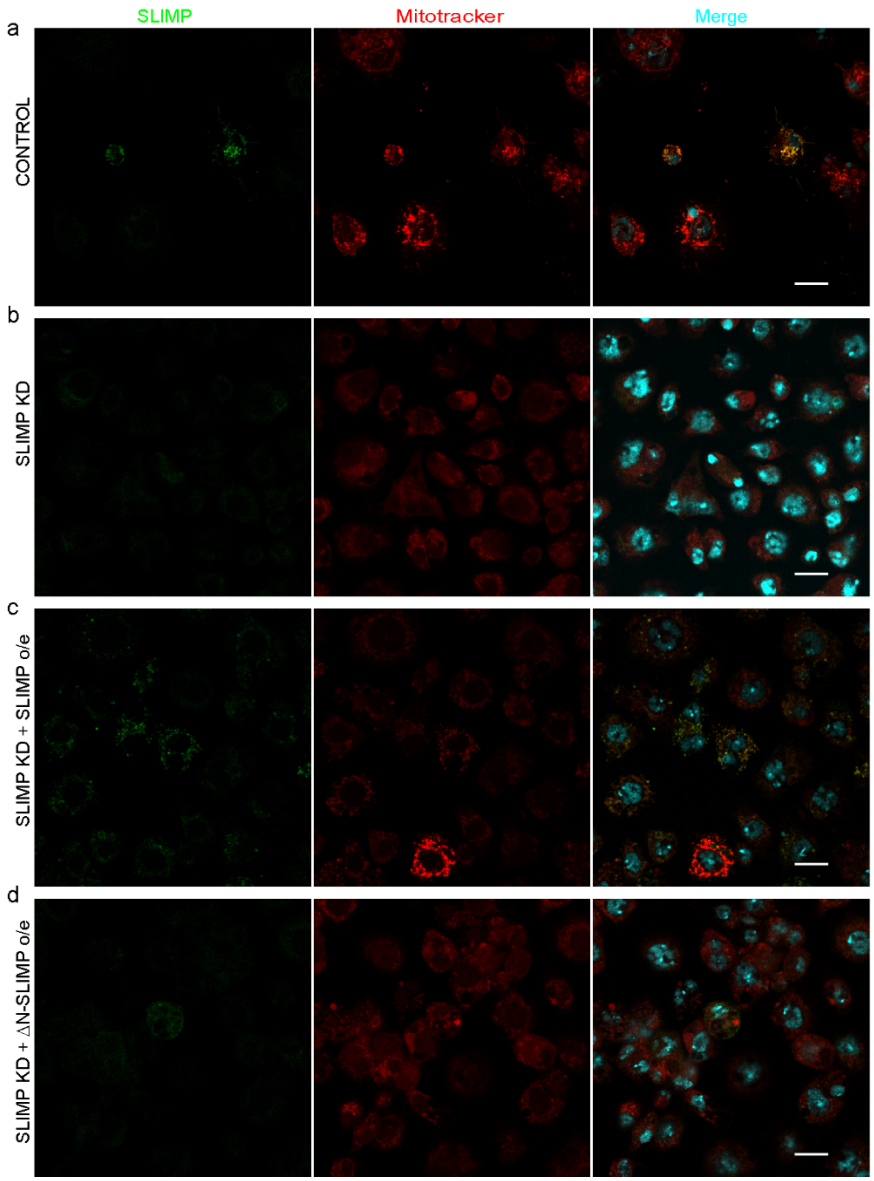

Figure 23| SLIMPr and ΔN-SLIMP subcellular localization. Representative immunocytochemistry analysis of control (empty vector), SLIMP-depleted (SLIMP KD) and the rescued SLIMP KD with SLIMPr or ΔN-SLIMP-overexpression. SLIMP was detected with α-SLIMP antibody and Alexa488 secondary antibody (in green), mitochondria were detected by using Mitotracker Red and nuclei were stained with DAPI (in blue). Scale bar corresponds to 10 μm.

2.2 SLIMP/SerRS2 heterodimer is essential for mitochondrial protein translation

It was previously shown in our group that SLIMP and the homologous protein SerRS2 are forming heterodimers and we also confirmed in the previous section that their protein levels are interdependent. Keeping in mind that both proteins are needed for the aminoacylation reaction, we tested the effect of SLIMP/SerRS2 heterodimer depletion on mitochondrial translation. We performed *in vivo* labelling of mitochondrial translation products in S2 cells, with SLIMP or SerRS2 knockdown cells (Figure 24a). Induced S2 cells were cultured in Schneider's media without methionine before performing a pulse of radiolabelled methionine. Control cells without any treatment did not show any clear band due to the high number of cytosolic and mitochondrial translated products that run as a smear of proteins. As a negative control, cells were incubated with chloramphenicol to inhibit cytosolic and mitochondrial translation. In order to visualize only the mitochondrial proteins, we incubated all the samples with emetine and cycloheximide to inhibit cytosolic translation. The mitochondrial proteins translated during the pulse time incorporated the radiolabelled methionine and were visualized in a Storage Phosphor Screen.

The results from pulse-labelling experiments showed that SLIMP/SerRS2 heterodimer was essential for mitochondrial protein translation, which was reduced 56.22±8.5 % in SLIMP-depleted cells and 50.15±6.5 % in SerRS2 knockdown cells (Figure 24b), as estimated by the quantification of the COX1/ND4 band to VDAC/porin rations in western blot.

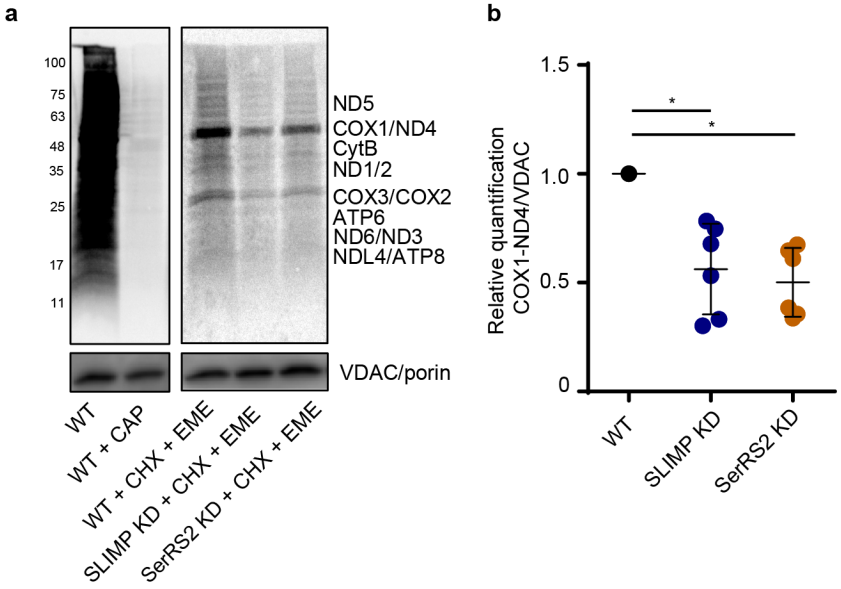

Figure 24| *In vivo* labelling of mitochondrial translation products. SLIMP and SerRS2 levels affected mitochondrial translation. (a) Phosphorimager images of S35 labelled mitochondrial translation products separated by SDS-PAGE and blotted to PVDF membranes are shown for the indicated cell lines. Untreated control cells (WT) and treated with chloramphenicol (WT+CAP) were evaluated. SLIMP or DmSerRS2 depleted and control cells were treated with cycloheximide and emetine (+CHX+EME) to analyse mitochondrial translation. SLIMP and DmSerRS2 protein levels were analysed by immunoblot, and VDAC protein level was analysed to ensure equal loading. (b) Individual values quantification of two independent experiments performed in triplicates is represented. *p value* *≤0.05.

2.3 SLIMP/SerRS2 heterodimer is required for mitochondrial respiration

Mitochondrial translation is essential for the correct coordination of the assembly of the oxidative phosphorylation system (OXPHOS) and mitochondrial respiration activity (Pearce et al., 2017; Smits et al., 2010; Wasilewski et al., 2017). Therefore, we analysed how SLIMP and SerRS2

levels affects mitochondrial oxygen consumption rate (OCR) by using a Seahorse XF24 bioanalyser. We calculated the basal OCR in SLIMP or SerRS2-depleted cells, as well as the overexpressed SLIMP-FLAG, and rescued SLIMP-depleted cells with SLIMPr or ΔN-SLIMPr overexpression (Figure 25).

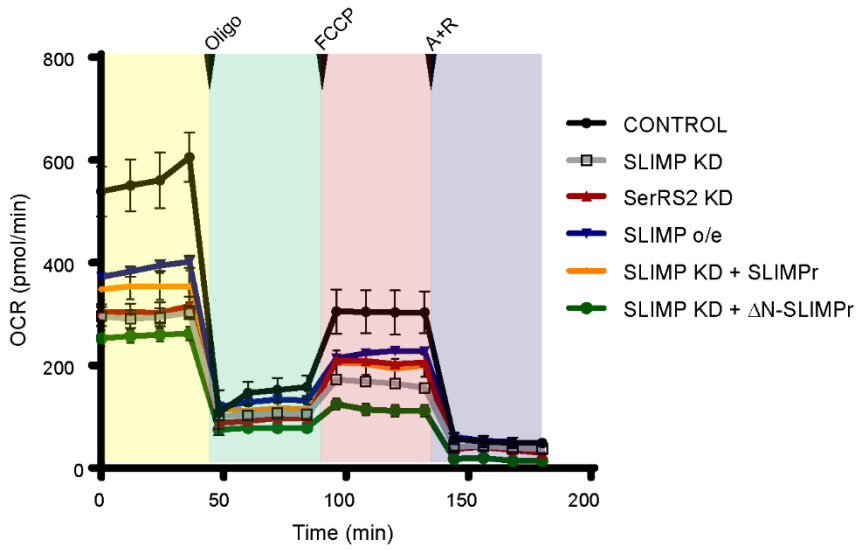

Figure 25| Oxygen consumption rate. Graphical representation the oxygen consumption rate from control, SLIMP or SerRS2-depleted cells, SLIMP-overexpressed cells and SLIMP rescued cells (SLIMPr and ΔN-SLIMPr) during the time. The mean of two independent experiments with four technical replicates is represented during time. Addition of oligomycin (0.5 μM), FCCP (2 μM), antimycin (5 μM) and rotenone (5 μM) was performed in the indicated time points. Maximal respiration could not be assessed as FCCP addition was not able to increase cells OCR.

We observed a significant OCR reduction in SLIMP or SerRS2 knockdown, while the decrease in basal respiration was not severe in SLIMP-overexpressing cells. OCR was partially rescued when expressing SLIMPr in a SLIMP-depleted context, while ΔN-SLIMPr was not able to rescue this

mitochondrial defect (Figure 26a). These results indicated that mitochondrial SLIMP levels were necessary for correct mitochondrial respiration activity.

We also evaluated the ATP-linked respiration by comparing OCR before and after inhibition of the ATP-synthase with oligomycin (Figure 26b). The OCR linked to ATP-production was partially reduced in SLIMP and SerRS2-depleted cells, as well as in the complementation with ΔN-SLIMPr, compared to control cells. SLIMP-overexpressed cells or cells complemented with SLIMPr presented similar ATP-synthase activity as control cells.

Furthermore, we analysed proton leak intensities, an indicator of mitochondrial integrity (Brand, 1990; Brand and Nicholls, 2011). We found that the organelle was not immediately compromised (Figure 26c) as proton leak levels remain low in all the analysed conditions. Finally, we calculated the non-mitochondrial respiration, or the OCR after inhibiting mitochondrial respiration with antimycin and rotenone, and we found it not altered among the different conditions (Figure 26d), indicating that the OCR calculated was entirely mitochondrial.

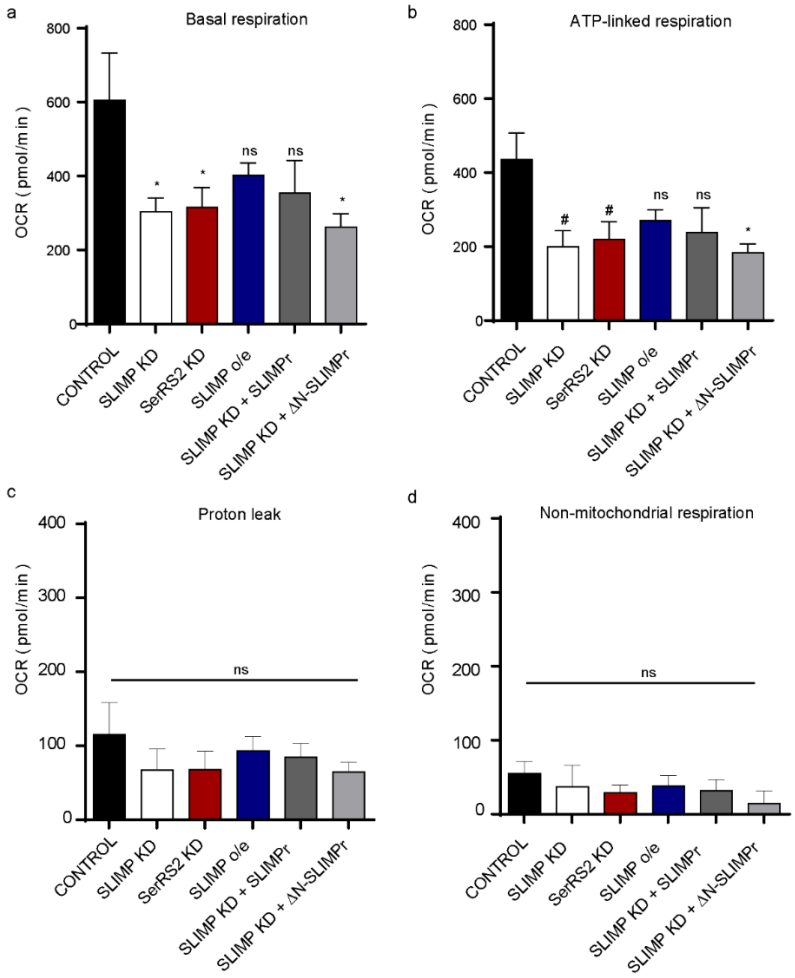

Figure 26| Oxygen consumption rate. (a) Basal respiration was calculated as the OCR in basal conditions before inhibiting ATP synthase with oligomycin. SLIMP and SerRS2-depleted cells presented decreased respiration while this reduction was milder in cells overexpressing SLIMP or SLIMPr. (b) The OCR linked to ATP production was calculated by subtracting oligomycin OCR to the basal. As observed with the basal respiration, ATP-linked respiration was decreased in SLIMP and SerRS2-depleted cells, while SLIMP-overexpressing or SLIMPr complemented cells was slightly higher than SLIMP knockdown mitochondria. (c) Proton leak, the OCR remaining after the inhibition of ATP synthase, was not significantly changed between conditions. (d) Non-mitochondrial respiration is the remaining OCR after completely inhibiting mitochondrial activity that was unchanged between the different conditions. *p value* *≤0.05, #≤0.07, ns – not significant.

We then calculated the coupling efficiency, or the proportion of respiratory activity that is used to produce ATP. We found that coupling efficiency was equal between the different conditions, showing that the measured respiration was produced from the activity linked to complex V of the OXPHOS complex (Figure 27).

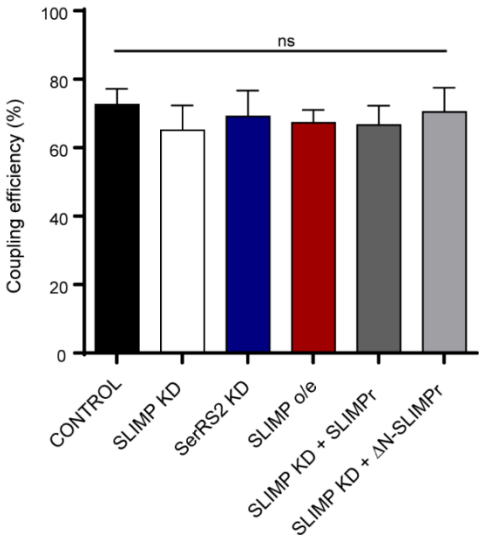

Figure 27| Mitochondrial coupling efficiency. The ratio between basal respiration and the ATP linked respiration indicated mitochondrial coupling efficiency was not different between samples. *p value* ns – not significant.

2.4 SLIMP/SerRS2 depletion does not increase ROS production in S2 cell mitochondria

Mitochondria are major sites of ROS production that mainly occurs at complexes I and III of the respiratory chain. ROS generation is increased when ETC function is compromised, leading to increased leakage of electrons, which react with oxygen to form superoxide (Murphy, 2009).

Mitochondrial dysfunction has also been linked to increased ROS production outside the mitochondria (Leadsham et al., 2013).

In order to study cellular ROS, we first analysed MitoSox staining by cell cytometry, which specifically detects mitochondrial superoxide. SLIMP- or SerRS2-depleted cells showed a decrease in mitochondrial ROS (Figure 28a). We also assessed total superoxide production by using dihydroethidium (DHE) staining and cell cytometry quantification. We found an increase in cellular superoxide in SLIMP knockdown or SerRS2 knockdown cells (Figure 28b), as it was previously reported *in vivo* (Guitart et al., 2010; Guitart et al., 2013). These results were in concordance with our mitochondrial respiration results, where SLIMP and SerRS2-depleted cells did not present an increased proton leak, suggesting that the mitochondria were not directly compromised.

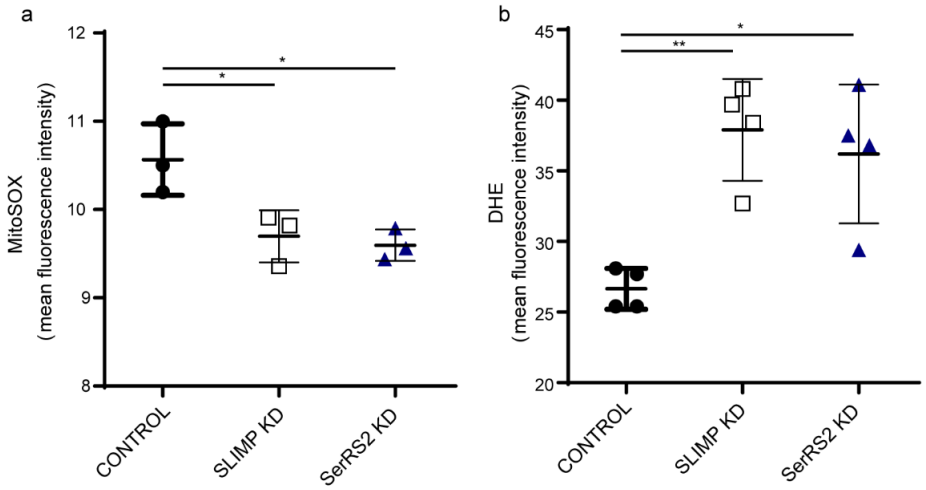

Figure 28| Superoxide production in SLIMP and SerRS2-depleted cells. (a) MitoSOX levels were reduced upon SLIMP or SerRS2 depletion showing a decreased mitochondrial superoxide production. (b) Total cellular superoxide production was evaluated using dihydroethidium (DHE) and quantified by cell cytometry. It was shown to be upregulated in SLIMP or SerRS2 knockdown cells. *p value* * ≤ 0.05, ** ≤ 0.001.

Chapter 3: SLIMP and LON protease interaction represses mtDNA replication

In collaboration with: Núria Bosch, Panagiota Siatra, Antigoni Machallekidou, Merve Nur Güller, Laurie Kaguni and Míriam Royo.

3.1 SLIMP interacts with the substrate binding domain of LON protease

SLIMP was previously described to interact with LON protease and this interaction was confirmed in the BioID analysis previously shown. In order to determine the interaction domain between LON and SLIMP, we cloned ΔN-LON (without the mitochondrial signal peptide), or each of the individual subdomains: the substrate binding domain (SBD), the ATPase domain (AAA^+), and the proteolytic domain (PD). First, we determined the mitochondrial signal peptide (1-56 N-terminal amino acids) by TPpred online software (Savojardo et al., 2015). To define the length and structure of each subdomain in the *Drosophila melanogaster* LON protease (CG8798) we performed sequence alignment and PFAM analysis (El-Gebali et al., 2018). To avoid α-helix or β-sheets disruption between subunits we predicted the secondary structure, and the edge of each subdomain was delimited within a loop with Phyre2 software (Kelley et al., 2015) and PsiPred online tools (McGuffin et al., 2000). LON subdomains were finally annotated between the following amino acid sequence positions: 57-433 for SBD, 434-754 for AAA^+ and 755-1006 for PD (Figure 29).

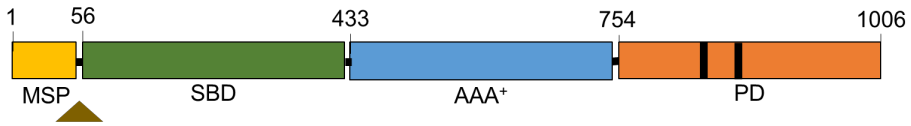

Figure 29| *Drosophila melanogaster* LON protease subdomains. LON protease subdomains illustration with the mitochondrial signal peptide (MSP), substrate binding domain (SBD), AAA+ (ATPase domain) and proteolytic domain (PD) are shown with the amino acid sequence number.

ΔN-SLIMP-HIS and ΔN-LON-FLAG, or the defined subdomains tagged with FLAG, were cloned into the pET-duet vector that contains two expression promoters. ΔN-SerRS2 and ΔN-LON-FLAG were also cloned following the same strategy. All proteins were co-expressed in *E. coli* and purified with FLAG-Dynabeads. We found that LON and the isolated SBD domain of LON readily co-purified with SLIMP (Figure 30a-b) but no interaction was detected between SLIMP and the active site or the ATPase domains (Figure 30c-d). SerRS2 was not found in the ΔN-LON immunoprecipitation confirming previous results from our lab where we showed no interaction between SerRS2 and LON (Figure 30e).

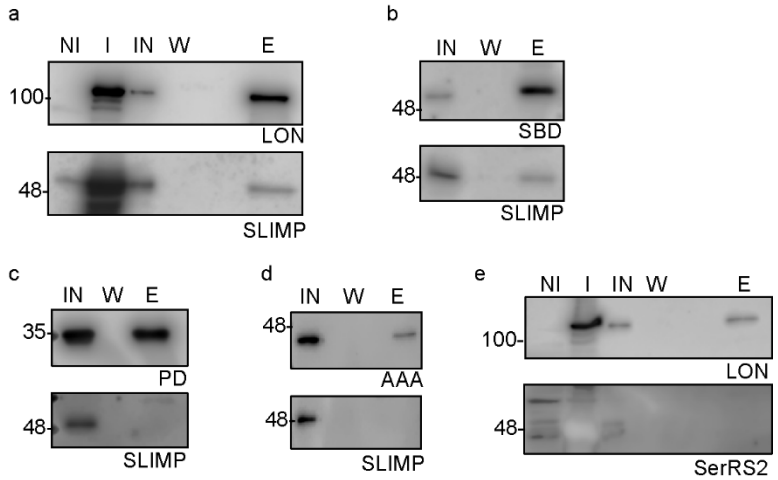

Figure 30| SLIMP interacts with the LON substrate binding domain. Immunoblot analysis of immunoprecipitated LON protease with α-FLAG magnetic beads, detected with α-FLAG antibody. Western blot for the non-induced (NI), induced (I), input (IN), wash (fifth wash) and elution (E) fractions are shown. ΔN-SLIMP was detected in (a) LON and (b) SBD immunoprecipitation samples. (c) PROT and (d) AAA^+ were correctly expressed but not immunoprecipitated with LON. (e) ΔN-SerRS2 was highly expressed but was not found to interact with LON.

3.2 SLIMP represses TFAM degradation by LON protease

LON is a mitochondrial protease of broad specificity. It was described in our laboratory that LON does not degrade SLIMP and that their protein and transcript levels are not interdependent. In *Drosophila melanogaster*, LON is known to regulate the levels of the DNA-binding protein TFAM (Matsushima et al., 2010). Thus, we analysed the impact of SLIMP depletion upon the degradation of TFAM by LON.

We observed that TFAM levels were increased two-fold in cells depleted of

SLIMP (Figure 31a-b), while they were not altered in SLIMP-overexpressing cells. The effect of SLIMP depletion upon TFAM levels was eliminated by overexpressing LON but not an inactive form of LON (LON S880A) (Figure 31b). This result indicated that SLIMP might be driving TFAM degradation by LON.

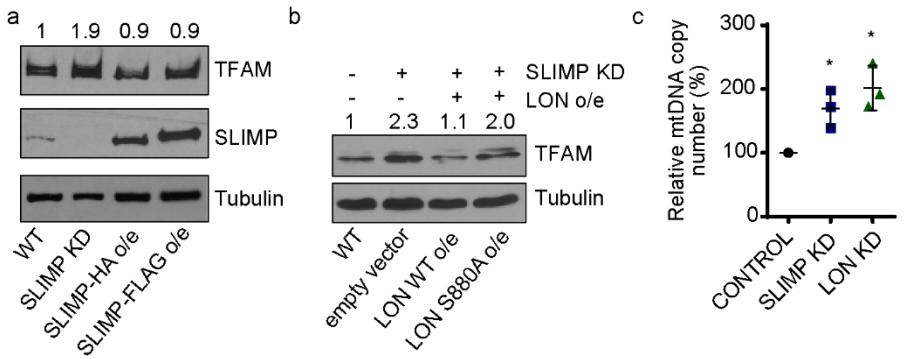

Figure 31| SLIMP drives TFAM degradation by LON. (a) Western blot analysis of SLIMP-depleted or SLIMP-overexpressed cells (with two different tags) compared to control wild type cells (WT). TFAM band quantification is shown and normalized to loading control. TFAM levels were increased upon SLIMP depletion. (b) Immunoblot analysis of TFAM levels in SLIMP-depleted cells, and SLIMP-depleted cells with the overexpression of LON WT (wild type) and LON S880A (inactive). TFAM band quantification is shown above. (c) Mitochondrial DNA quantification by RT-qPCR in control (empty vector), SLIMP or LON-depleted cells, normalized to nuclear DNA. *p value* * ≤0.05. (a) and (b) were performed in collaboration with Dr. Laurie Kaguni Lab.

It has been described that, in *Drosophila,* LON stabilizes the TFAM:mtDNA ratio and plays a crucial role in mtDNA replication. In order to determine the effect of SLIMP depletion and increased TFAM levels on the levels of mitochondrial DNA (mtDNA), we isolated total DNA from SLIMP and LON knockdown cells and we measured the amount of mtDNA

normalized to nuclear DNA. As previously reported *in vivo* (Guitart et al., 2010) we confirmed that SLIMP-depleted S2 cells presented an increase in mtDNA levels. In concordance to previously described studies (Matsushima et al., 2010), LON-depleted cells also presented a higher mtDNA copy number (Figure 31c).

3.3 LON general mitochondrial protease activity is not affected by SLIMP

We then sought to determine if the activation of LON activity by SLIMP was specific for TFAM, or extensive to any LON substrate. To answer this question we synthesized FRETN 89-98Abu (Fishovitz et al., 2011), a synthetic peptide used to monitor LON protease activity. By incubating the peptide with crude mitochondrial extracts from S2 cells we could monitor the fluorescence emission resulting from the cleavage of the peptide by LON. We then used different cellular models to monitor SLIMP influence on LON activity.

First, LON expression was evaluated by western blot (Figure 32). We confirmed that SLIMP and LON protein levels were not interdependent, and we found that LON protein levels were not changed in SLIMP-depleted, SerRS2-depleted or SLIMP-overexpressing cells.

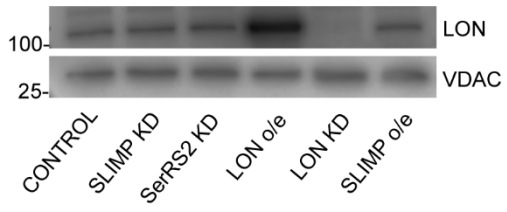

Figure 32| LON protein expression levels. Immunoblot of control (empty vector), SLIMP, SerRS2 or LON-depleted cells, and LON or SLIMP-overexpressed cells, induced with 400μM $CuSO_4$ for eight days. LON was detected with custom α-LON antibody and VDAC was used as a loading control.

Isolated mitochondrial extracts from LON and SLIMP-overexpressing cells, as well as SLIMP- and LON-depleted cells were analysed (Figure 33). Trypsin was added in control reactions to monitor peptide cleavage, and reactions with only peptide were used to monitor spontaneous cleavage.

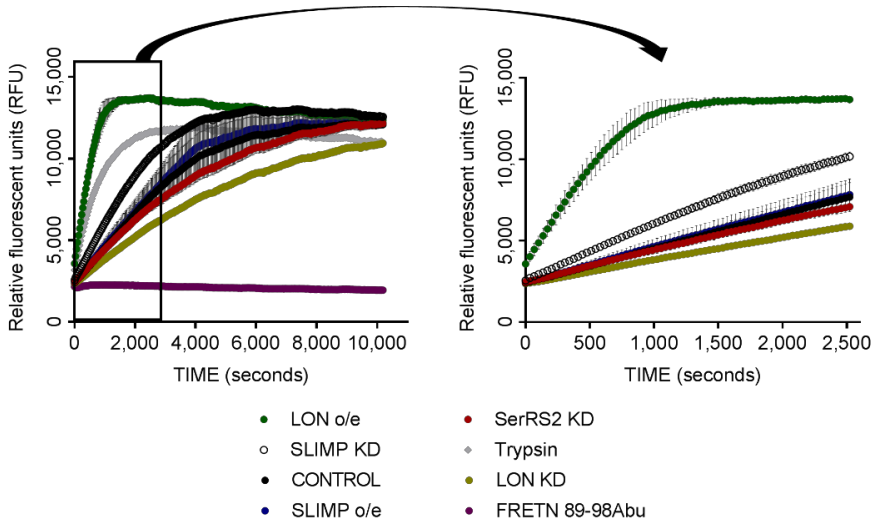

Figure 33| General LON activity was not affected by SLIMP. FRETN89-98Abu degradation monitored during 10,193 seconds with crude mitochondrial extracts of control

(empty vector); SLIMP-, LON- or SerRS2-depleted cells; LON and SLIMP-overexpressing cells. Reactions with only FRETN89-98Abu, and a peptide cleavage control with trypsin without any mitochondrial extract were analysed. Zoom into the first 2,500 seconds is shown.

We monitored peptide cleavage for approximately three hours (Figure 34a) and we observed that LON-overexpressing cells cleaved the peptide with a maximum activity of 13,727±97 relative fluorescence units (RFU). We detected a significant decrease in peptide cleavage in the LON-depleted mitochondria (5,855±68 RFU) compared to LON-overexpressing or wild type cell extracts (7,618±862 RFU). FRETN 89-98Abu degradation was also monitored in SLIMP-depleted and SLIMP-overexpressed mitochondria. LON activity in SLIMP-overexpressing cells was equal than control cells, while in SLIMP knockdown cells, the monitored activity was increased.

We also checked the protease activity of LON when the control cells reached the plateaux phase and we discovered that all the cellular conditions had already reached the same activity, except for LON-depleted cells that was lower (Figure 34b).

Altogether, our results show that the activation by SLIMP of LON is not general and might be specific for TFAM, suggesting that SLIMP is modulating LON specificity through interactions with the SBD of the protease.

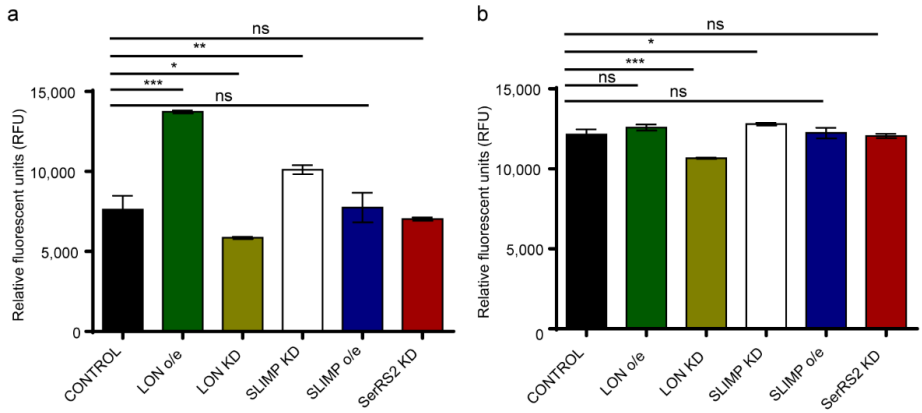

Figure 34| Activation of LON is not affected by SLIMP levels. (a) Relative fluorescence units (RFU) measurements in the plateaux point of LON-overexpressing cells and (b) in the control cells plateaux point. *p value* *≤0.05, ** ≤ 0.01, *** ≤ 0.001, ns – not significant.

Chapter 4: SLIMP controls cell cycle progression

In collaboration with: Maria Carretero, Camille Otto and Sue Cotterill.

4.1 SLIMP is required for cell cycle progression

SLIMP has been shown to be an essential gene involved in cell cycle progression (Ambrus et al., 2009; Liang et al., 2014). Thus, we decided to evaluate cellular growth and cell cycle progression in SLIMP-depleted S2 cells. SerRS2 knockdown cells growth were also monitored as controls. Cellular growth curves demonstrated that SLIMP is required for cell proliferation (Figure 35a). We observed the reduction of cellular proliferation was more acute in SLIMP-depleted cells than in SerRS2 knockdown cells. SLIMP protein levels were found to correlate with the reduction of cellular proliferation, and the phenotype defect was increased when SLIMP protein levels were diminishing (Figure 35b).

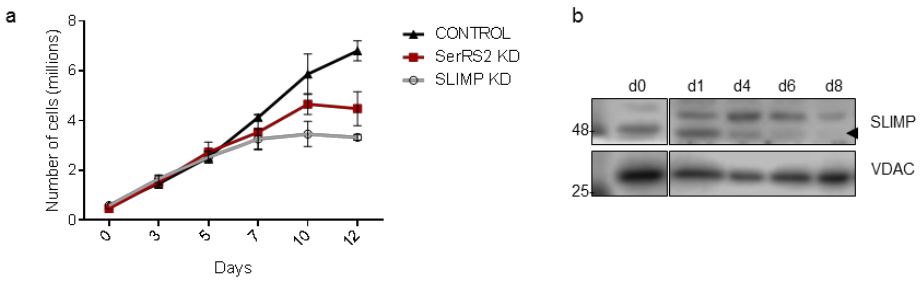

Figure 35| Cellular growth curve and SLIMP knockdown induction. (a) Growth curve of control cells (with an empty vector), SLIMP knockdown and SerRS2-depleted

cells during twelve days of induction with $CuSO_4$. Average cell number of biological triplicates ± SD of live cells is shown (in millions). (b) Western blot to detect the decrease in SLIMP (arrow) protein levels during SLIMP knockdown induction process (day 0, 1, 4, 6 and 8). VDAC was used as a loading control.

Interestingly, we observed that *Drosophila melanogaster* S2 cells undergo a visible cell shape change from a spherical/round shape to a spindle morphology in SLIMP-depleted cells during longer times of knockdown induction (Figure 36). Related to the lower proliferation we also observed a lower cell confluency. Furthermore, we found bi-nucleated cells or cells with mitotic defects (Figure 36) in SLIMP-depleted cells, while control and SerRS2-depleted cells presented a wild type phenotype.

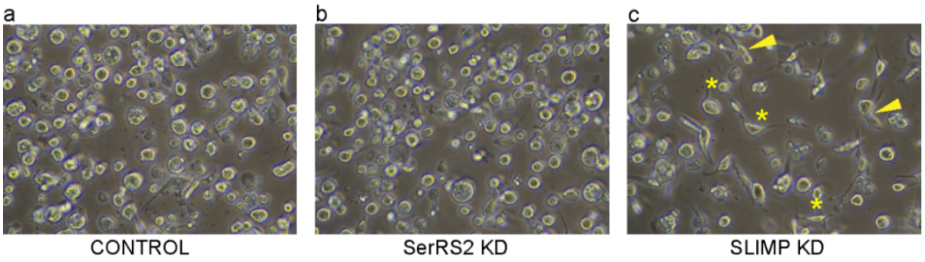

Figure 36| S2 cell phenotype and morphology. Representative S2 cell imaging of stable cell lines induced for twelve days in (a) control, (b) SerRS2 or (c) SLIMP-depleted cells. In SLIMP knockdown cells, binucleated cells are marked with arrows and morphology changes are marked with asterisks.

4.2 SLIMP-depleted cells accumulate in G2 cell cycle phase

Considering the defective growth and cell morphology changes, as well as previous publications where SLIMP has been implicated in cell cycle, we examined cell cycle progression in *Drosophila melanogaster* embryonic S2 cells following SLIMP depletion. We performed cell cycle analysis using cell cytometry, calculated as the fluorescence emitted by propidium iodide that intercalates between DNA bases. DNA content can be evaluated in each single cell and a minimum of 10,000 cells were analysed (Figure 37).

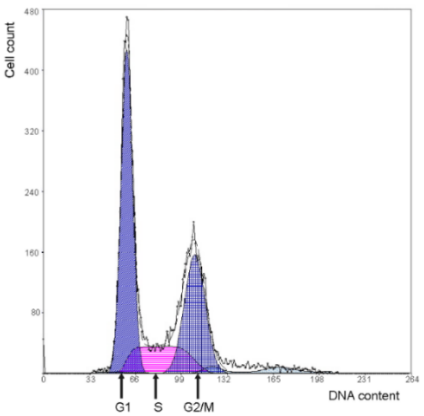

Figure 37| Cell cycle analysis example. Cell cycle was analysed by cell cytometry and PI fluorescence was projected on a monoparametrical histogram. Histograms were analysed using Multicycle Software. G1, S and G2/M cell cycle phases were calculated according to the DNA content of each cell.

We evaluated the cell cycle profile of SLIMP knockdown and overexpressing cells, as well as cells depleted of its protein interactors SerRS2 and LON. We observed that the cell cycle was altered only in SLIMP-depleted cells, while in SerRS2 or LON knockdown cell the cycle was not changed. SLIMP knockdown cells were significantly accumulated

in G2/M cell cycle phase (61.3±4.1%). Moreover, we found that the cell cycle profile was not altered when overexpressing SLIMP (Figure 38).

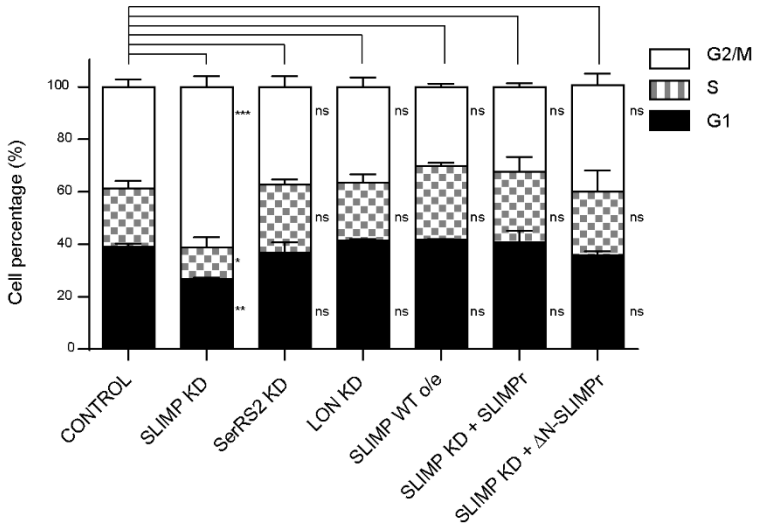

Figure 38| Cell cycle profile. Cell cycle analyses of control, SLIMP-, SerRS2- or LON-depleted cells, SLIMP-overexpressing cells and SLIMP knockdown cells rescued with either full SLIMP RNAi resistant (SLIMPr) or SLIMPr without the mitochondrial signal peptide (ΔN-SLIMPr). Percentages for each cell cycle phase are coloured in black (G1), grey pattern (S) and white (G2). Data represents the average from three independent experiments, mean and standard deviations are shown. *p value* comparing each cell cycle phase to the corresponding cell phase in control cells *≤0.05, **≤0.01, *** ≤ 0.001, ns – not significant.

To confirm this phenotype with another technique we used cellular lysates to measure cyclin E and cyclin B protein concentrations by western blot. We selected cyclin E as a G1 phase determination and cyclin B for G2/M assessment (Siu et al., 2012; Whitfield et al., 1990). As expected, we found cyclin B protein levels increased in total cellular extracts upon SLIMP depletion while cyclin E levels were decreased (Figure 39), thus confirming

that SLIMP knockdown cells accumulate in G2/M phase. On the other hand, although SLIMP and SerRS2 protein levels were found to be interdependent, we found that SerRS2-depleted cells present normal cyclins levels compared to control cells, confirming our previous cell cytometry results. Altogether, our data support the hypothesis that the lack of SLIMP is responsible for the cell cycle phenotype and indicate that SLIMP is needed for cell cycle progression.

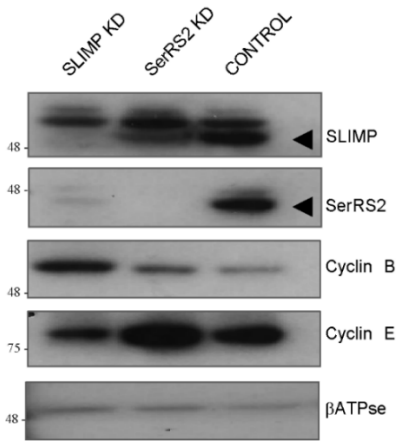

Figure 39| Cyclin protein levels upon SLIMP and SerRS2 knockdown. Western blot analysis of control (empty vector), SLIMP and SerRS2-depleted cells. SLIMP, SerRS2, cyclin B and cyclin E were analysed. βATPase was used as a loading control. Representative immunoblot is shown.

We then asked whether the G2 arrest caused by SLIMP depletion could be rescued by the overexpression of a RNAi resistant SLIMP (SLIMPr). Thus, we performed cell cycle analyses with the overexpression of SLIMPr or ΔN-SLIMPr in a SLIMP-depleted context, and we found that G2/M accumulation could be recovered by both SLIMP isoforms (Figure 38). These results suggested that the role of SLIMP in cell cycle was being performed from outside the mitochondria.

To further study this cell cycle phase accumulation, we analysed cell cycle progression and mitotic status in SLIMP-depleted cells. We performed a 5-bromouridine (BrdU) pulse and we monitored during one cycle those cells in S that had incorporated the analogue of thymidine (Figure 40a). This analysis revealed that G2/M phase in the SLIMP knockdown cells was longer that in control cells. After ten hours of the BrdU pulse incubation SLIMP-depleted cells were still in G2/M phase, while control cells had completed the cycle and already undergone mitosis (Figure 40b).

By evaluating the cell cycle after 24h of the pulse labelling, we observed that SLIMP-depleted cells eventually finished mitosis and divided, as we found G1 phase stained cells (Figure 40). We also observed that SLIMP-depleted cells and control cells progress through S phase to G2/M at the same ratio.

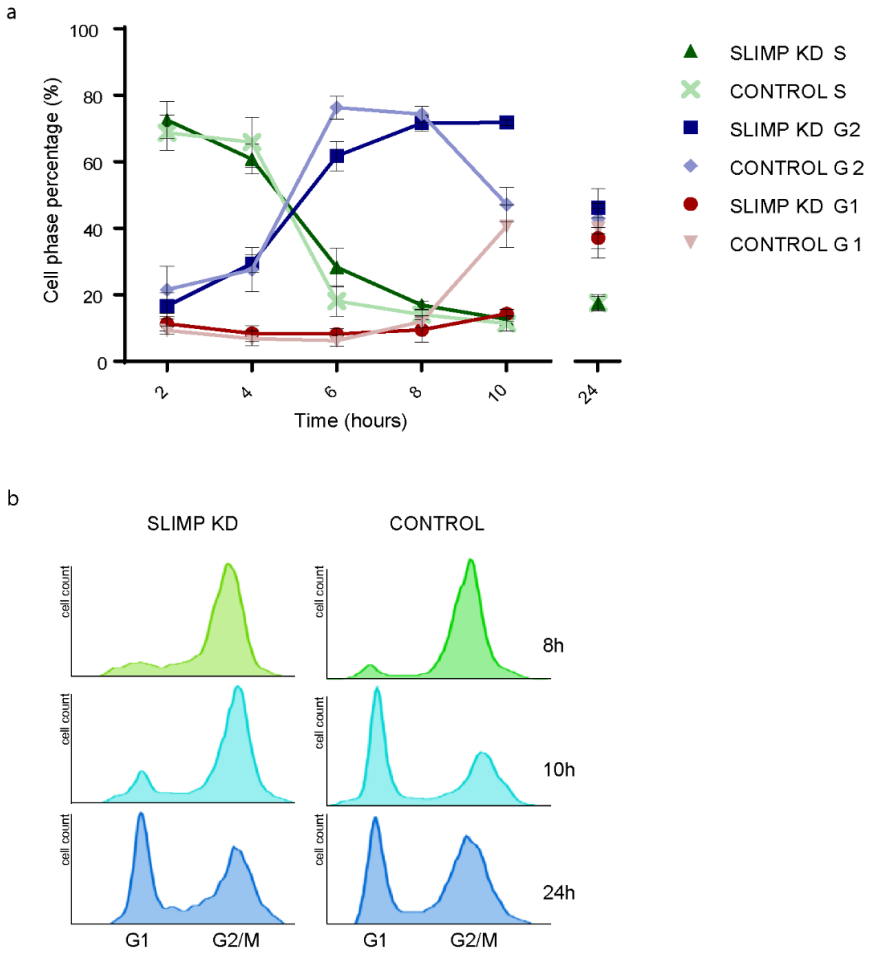

Figure 40| S phase to G2 phase cell cycle progression. SLIMP-depleted cells and control cells were incubated with BrdU for one hour, washed, plated back in Schneider's media and collected every two hours. Cells that incorporated BrdU were tracked for 10 hours and analysed by cell cytometry. (a) Cell cycle percentage is represented during time of two independent experiments and standard deviation are shown. SLIMP-depleted cells are represented in dark colours and control cells in light colours (G1 phase in red, S phase in green and G2/M phase in blue) (b) Representative cell cycle profile histograms at 8h, 10h and 24h in control cells of SLIMP-depleted and control cells.

Next, to evaluate the mitotic status under SLIMP depletion we performed histone H3 phosphorylation (H3P) immunostaining followed by cell cytometry. It has been long described that histone H3 is phosphorylated during metaphase at a single tryptic peptide by a cAMP-independent protein kinase (Shoemaker and Chalkley, 1978). Histone H3 is phosphorylated at Serine-10 (H3S10P) in all eukaryotes and this modification was demonstrated to be associated with transcriptional activation and chromosome condensation (Bode and Dong, 2005; Goto et al., 1999; Rossetto et al., 2012). We found H3S10P levels decreased in SLIMP knockdown cells (Figure 41) denoting a lower mitotic cell percentage upon SLIMP depletion. This result indicated that SLIMP-depleted cells had less mitotic cells, consistent with an elongated G2 phase.

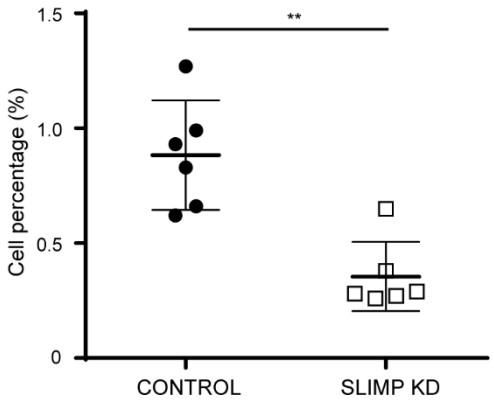

Figure 41| Mitotic cell percentage. Histone H3 phosphorylation analysed by cell cytometry indicating percentage of mitotic cells. In control cells mitosis represented 0.88±0.09 and in SLIMP-depleted cells was 0.35±0.06. *p value* ** ≤ 0.01.

4.3 G1 to S cell cycle progression is repressed by SLIMP

It has been reported in *Drosophila* that compensatory mechanisms occur to maintain normal rates of proliferation when one of the cell cycle phases is perturbed (Reis and Edgar, 2004). Considering that SLIMP-depleted cells presented an elongated G2 phase we decided to also investigate G1 to S phase progression. We synchronized SLIMP knockdown cells and control cells in G1 phase by adding 0.5 mM hydroxyurea (HU) to the media for 24 hours, washing with PBS and collecting the cells after two and four hours to analyse the cell cycle. The results showed that the percentage of SLIMP-depleted cells in S phase was highly increased after two hours of HU treatment, suggesting that SLIMP knockdown cells progress faster from G1 phase to S cell cycle phase (Figure 42).

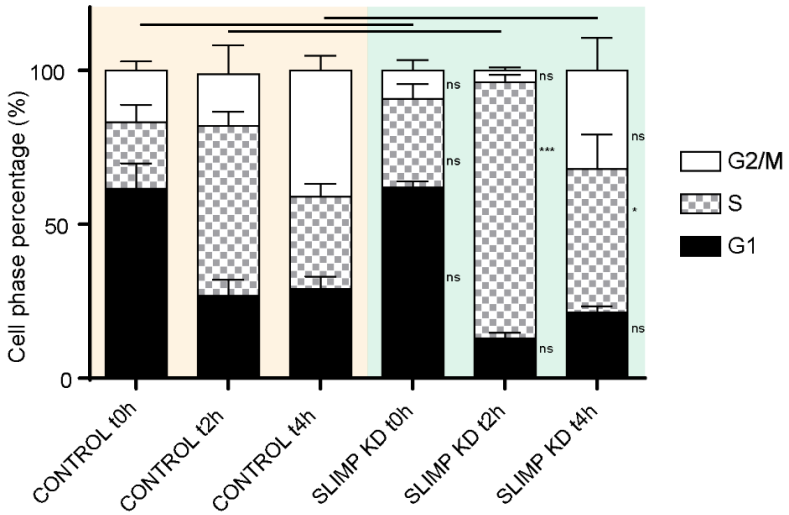

Figure 42| SLIMP-depleted cells display a faster G1/S transition. Control cells (light orange) and SLIMP-depleted (light green) cells were synchronized in G1 phase with the incubation of 1mM hydroxyurea for 24 h. Cells were washed and cultured back to be analysed by cell cytometry every 2 h. At time 0 h, the cell cycle of SLIMP KD or control

cells was synchronized in G1 phase, while after 2 h, upon the SLIMP depletion more cells already had passed from G1 to S phase. After 4 h, SLIMP-depleted cells still present more cells in S phase. *p value* * ≤ 0.05, *** 0.001, ns – not significant.

4.4 SLIMP is not differentially expressed during cell cycle

We described in the previous sections that SLIMP is necessary for cell cycle progression. Moreover, SLIMP was previously described to be differentially expressed during cell cycle phases in an analysis of the periodic transcriptome in *Drosophila* wing discs and in S2 cells (Liang et al., 2014). Thus, we hypothesised that SLIMP transcription could be regulated during cell cycle progression. To validate this results in our cellular model, we performed cell sorting of S2 wild type cells in G1 or in G2/M phase and analysed protein levels by immunoblot and transcript levels by RT-qPCR. Contrary to our hypothesis, results showed that SLIMP protein and transcript levels did not significantly change along the cell cycle (Figure 43).

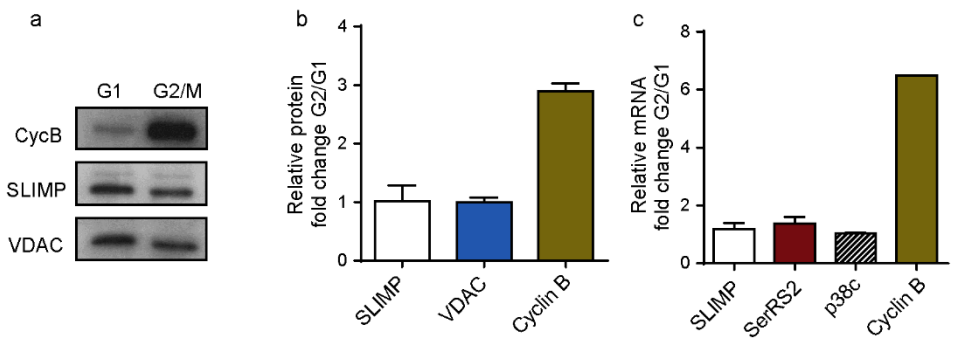

Figure 43| SLIMP expression during cell cycle. (a) SLIMP immunoblot in wild type cells sorted in G1 or G2/M phase. VDAC was used as loading control and cyclin B was used as a positive G2/M control. (b) Quantification of two independent western blots for SLIMP, VDAC and cyclin B. Values were normalized to G1. (c) Transcript quantification calculated by RT-qPCR for SLIMP, SerRS2, p38c (n=3) and cyclin B (n=1). Values were normalized to G1.

4.5 SLIMP depletion induces gene transcription and G2/M checkpoint

Considering the role of SLIMP in cell cycle and its identification as a suppressor of the dE2F1 mutation phenotype (Ambrus et al., 2009), we sought to determine the effect of SLIMP depletion in the cellular transcriptome. Thus, we performed a transcriptomic analysis of SLIMP-depleted cells and control cells, with the same number of G1 and G2 phase sorted cells. The top 10 upregulated and downregulated genes identified are shown in table 4, and SLIMP was detected as the most downregulated gene. Moreover, we confirmed that SLIMP transcript levels were not different between G1 and G2 cell cycle phases. Data is fully available at Gene Expression Omnibus with the number GSE104516.

Gene.Symbol	Entrez.Gene	Gene.Title	fc	KD.mean	WT.mean	pval	adj.pval
Slimp	318604	Seryl-tRNA synthetase-like insect mitochondrial protein	-13.3316	12.78242	9.045645	2.13E-12	4.03E-08
CG3397	41454	CG3397 gene product from transcript	-12.8702	8.68964	5.00368	5.69E-10	7.19E-07
CG1208	40727	CG1208 gene product from transcript	-11.6553	8.548684	5.005774	6.91E-11	1.87E-07
Ir75a	39982	Ionotropic receptor 75a	-11.6058	7.854093	4.317325	3.50E-11	1.33E-07
CG43074	12798579	CG43074 gene product from transcript	-8.70586	7.907925	4.785939	1.50E-10	3.02E-07
Ir75b	8673994	Ionotropic receptor 75b	-8.21108	7.700599	4.663027	1.05E-09	1.18E-06
Obp83cd	40746	Odorant-binding protein 83cd	-7.91212	6.927069	3.943005	2.07E-08	5.54E-06
Tsp42Ec	35612	Tetraspanin 42Ec	-6.4493	8.993416	6.304273	6.47E-11	1.87E-07
CG8160	36701	CG8160 gene product from transcript	-6.15803	6.991076	4.368608	1.34E-09	1.25E-06
mfas	41455	midline fasciclin	-5.85306	9.328916	6.779724	3.96E-10	5.77E-07
RhoGEF3	38050	Rho guanine nucleotide exchange factor 3	3.219747	7.052645	8.739592	5.50E-09	2.26E-06
CG3526	31277	CG3526 gene product from transcript	3.371874	5.203119	6.95667	5.90E-09	2.38E-06
sog	32498	short gastrulation	3.463367	5.342685	7.13486	6.94E-09	2.74E-06
CG5863	42096	CG5863 gene product from transcript	3.578146	5.249735	7.088947	3.97E-07	3.82E-05
ND-75	31762	NADH dehydrogenase (ubiquinone) 75 kDa subunit	4.078077	8.214082	10.24197	1.97E-09	1.29E-06
CG43736	3771905	CG43736 gene product from transcript	4.769327	5.14078	7.394565	3.21E-09	1.84E-06
CG34330	2768869	CG34330 gene product from transcript	4.99783	6.023123	8.344425	6.87E-07	5.61E-05
Taf12L	33672	TBP-associated factor 30kD subunit alpha-2	5.164775	5.427749	7.796454	3.82E-07	3.77E-05
CG4733	42368	CG4733 gene product from transcript	5.798274	5.162278	7.697901	1.76E-11	1.33E-07
CG11313	43646	CG11313 gene product from transcript	6.604416	7.270502	9.993933	2.17E-10	3.74E-07

Table 4| Top genes up and down regulated upon SLIMP knockdown. Gene symbol, Entrez gene, gene title, fold change (fc), mean value in KD or control cells, *p value* and adjusted *p value* are represented.

We then performed gene ontology (GO) studies comparing SLIMP-depleted cells to control cells. By assessing the GO Broad Hallmarks category, we found E2F target genes as the highest upregulated and significant category, with a *p value* smaller than 0.001 and an enrichment score of 0.65. The following upregulated category was G2/M checkpoint genes, with a *p value* smaller than 0.005 and an enrichment score of 0.59. Finally, Myc targets category was also upregulated with a *p value* minor than 0.023 and an enrichment score of 0.55 (Figure 44). It is interesting to note that no GO category was significantly downregulated, indicating that SLIMP depletion was producing a general upregulation of transcription.

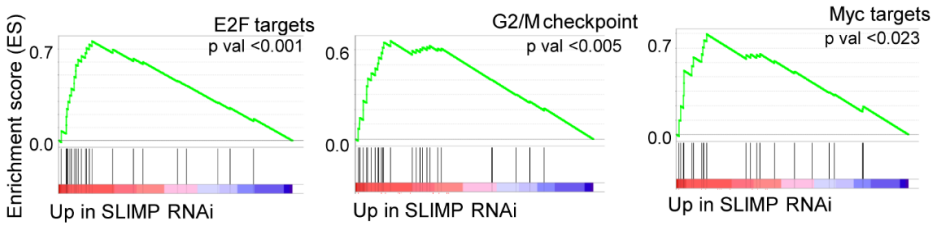

Figure 44| Microarray upregulated GO categories. Broad hallmarks upregulated GO in the SLIMP-depleted cells.

Results showed that the upregulation of the genes in these categories was higher in G2 phase sorted samples. We checked which genes contribute the most to the upregulation of E2F targets, G2/M checkpoint or Myc targets categories. Interestingly, we observed that many upregulated genes coded for replication fork proteins (Table 5), such as open reading frame proteins components (ORCs) or the minichromosome maintenance proteins (MCMs), suggesting that replication forks could be upregulated upon SLIMP depletion. We also found upregulated genes involved in mitotic entry control such as Wee1 (Di Talia and Wieschaus, 2012; Stumpff et al.,

2004), or Bub3, associated with the regulation of the spindle assembly checkpoint (Derive et al., 2015; Lopes et al., 2005).

	Gene	Fc	*pvalue*		Gene	Fc	*pvalue*
E2F targets	Mcm2	1.632236	0.001049	**G2/M checkpoint**	Orc5	1.389678	0.009987
	Mcm7	1.337468	0.005019		Cdk1	1.253367	0.010014
	Mcm5	1.450156	0.005224		Nek2	1.365188	0.01136
	Wee1	1.381788	0.005703		Mcm6	1.278536	0.016278
	Spc25	1.247871	0.007302		Mcm3	1.221756	0.024944
	Cdk1	1.253367	0.010014		Incenp	1.258085	0.030338
	Zw10	1.253518	0.011968		Orc6	1.260618	0.033033
	Slbp	1.223056	0.016191		Bub3	1.180506	0.039573
	Mcm6	1.278536	0.016278		Cdc7	1.170344	0.043571
	Orc2	1.431965	0.020072		Cdk4	1.161705	0.046205
	Mlh1	1.394759	0.020299	**Myc targets**			
	Mcm3	1.221756	0.024944		Mcm2	1.632236	0.001049
	Orc6	1.260618	0.033033		Set	1.328365	0.001978
	Pms2	1.168902	0.043739		Cdk2	1.408006	0.004965
	Cdk4	1.161705	0.046205		Mcm7	1.337468	0.005019
G2/M checkpoint					Mcm5	1.450156	0.005224
	Mcm2	1.632236	0.001049		Mcm6	1.278536	0.016278
	Cdc6	1.969177	0.001863		Orc2	1.431965	0.020072
	Ndc80	1.299852	0.005211		Bub3	1.180506	0.039573
	Mcm5	1.450156	0.005224		Uba2	1.17849	0.043598
					Cdk4	1.161705	0.046205

Table 5| Top upregulated genes in the significant upregulated categories E2F targets, G2/M checkpoint and Myc targets. Gene name, fold change and *p value* for each gene is indicated.

To better define the biological pathway affected by SLIMP, we also analysed the GO category of Biological Processes. The more upregulated categories in SLIMP-depleted cells were found to be involved in RNA processing, DNA replication or DNA conformational change (Table 6). Thus, we hypothesised that SLIMP depletion might be affecting the essential processes of DNA maintenance and expression.

GO category	SIZE	NOM p-val
GO0006397 MRNA PROCESSING	12	<0.000001
GO0071103 DNA CONFORMATION CHANGE	10	0.002053
GO0006261 DNA-DEPENDENT DNA REPLICATION	16	0.004329
GO0006259 DNA METABOLIC PROCESS	59	0.005155
GO0016071 MRNA METABOLIC PROCESS	16	0.006696
GO0006260 DNA REPLICATION	32	0.011601
GO0007049 CELL CYCLE	92	0.012788
GO0006396 RNA PROCESSING	19	0.014862
GO0006974 RESPONSE TO DNA DAMAGE STIMULUS	43	0.019048
GO0044057 REGULATION OF SYSTEM PROCESS	19	0.021645
GO0051704 MULTI-ORGANISM PROCESS	26	0.035294
GO0044772 MITOTIC CELL CYCLE PHASE TRANSITION	24	0.03838
GO0051325 INTERPHASE	18	0.041758
GO0006952 DEFENSE RESPONSE	14	0.047722

Table 6| Biological Process gene ontology categories significantly upregulated in SLIMP knockdown cells. GO category, number of genes in each category (size) and *p value* are represented.

As it was previously mentioned, E2F targets genes were upregulated upon SLIMP depletion, driving the hypothesis that E2F could be upregulated in SLIMP knockdown cells. Thus, we performed RNA extraction and RT-qPCR analysis of E2F pathway transcripts following SLIMP depletion. We confirmed that transcripts of the E2F pathway proteins were not altered, including dE2F1, dE2F2, dRBF1, and dDP (Figure 45a). Although transcript levels were not upregulated we hypothesized that dE2F1 protein levels could be increased triggering an upregulation of transcription. Thus, we performed an immunoblot analysis to detect changes in dE2F1 protein levels. Results showed that they were not affected by SLIMP depletion (Figure 45b-c), confirming previously published results (Ambrus et al., 2009).

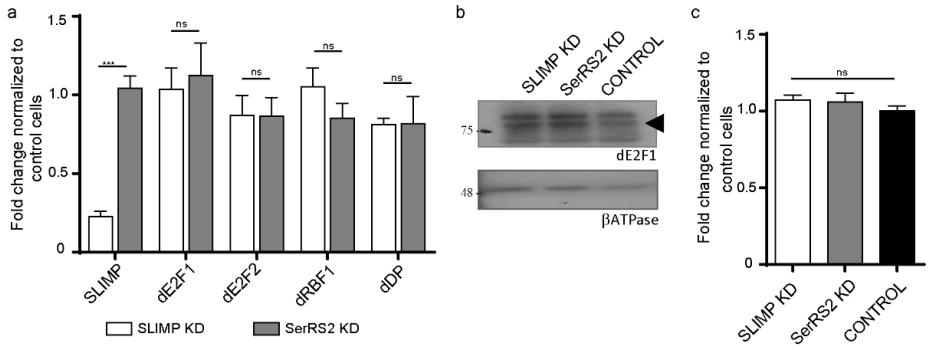

Figure 45| dE2F1 and E2F pathway genes are not differentially expressed. (a) Transcript levels determined by RT-qPCR for SLIMP, dE2F1, dE2F2, dRBF1 and dDP. SLIMP- or SerRS2-depleted values were normalized to control cells and RP49 was used as an internal control. (b) dE2F1 protein levels were determined for SLIMP knockdown, SerRS2-depleted and control cells by western blot. βATPase was used as a loading control. Representative immunoblot is shown. (c) Quantification of three independent experiments was performed for dE2F1 protein levels upon SLIMP- or SerRS2-depleted cells normalized to control cells. *p value* *** ≤ 0.001, ns – not significant.

4.6 Cdc6 and ORC2 protein levels increase upon SLIMP knockdown

Having previously demonstrated that E2F target genes were upregulated upon SLIMP knockdown, we then wanted to evaluate whether transcript upregulation was translated into protein upregulation. To answer this question, we performed immunoblot analyses with available antibodies and detected a significant upregulation of Cdc6 and ORC2 protein levels (Figure 46a-b). Although transcript levels were upregulated for MCM2, MCM5 or ORC5, the corresponding protein levels did not change. Altogether, these results suggest that SLIMP depletion drives the transcription of E2F targets and replication fork formation to boost progression from G1 to S phase.

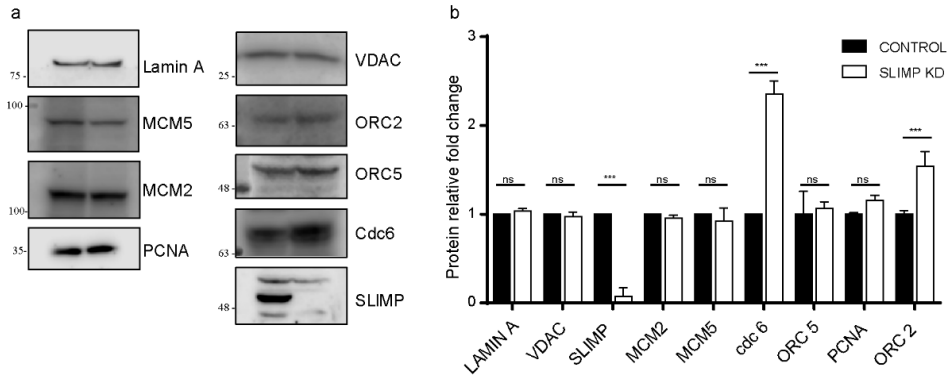

Figure 46| SLIMP-depleted cells presented an increased replication fork protein level. Control cells and SLIMP knockdown cell lysate was analysed by western blot, for MCM2/5, ORC2/5, Cdc6 and PCNA. SLIMP protein levels were used to confirm the correct induction of the knockdown. Lamin A and VDAC were used as a loading control. (a) Representative immunoblot is shown and (b) three independent experiments were quantified. *p value* ***≤0.001, ns – not significant.

4.7 SLIMP depletion does not trigger apparent DNA damage

Upregulation of E2F target genes combined with the upregulation of the G2/M checkpoint in SLIMP-depleted cells rise the question whether the lack of SLIMP could be leading to DNA damage problems. One of the earliest events after DNA damage, regardless of whether it is a biological, chemical or physical event, is the activation of protein kinases that rapidly phosphorylate the C-terminal tail of the histone 2A variant (H2Av) (Talbert and Henikoff, 2010). Therefore, we analysed DNA damage in the SLIMP knockdown cells by assessing histone H2Av phosphorylation by immunoblot. Control cells or SLIMP-depleted cells were cultured at very low confluency before cell lysis and subsequent western blot analysis. Contrary to our hypothesis, an increase in phosphorylation signal was not

detected in SLIMP knockdown cells (Figure 47). We also assessed H2Av phosphorylation status upon DNA damage in SLIMP-depleted and in control cells. We applied γ-irradiation to activate H2Av phosphorylation and we found that both cell lines trigger the same phosphorylation response, higher than in non-irradiated cells.

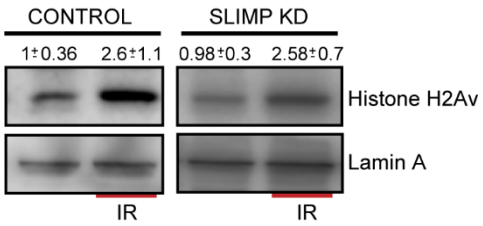

Figure 47| DNA damage assessed by H2Av phosphorylation. Immunoblot assay in control (empty vector) and SLIMP-depleted cells against histone H2Av and Lamin A, as a nuclear loading marker. In red, irradiated (IR) samples were used as a positive control. Representative western blot from three independent experiments with band quantification mean and standard deviation are shown.

Replication fork movement heavily depends on deoxyribonucleoside triphosphate (dNTPs) availability (Kunz et al., 1994; Pai and Kearsey, 2017; Siddiqui et al., 2013). Therefore, in order to further explore our hypothesis of DNA instability upon SLIMP depletion, we incubated SLIMP-depleted and control cells with nucleosides for 24 hours and analysed cell cycle progression by cell cytometry. Results showed that SLIMP knockdown cells G2 phase accumulation was increased with nucleosides incubation (Figure 48a) and supported the idea that SLIMP depletion triggers DNA replication problems. It is well known that unbalanced nucleosides pools cause genetic abnormalities and cell death (Reichard, 1988). Thus, we carried out a cell viability analysis with WST-1 upon nucleoside supplementation in control

and SLIMP-depleted cells, with the previous supplementation concentration (1x) and ten times higher concentration (10x) (Figure 48b). We found that the lower nucleoside concentration was not toxic for control or SLIMP knockdown cells, while the higher concentration compromised S2 cells.

Taken together, these results suggest that although SLIMP depletion does not trigger apparent DNA damage, it could be generating replicative instability that would lead to an increased G2 arrest upon nucleosides incubation.

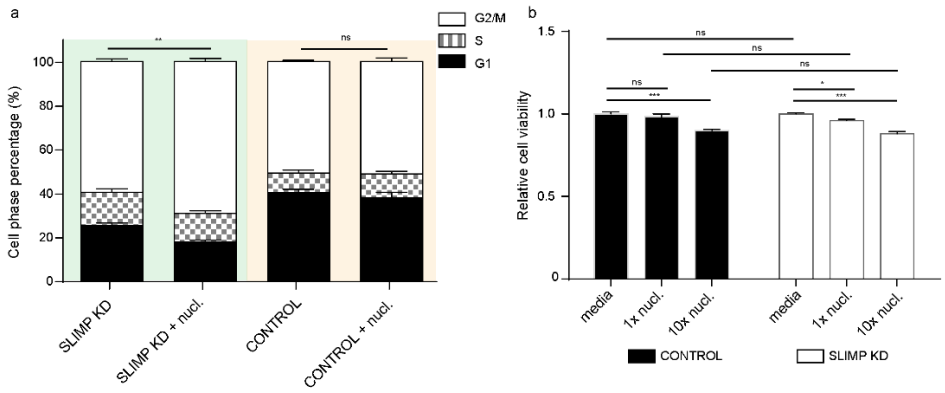

Figure 48| Nucleoside supplementation caused a severe G2 accumulation in SLIMP-depleted cells. (a) Supplementation of SLIMP-depleted (light orange) and control cells (empty vector – light green) with 1x nucleosides mix for 24 hours resulted in an increased G2 accumulation in the SLIMP knockdown conditions. (b) WST-1 viability test in control and SLIMP knockdown cells incubated with 1x or 10x nucleosides. *p value* *≤0.05, **≤0.01, ***≤0.001, ns – not significant.

Chapter 5: SLIMP in human cells

In collaboration with: David Piñeyro and Federica Lombardi.

The mitochondrial and cell cycle function of SLIMP described in this work, as well as other reports that showed that cytosolic SerRS regulates vascular development in animals (Amsterdam et al., 2004; Herzog et al., 2009; Xu et al., 2012), highlight the disposition of SerRS structures to incorporate non-canonical regulatory functions in animals. Many evolutionary and mechanistic aspects of this regulatory network remain unknown, including whether functional equivalents to SLIMP exist in mammals.

With this goal in mind we decided to inhibit the closest SLIMP homologue in human cells, the mitochondrial seryl-tRNA synthetase (SARS2), and study its impact on cell cycle progression. By synchronizing HeLa cells with a double blockage of thymidine, we observed that cell cycle progression was not affected by the depletion of SARS2 or its overexpression (Figure 49). Moreover, cell cycle progression was also not affected when we performed cell cycle experiments with stable HeLa cells heterologously overexpressing *Drosophila melanogaster* SLIMP.

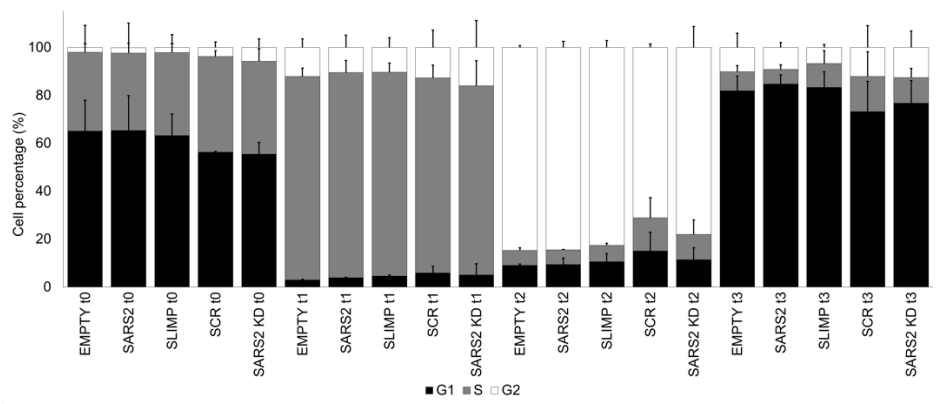

Figure 49 |HeLa cell cycle progression study. Cells synchronized in G1 with a double blockage in thymidine were released and the cell cycle was analysed by cell cytometry every two hours. We used control cells with an empty vector, SARS2-depleted cells, and SLIMP-overexpressing cells. Control cells with a scrambled (SCR) shRNA or SARS2 shRNA were used to monitor the cell cycle progression upon SARS2 depletion. Mean and standard deviation of three independent experiments is shown.

DISCUSSION

Altogether, the work described in this thesis contributes to further characterize SLIMP, a seryl-tRNA synthetase paralog with essential mitochondrial and cell cycle functions in *Drosophila melanogaster*. We propose that SLIMP acts as a regulator of mitochondrial translation and DNA replication and, through a mechanism still not completely understood, it represses cell cycle progression.

ARSs are essential and universal components of the genetic code. They have undergone numerous events of duplication, insertion and deletion of protein domains during their extended evolution (Ibba and Soll, 2000). It is now well recognized that eukaryotic ARSs are a hot spot for the evolution of new functionalities, perhaps due to their ancient nature and multi-domain structures (Guo et al., 2010). In our lab, in the process of construction of a *Drosophila* model for mitochondrial diseases by depleting the mitochondrial Seryl-tRNA Synthetase (SerRS2) (Guitart et al., 2013), its paralog Seryl-tRNA synthetase-Like Insect Mitochondrial (SLIMP) protein was identified (Guitart et al., 2010). SLIMP is an ARS paralog that evolved via duplication of a mitochondrial SerRS gene early in the evolution of metazoans, which was fixed in the genomes of arthropods. It retains significant sequence identity with SerRS and data from our laboratory indicates that SLIMP forms a heterodimer with a catalytically active SerRS2 monomer.

SLIMP cellular environment and localization

SLIMP was initially described as a mitochondrial protein whose mitochondrial signal peptide (MSP) sequence was predicted using bioinformatics tools. We now refine the mitochondrial signal peptide cleavage site by mass spectrometry (Figure 16 and Supplementary table 1) and demonstrate by immunofluorescence that this N-terminal amino acid

sequence is indeed required for SLIMP internalization into the organelle (Figure 17). Paradoxically, although we described that SLIMP contains MSP, we also detected nuclear and cytosolic proteins in our BioID analysis (Figure 19), suggesting that SLIMP may be present outside of the mitochondria. Interestingly, it has been recently reviewed that some proteins containing a MSP can also be detected in low amounts in other cellular compartments than the mitochondria (Monaghan and Whitmarsh, 2015). For example, in mammalian cells, the transcription factor NRF2 associates with the outer mitochondrial membrane as part of a complex with KEAP1 and PGAM5, but it dissociates from the complex upon oxidative stress and translocates to the nucleus, where it targets the promoters of genes that contribute to antioxidant defences (Itoh et al., 2015). Also, the *Caenorhabditis elegans* transcription factor ATFS-1 is imported into the mitochondrial matrix and degraded by proteolysis and, in response to disrupted proteostasis, it is redirected from mitochondria to the nucleus (Nargund et al., 2012). Additional data that back up an extra-mitochondrial localization of SLIMP are cellular fractionation experiments performed in our laboratory in which SLIMP was detected not only in the mitochondria but also in the nuclear fraction and, as described in the results section 4.2, the rescue of the cell cycle arrest phenotype caused by the SLIMP depletion with the expression of the RNAi resistant SLIMP lacking the MSP (Figure 38).

These results raised the question whether SLIMP, although it was mainly detected in the mitochondria by immunofluorescence (Figure 17), could be translocated outside or not imported into the organelle under certain cellular conditions. We first asked whether the SLIMP transcript could be translated starting from a second methionine present in the *Drosophila melanogaster* SLIMP-coding gene downstream of the MSP, which would

generate two distinct SLIMP populations. However, an alignment of several *Drosophila* SLIMP sequences revealed that this second methionine is not conserved.

Further studies would be necessary in order to understand the presence of SLIMP outside the mitochondria and to determine the mechanism by which this is achieved, whether it might be translocated outside the mitochondria either during cell cycle or under particular stress or developmental conditions.

The role of SLIMP in mitochondrial translation

The association of SLIMP with SerRS2 and LON protease, together with its mitochondrial protein environment, support the idea that SLIMP is important for mitochondrial homeostasis. SLIMP function has been linked to mitochondria physical integrity and metabolism, and it was shown that SLIMP-depleted flies present a swollen matrix with loss of the inner-membrane *cristae*. Furthermore, one of the SLIMP-depleted *Drosophila melanogaster* lines presented a defect in mitochondrial respiration (Guitart et al., 2010), as analysed by Oxygraph – Oroboros. SerRS2-depleted *Drosophila* have been also described to present a defect in mitochondrial respiration (Guitart et al., 2013). We have now analysed mitochondrial respiration in *Drosophila* S2 cells (Figure 25) that were depleted of SLIMP or SerRS2, or that overexpressed SLIMP in either a wild-type or a SLIMP knockdown background (SLIMP rescued cell lines: SLIMPr and ΔN-SLIMPr). Mitochondrial respiration was significantly reduced in SLIMP- and SerRS2-depleted cells, as well as in the SLIMP knockdown cells that express the protein outside the mitochondria (ΔN-SLIMPr) (Figure 26). This is in agreement with our findings that the SLIMP-SerRS2 heterodimer is

essential for tRNA aminoacylation (Figure 14a). Interestingly, cells overexpressing SLIMP and SLIMP-depleted cells rescued by SLIMPr, did not show a clear reduction in respiration, but presented a tend towards a decrease in mitochondrial respiration compared to control cells. These results are in concordance with *in vitro* aminoacylation assays performed in our laboratory showing that while tRNA aminoacylation by the SLIMP-SerRS2 heterodimer increases with the SLIMP/SerRS2 ratio, it reaches a saturation concentration after which the aminoacylation activity is decreased (Figure 14b). In addition, analyses of the SLIMP/SerRS2 complex by size exclusion chromatography and Multi Angle Light Scattering (MALS) unequivocally identified an αβ heterodimer in solution, while purifying SLIMP alone tends to form homodimers. Altogether, these results suggest that SLIMP-overexpressing cells could also present mitochondrial defects due to diminished tRNA aminoacylation.

In agreement with the reduced aminoacylation activity, we demonstrate that mitochondrial translation is reduced in SLIMP or SerRS2 knockdown cells (Figure 24). Therefore, the reduced availability of charged tRNA affects mitochondrial translation, and the same effect is observed whether SLIMP or SerRS2 are depleted. Interestingly, *Drosophila melanogaster* SerRS2 is shorter than other SerRS proteins, suggesting the need for a cofactor protein to perform aminoacylation activity (Chimnaronk et al., 2005). Future work with SLIMP-depleted cells rescued by SLIMPr or ΔN-SLIMPr, and cells overexpressing SerRS2 will allow us to further determine the function of SLIMP in mitochondrial translation.

Although mitochondrial respiration and mitochondrial translation were reduced upon SLIMP or SerRS2 depletion, we observed no change in the

coupling efficiency or the proton leak (Figure 27). They have been described as indicators of mitochondrial integrity (Brand, 1990; Brand and Nicholls, 2011), and the fact that they were unchanged in our cells indicated that the respiratory complexes translated upon SLIMP or SerRS2 depletion would be functional and the OXPHOS system would be active. We therefore suggest that under these conditions, the mitochondrial status is not highly compromised as cells present less but equally active respiration complexes. In concordance with these results, we also showed that mitochondrial ROS was not increased, even though we detect elevated total cellular ROS (Figure 28), as previously reported *in vivo* (Guitart et al., 2010). Similar results have been shown for Drp1, a protein involved in the mitochondrial fusion/fission processes whose depletion causes less mitochondrial respiration but also less reactive species (Zhang et al., 2017). Further studies regarding the respiration complexes integrity will allow us to understand the OXPHOS system complex stability upon SLIMP or SerRS2 depletion.

The role of SLIMP in the activity of LON in the mitochondria

BioID analysis confirmed that SLIMP interacts with mitochondrial LON protease (Figure 19). We described that SLIMP interacts with the substrate binding domain (SBD) of the protease (Figure 30) to stimulate the degradation of TFAM, thus repressing mtDNA replication (Figure 31). The cellular localization of SLIMP, together with the fact that the SLIMP-LON interaction does not generally activate LON (Figure 33), suggests that SLIMP could be recruiting LON to the vicinity of ribosome granules in order to stimulate TFAM degradation. This would be in concordance with previous results from our research group showing that SLIMP interacts with mitochondrial RNAs without specificity. However, the fact that SLIMP interacts with the SBD of LON also opens the possibility that the

LON-SLIMP complex more efficiently recognizes TFAM for degradation than LON alone.

Interestingly, SLIMP-overexpression did not affect neither LON activity *in vitro*, nor TFAM protein levels in S2 cells (Figure 31 and Figure 33). Titration assays with increasing concentration of SLIMP should provide more insight about the regulation of the SLIMP-LON interaction. LON has also been described to be involved in the mitochondrial misfolded protein quality control (Bezawork-Geleta et al., 2015; Friguet et al., 2008) and in the degradation of proteins such as aconitase (Bota and Davies, 2002) or cystathionine beta-synthase (Teng et al., 2013). Therefore, future work is also needed to completely define the effect of SLIMP depletion on other LON substrates.

During the writing of this thesis, a report was published describing that, in *Drosophila*, a LON null allele causes early larval lethality and that LON depletion shortens lifespan and causes locomotor impairment and respiration defects specific to respiratory chain complexes that contain mitochondrial encoded subunits. The later phenotype appeared to result from reduced mitochondrial translation, due to a sequestration of mitochondrial encoded transcripts in highly dense ribonucleoparticles (Pareek et al., 2018). This work supports our proposal that disrupting the interaction of SLIMP with LON might enhance mitochondrial translation defects. Moreover, Pareek et al. propose that these defects are induced by the mitochondrial unfolded protein response (mtUPR). Thus, we asked whether we could detect upregulation of genes involved in this cellular pathway in our model. Our microarray data for SLIMP-depleted cells does not indicate upregulation of NRF1/NRF2 *Drosophila* homologous *cnc* gene (Pitoniak and Bohmann, 2015), PGC-1 homologous *spargel* gene or KEAP-1 (Deshmukh et al., 2017; Fuse and Kobayashi, 2017), suggesting that the

mitochondrial translation defects in SLIMP-depleted cells were not triggering a nuclear response.

Altogether, we propose that SLIMP in the mitochondria helps coordinate two intrinsically conflictive activities. SLIMP activity would repress mtDNA replication and stimulate the translation of transcription products. Under conditions where mtDNA replication is preferential, attenuating SLIMP function would simultaneously reduce translation activity and stimulate mtDNA replication through increased TFAM levels.

SLIMP cell cycle function

In this section we will discuss the results about the role of SLIMP in cell cycle regulation previously showed in the results chapter 4. Generation of mitochondrial biomass depends on the expression of genes encoded in both the nucleus and mitochondria whose translation must be coordinated in order to prevent an imbalanced composition of the mitochondrial proteome (Couvillion et al., 2016). At the same time, RNA transcription and DNA replication are potentially exclusive processes whose mutual interference must be prevented (Agaronyan et al., 2015). Thus, mechanisms must exist to control the levels of DNA replication and transcription according to the translational needs of mitochondria and cell cycle.

Previous reports have highlighted the involvement of SLIMP in the control of cell cycle progression in *Drosophila* (Ambrus et al., 2009; Liang et al., 2014). Liang et al., described in a functional genomic analysis of the periodic transcriptome in *Drosophila melanogaster* a core set of cell-cycle-dependent periodic genes in *Drosophila* wing disc and S2 cultured cells. On a genomic level, these authors defined the global cell-cycle-associated transcriptome by microarray and identified more than 700 cell-cycle-associated genes in

wing discs and more than 600 in S2 cells. The intersection of these sets included 150 genes with similar patterns of periodic expression in both cell types, which included SLIMP (CG31133). Knockdown mutants were then generated for all the differentially expressed genes and the effect of this depletion was analysed. SLIMP depletion resulted in an accumulation of cells in the G2/M phase.

Our results confirm and extend these observations. First, as it was previously reported *in vivo* (Guitart et al., 2010), we described that the depletion of SLIMP severely affects cell growth in S2 cells (Figure 35). Moreover, we observed a clear phenotype effect when depleting SLIMP for long periods of time (Figure 36). We noticed that cell culture confluency was reduced, and some cells presented an elongated shape or were binucleated. We find that the involvement of SLIMP in the regulation of cell cycle progression is likely independent of its interactions with SerRS2 and LON, as depleting SerRS2 or LON did not affect cell cycle (Figure 38). In contrast, and as previously mentioned, we described that the mitochondrial defects are indeed similar for the SLIMP- or SerRS2-depleted cells (Figure 25).

Furthermore, we were able to rescue the cell cycle accumulation in SLIMP-depleted cells by expressing either the full length SLIMP or an ex-mitochondrial form, indicating that the cell cycle role of the protein is likely taking place outside the organelle. This result, together with the SLIMP protein interactome study previously described (Figure 21), and cell fractionation studies performed in our lab, strengthen the hypothesis that SLIMP might be affecting cell cycle progression independently from the mitochondria.

Although we confirmed the cell cycle phenotype caused by the depletion of SLIMP, we could not ratify in our cellular model the results of Liang et al.

about SLIMP being differentially expressed through cell cycle, since we detected equal protein and transcript level in G1 and G2 sorted cells (Figure 43). Moreover, we also obtained the same results for the transcript levels in the microarray analysis and confirmed the results from the RT-qPCR.

To further characterize the observed G2 accumulation we studied cell cycle progression by performing BrdU pulse labelling experiments. We observed that SLIMP-depleted cells presented an elongated G2 phase compared to control cells (Figure 40). Although we also found less mitotic cells upon SLIMP depletion (Figure 41), we proved that mitosis is not compromised, as we observed BrdU positive cells in G1 after 24h.

The cell shape phenotype we observed in our SLIMP-depleted cells (Figure 36) has been previously described in the literature for cells accumulated in G2 cell cycle phase (Guo et al., 2016), when the protein Wee1, upregulated in our microarray (Table 5), phosphorylates cdc2 and inhibits the mitotic entry (Campbell et al., 1995). Moreover, cells with higher levels of Wee1, despite elongated G2 phases, divide at wild-type rates by compensating and shortening their G1 phases (Reis and Edgar, 2004). This is in concordance with our BrdU results showing that SLIMP-depleted cells were able to divide. These compensatory mechanisms have been described to maintain normal rates of proliferation when one of the cell cycle phases is perturbed (Neufeld et al., 1998; Reis and Edgar, 2004).

In agreement with this idea, we found that SLIMP-depleted cells enter S phase faster than control cells (Figure 42). Further studies would be needed to confirm this hypothesis since we also observed a modest accumulation in S phase four hours after synchronization release, suggesting that S phase in SLIMP-depleted cells may be slower.

Altogether, this data would indicate that SLIMP-depleted cells present a faster progression from G1 to S phase, and by the overexpression of Wee1, among others, an inhibition of the mitotic entry. Future experiments to detect a possible role and contribution of Wee1 in our G2 accumulation phenotype would allow us to further understand the mechanism of SLIMP in cell cycle regulation.

In concordance with this idea and as previously mentioned, SLIMP was found in a mosaic genetic screen utilizing the dE2F1 mutant phenotype to identify suppressors that could overcome the dE2F2/pRB-dependent proliferation blockage. Ambrus et al. identified *l(3)mbt* and *B52*, which are known to be required for dE2F2 function, as well as genes that were not previously linked to the E2F/pRB pathway such as *Doa*, *gfzf*, and *SLIMP* (*CG31133*). Both *gfzf* and *SLIMP* potentiate E2F-dependent activation and synergize with inactivation of RBF, suggesting that they may act in parallel to E2F. Consistent with this report, our transcriptomic analysis of SLIMP-depleted S2 cells found E2F target genes upregulated (Figure 44).

In order to determine whether the observed increase in transcript levels resulted in increased protein levels, we performed western blot analyses of several upregulated genes in the microarray (Figure 46). We analysed by immunoblot all the proteins with available *Drosophila* antibodies. We were able to detect that, upon SLIMP depletion, Cdc6 and ORC2 protein levels were upregulated. On the other hand, we could not detect increased protein levels for ORC5 or MCM2/5. Since these proteins had been described to be regulated during cell cycle progression (Ishimi, 2018; Ohta et al., 2003; Yan et al., 1993), it would be interesting to perform immunoblot analyses in cell sorted or synchronized cells, to check protein levels upon SLIMP depletion in the different cell cycle phases. Cdc6 has been extensively

described as a factor involved in DNA replication, also in *Drosophila* (Crevel et al., 2005). However, differences between species have been observed when Cdc6/18 is overexpressed. In *S. pombe*, overexpression of cdc18 causes overreplication of the DNA especially when in combination with Cdt1 overexpression (Yanow et al., 2001). In *S. cerevisiae* a delay in the initiation of M phase has been observed in a Cdc6 context, although the overall growth rate was not affected (Elsasser et al., 1996). In higher eukaryotes the effect of increased expression of Cdc6 is dependent on the phase of the cell cycle. It has been reported that in non-synchronised cells retrovirally overexpressed protein shows no effects (Petersen et al., 2000), while Cdc6 microinjection into cells in G2 phase prevented them from entering mitosis (Clay-Farrace et al., 2003). Also, adenoviral directed expression of Cdc6 in quiescent mammalian cells where is normally absent causes MCM loading, and accelerates S phase entry when coupled with serum stimulation (Cook et al., 2002). Moreover, disturbed expression of pre-RC proteins and the overexpression of Cdc6, had been described to induce rereplication (Bartkova et al., 2006; Green et al., 2010; Vaziri et al., 2003), a form of replication stress that would be fuelling genomic instability (Hanahan and Weinberg, 2011; Siddiqui et al., 2013).

Overall, these results also support the hypothesis that SLIMP-depleted cells are progressing faster from G1 to S phase. Also, we observed an increase in proteins of the replication machinery and therefore we hypothesize that SLIMP-depleted cells suffer from aberrant accumulation of replication forks. Future work may determine the role of SLIMP in replication fork regulation. DNA combing would allow us to determine the number and the correct functionality of the replication forks. Also, although we do not observe an increase in total PCNA protein, it would be interesting to

determine whether the amounts of its DNA bound form vary upon SLIMP depletion.

Our transcriptomic data, together with the upregulation of replication fork proteins and the G2 cell cycle phase accumulation, raised the question whether the SLIMP-depleted cells would have DNA damage problems. We analysed H2Av phosphorylation status by immunoblot (figure 47), but we detected normal levels of H2Av phosphorylation, indicating that SLIMP depletion does not cause DNA damage. On the other hand, the exacerbating effect of nucleoside supplementation would again suggest that SLIMP-depleted cells present a replicative problem, which is enhanced when nucleoside availability is not limiting (Figure 48).

These results suggest that SLIMP blocks nuclear DNA replication or the process of transition from G1 to S phase. Under SLIMP depletion, transcription of genes involved in replication fork formation is upregulated, inducing a faster G1 to S progression that causes temporal DNA replicative problems that need to be solved in the G2 phase, where SLIMP-depleted cells accumulate.

SLIMP homologous protein in human cells

No ortholog of SLIMP has been detected or can be found by sequence homology in the mammalian system and the search for a functional homolog is challenging. Previous studies in our laboratory have shown that the heterologous expression of SLIMP in human cell lines produces mitochondrial network fragmentation. Since the closest SLIMP homologue in mammals is SARS2, in the last chapter of this thesis we aimed to study the impact upon cell cycle progression in human cells the of overexpression or the depletion of SARS2, and the heterologous expression of *Drosophila*

melanogaster SLIMP. Cell cytometry assays showed that cell cycle was not affected under any of these conditions (Figure 49). The fact that HeLa gene expression profiles diverge significantly from those of in normal human tissues is a factor to be taken into consideration when evaluating these results, and it is possible that a primary cell culture could better help us to understand the effect of SLIMP or SARS2 in human cell cycle progression (Landry et al., 2013). Nevertheless, this work, together with other reports showing that cytosolic SerRS regulates vascular development in animals (Amsterdam et al., 2004; Herzog et al., 2009; Xu et al., 2012), highlight the facility with which the SerRS structure incorporates non-canonical regulatory functions in animals.

In summary, we propose that SLIMP evolved in arthropods as a mechanism to regulate translation and replication in mitochondria. It is possible that the coordination role of SLIMP extends to link mitochondrial physiological status with cell cycle progression. Many evolutionary and mechanistic aspects of this regulatory network remain unknown, including whether functional homologs of SLIMP exist in mammals.

CONCLUSIONS

SLIMP contains a mitochondrial signal peptide in the N-terminal region that is necessary for the protein import. SLIMP mitochondrial mature form starts form isoleucine 22.

SLIMP is localized in the mitochondrial RNA granules, interacting with SerRS2 and LON protease.

Mitochondrial SLIMP and SerRS2 protein levels are interdependent.

SLIMP/SerRS2 heterodimer is essential for mitochondrial protein translation.

SLIMP and SerRS2 are required for mitochondrial OXPHOS activity and its deficiency impairs cellular respiration.

SLIMP or SerRS2 depletion in S2 cells does not increase mitochondrial ROS production.

SLIMP interacts with the substrate binding domain of mitochondrial LON protease.

SLIMP represses TFAM degradation by LON, affecting mtDNA levels.

LON general mitochondrial protease activity is not affected by SLIMP protein levels.

SLIMP is required for cell cycle progression and its depletion accumulates *Drosophila* cells in G2 cell cycle phase.

G1 to S cell cycle phase progression is repressed by SLIMP.

SLIMP is not differentially expressed during cell cycle.

SLIMP depletion induces gene transcription and G2/M checkpoint, and upregulation of Cdc6 and ORC2 protein levels.

SLIMP depletion does not trigger apparent DNA damage.

SUPPLEMENTARY MATERIAL

Supplementary figure 1| SLIMP mitochondrial signal peptide identification. SLIMP peptides identified by mass spectrometry (in green) and the targeted peptides with the digestion of trypsin (yellow), Glu-C (blue) and Lys-C (red).

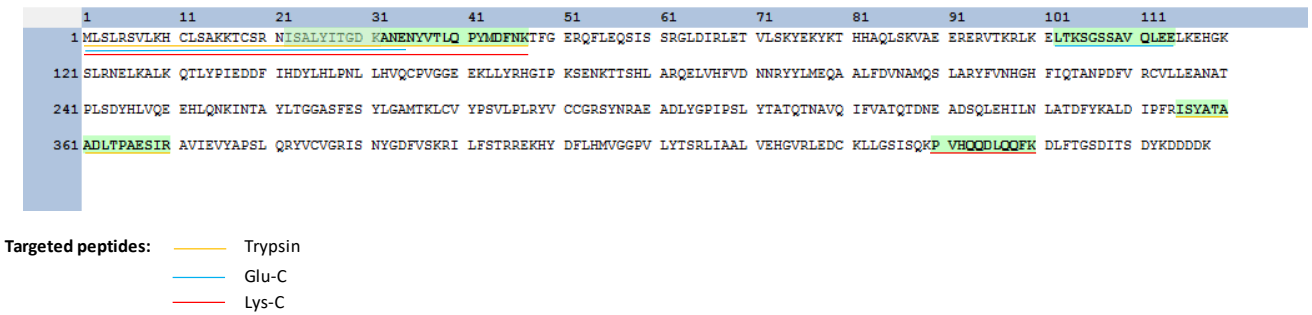

Supplementary table 1|Raw MS data for SLIMP mitochondrial signal peptide identification. Peptides detected with mass spectrometry to detect the N-terminal cleavage site of SLIMP in S2 cells.

Confidence	Identifying Node	Annotated Sequence	Protein Accessions	#Missed Cleavages	Charge	Delta Score	Delta Cn	Rank	Search Engine Rank	m/z [Da]	MH+ [Da]	DeltaM [ppm]	Deltam/z [Da]	Activation Type	MS Order	Ion Inject Time [ms]	RT [min]	First Scan
High	Trypsin	ISYATAADLTPAESIR	SLIMP	0	2	0.587	0	1	1	839.936	1678.8647	0.02	0.00002	HCD	MS2	55.5	113.214	44050
High	Trypsin	ISYATAADLTPAESIR	SLIMP	0	2	0.679	0	1	1	839.936	1678.8647	0.02	0.00002	HCD	MS2	55.5	113.266	44075
High	Trypsin	ISYATAADLTPAESIR	SLIMP	0	2	0.736	0	1	1	839.936	1678.8647	0.02	0.00002	HCD	MS2	55.5	113.307	44100
High	Trypsin	ANENYVTLQPYMDFNK	SLIMP	0	2	0.553	0	1	1	973.9513	1946.8953	0.01	0.00001	HCD	MS2	133.262	135.617	26899
High	Trypsin	ANENYVTLQPYMDFNK	SLIMP	0	2	0.83	0	1	1	973.9513	1946.8953	0.01	0.00001	HCD	MS2	216.857	135.665	26924
High	Trypsin	ANENYVTLQPYMDFNK	SLIMP	0	2	0.838	0	1	1	973.9513	1946.8953	0.01	0.00001	HCD	MS2	64.756	135.716	26949
High	Trypsin	ANENYVTLQPYMDFNK	SLIMP	0	2	0.82	0	1	1	973.9513	1946.8953	0.01	0.00001	HCD	MS2	71.923	135.759	26974
High	Trypsin	ANENYVTLQPYMDFNK	SLIMP	0	2	0.81	0	1	1	973.9513	1946.8953	0.01	0.00001	HCD	MS2	55.5	135.808	26999
High	Trypsin	ANENYVTLQPYMDFNK	SLIMP	0	2	0.82	0	1	1	973.9513	1946.8953	0.01	0.00001	HCD	MS2	60.046	135.854	27024
High	Trypsin	ANENYVTLQPYMDFNK	SLIMP	0	2	0.839	0	1	1	973.9513	1946.8953	0.01	0.00001	HCD	MS2	65.018	135.899	27049
High	Trypsin	ANENYVTLQPYMDFNK	SLIMP	0	2	0.712	0	1	1	973.9513	1946.8953	0.01	0.00001	HCD	MS2	300	135.945	27074
High	Trypsin	ANENYVTLQPYMDFNK	SLIMP	0	2	0.689	0	1	1	973.9513	1946.8953	0.01	0.00001	HCD	MS2	127.705	135.994	27099
High	LysC	PVHQQDLQQFK	SLIMP	0	3	0.515	0	1	1	456.5737	1367.7066	-0.06	-0.00003	HCD	MS2	55.5	62.509	13110
High	LysC	PVHQQDLQQFK	SLIMP	0	2	0.709	0	1	1	684.357	1367.7067	0.06	0.00004	HCD	MS2	187.884	62.5055	13109
High	LysC	PVHQQDLQQFK	SLIMP	0	3	0.618	0	1	1	456.5737	1367.7066	-0.06	-0.00003	HCD	MS2	113.994	62.4367	13087
High	LysC	PVHQQDLQQFK	SLIMP	0	2	0.804	0	1	1	684.357	1367.7067	0.06	0.00004	HCD	MS2	152.056	62.4338	13086
High	LysC	PVHQQDLQQFK	SLIMP	0	3	0.621	0	1	1	456.5737	1367.7066	-0.06	-0.00003	HCD	MS2	81.357	62.2909	13041
High	LysC	PVHQQDLQQFK	SLIMP	0	2	0.775	0	1	1	684.357	1367.7067	0.06	0.00004	HCD	MS2	300	62.3551	13063
High	LysC	PVHQQDLQQFK	SLIMP	0	2	0.755	0	1	1	684.357	1367.7067	0.06	0.00004	HCD	MS2	167.21	62.2857	13040
High	LysC	PVHQQDLQQFK	SLIMP	0	3	0.631	0	1	1	456.5737	1367.7066	-0.06	-0.00003	HCD	MS2	91.892	62.3605	13064
High	GluC	ISALYITGDKANE	SLIMP	1	2	0.649	0	1	1	697.8617	1394.7161	-0.05	-0.00004	HCD	MS2	300	102.07	19247
High	GluC	LTKSGSSAVQLEE	SLIMP	1	2	0.6	0	1	1	674.8514	1348.6955	0.02	0.00002	HCD	MS2	300	69.3852	13008
High	GluC	LTKSGSSAVQLEE	SLIMP	1	2	0.551	0	1	1	674.8514	1348.6955	0.02	0.00002	HCD	MS2	300	69.4715	13024
High	GluC	LTKSGSSAVQLEE	SLIMP	1	2	0.516	0	1	1	674.8514	1348.6955	0.02	0.00002	HCD	MS2	300	69.5577	13040
High	GluC	ISALYITGDKANE	SLIMP	1	2	0.656	0	1	1	697.8617	1394.7161	-0.05	-0.00004	HCD	MS2	300	101.898	19215
High	GluC	ISALYITGDKANE	SLIMP	1	2	0.665	0	1	1	697.8617	1394.7161	-0.05	-0.00004	HCD	MS2	300	101.984	19231
High	GluC	ISALYITGDKANE	SLIMP	1	2	0.681	0	1	1	697.8617	1394.7161	-0.05	-0.00004	HCD	MS2	300	102.156	19263

Supplementary table 2| BioID data. Results of BioID analysis with a SAINTscore >0.7. Data is plotted schematically in Figure 19.

Bait	Prey	PreyGene	Homology	SpecSum	ctrlCounts	SaintScore	FoldChange	BFDR
SLIMPBirA	Q95T19	SLIMP CG31133		426	0	1	387,27	0
SLIMPBirA	D2NUH5	c12.2 CG12149	VWA8	162	0	1	147,27	0
SLIMPBirA	M9PHH0	Glutaminase CG42708	GLS	93	1	1	76,09	0
SLIMPBirA	Q9VXY3	GstT4 CG1681	GSTT2	78	1	1	63,82	0
SLIMPBirA	Q7K3W2	SerRS2 CG4938	SARS2	52	0	1	47,27	0
SLIMPBirA	Q9VU35	Ten-m CG5723	TENM1	51	0	1	46,36	0
SLIMPBirA	M9NFI9	Prx3 CG5826	PRDX3	45	0	1	40.91	0
SLIMPBirA	Q961I1	anon-35F/36A CG4278	NIF3L1	42	0	1	38,18	0
SLIMPBirA	H8F4R0	CG10585	PDSS2	32	0	0.97	29,09	0
SLIMPBirA	Q24020	CG8728	PMPCA	142	4	1	29,05	0
SLIMPBirA	Q8MRM0	ZnT49B CG8632	SLC30A9	30	0	0.99	27,27	0
SLIMPBirA	Q95NR4	Plod CG6199	PLOD3	27	0	1	24,55	0
SLIMPBirA	Q9VYD5	Crinkled CG7595	MYO7A	28	1	0.99	22,91	0
SLIMPBirA	Q9VFF0	CG13551	ATPIF1	24	0	1	21,82	0
SLIMPBirA	P33438	GstT1 CG30000		24	0	0.95	21,82	0
SLIMPBirA	B3DN78	mRpS23 CG31842	MRPS23	24	0	0.94	21,82	0.01
SLIMPBirA	Q9VAY9	CG4882	MRPS27	22	0	0.99	20	0
SLIMPBirA	Q9VF85	CG3107	PITRM1	18	0	0.86	16,36	0.03

SLIMPBirA	Q9VPJ9	LanB2 CG3322	LAMC1	18	0	0.94	16,36	0.01
SLIMPBirA	M9PGF7	mRpS15 CG4207	MRPS15	17	0	0.84	15,45	0.04
SLIMPBirA	A0A0B4KEJ7	ref(2)P CG10360	SQSTM1	16	0	0.94	14,55	0.01
SLIMPBirA	A0APE4	Hml CG7002	OTOG	16	0	0.94	14,55	0.01
SLIMPBirA	Q9VEJ0	Myo31DF CG7438	MYO1D	17	1	0.99	13,91	0
SLIMPBirA	Q9NK57	mRF1 CG5705	MTRF1L	15	0	0.99	13,64	0
SLIMPBirA	D7QZ78	Citrate synthase CG3861	CS	15	0	0.84	13,64	0.04
SLIMPBirA	Q8T3K9	CG2100	TRNT1	15	0	0.77	13,64	0.06
SLIMPBirA	Q9VVL7	RNF-11 CG32850	RNF11	13	0	0.84	11,82	0.04
SLIMPBirA	Q9VP87	NAD kinase-2 CG8080	NADK2	13	0	0.92	11,82	0.02
SLIMPBirA	A1Z935	Got1 CG8430	GOT1	14	1	0.81	11,45	0.05
SLIMPBirA	Q7KTC0	Rme-8 CG8014		13	1	0.84	10.64	0.04
SLIMPBirA	G7H829	Lon CG8798	LON	13	1	0.71	10.64	0.08
SLIMPBirA	P11046	Ptp4E CG6899	PTPRB	11	0	0.77	10	0.06
SLIMPBirA	Q9VTH0	coro CG9446	CORO1C	47	4	1	9,61	0
SLIMPBirA	Q8MPP3	mRpS22 CG12261	MRPS22	57	5	0.99	9,33	0
SLIMPBirA	Q0E8X8	UQCR-C1 CG3731	PMPCB	68	6	1	9,27	0
SLIMPBirA	Q7K0B6	CalpB CG8107	CAPN9	10	0	0.88	9,09	0.03
SLIMPBirA	Q8IP62	Hsp10 CG11267	HSPE1	119	11	1	8,85	0
SLIMPBirA	O77477	TrpRS-m CG7441	WARS2	21	2	0.77	8,59	0.06
SLIMPBirA	Q9VVL8	CG3164	ABCG1	52	5	0.99	8,51	0
SLIMPBirA	Q9VW70	MRP CG6214	ABCC3	29	3	0.92	7,91	0.02
SLIMPBirA	A8JNU6	Nc73EF CG11661	OGDH	19	2	0.74	7,77	0.07

SLIMPBirA	Q9V9E3	LanB1 CG7123	LAMB2	28	3	0.87	7,64	0.03
SLIMPBirA	P15215	CG6459	C1QBP	46	5	0.99	7,53	0
SLIMPBirA	Q8WTC1	BSF CG10302	LRPPRC	78	9	1	7,09	0
SLIMPBirA	M9MRS7	Mmp2 CG1794		26	3	0.86	7,09	0.03
SLIMPBirA	P14199	Dihydrolipoyl dehydrogenase CG7430	DLD	35	5	0.81	5,73	0.05
SLIMPBirA	Q9U5D0	CG7668	ANGPTL5	21	3	0.76	5,73	0.07
SLIMPBirA	Q9VK20	Myo61F-RA	MYO6	90	13	1	5,66	0
SLIMPBirA	C6TP50	CG2970	STOML2	40	6	0.93	5,45	0.02
SLIMPBirA	Q9VNH2	env	CNTRL	41	7	0.92	4,79	0.02
SLIMPBirA	Q8IHB4	CG10236-RA	-	60	11	0.95	4,46	0.01
SLIMPBirA	A1Z7S0	Spn CG16757	PPP1R9A	102	22	0.93	3,79	0.02
SLIMPBirA	Q7KUT2	CG1673	BCAT1/2	69	16	0.74	3,53	0.07
SLIMPBirA	Q8SX35	Pxn CG12002	PXDN	322	77	0.91	3,42	0.02
SLIMPBirA	A0A0B4KEG0	CG5599	DBT	150	36	0.82	3,41	0.05
SLIMPBirA	Q9W4F5	fliI CG1484	FLII	87	23	0.94	3,09	0.01
SLIMPBirA	M9NE73	Glt CG9280	NLGN1	66	22	0.72	2,45	0.08

REFERENCES

Agaronyan, K., Morozov, Y.I., Anikin, M., and Temiakov, D. (2015). Mitochondrial biology. Replication-transcription switch in human mitochondria. Science *347*, 548-551.

Akiyama, H., Fujisawa, N., Tashiro, Y., Takanabe, N., Sugiyama, A., and Tashiro, F. (2003). The role of transcriptional corepressor Nif3l1 in early stage of neural differentiation via cooperation with Trip15/CSN2. The Journal of biological chemistry *278*, 10752-10762.

Alam, T.I., Kanki, T., Muta, T., Ukaji, K., Abe, Y., Nakayama, H., Takio, K., Hamasaki, N., and Kang, D. (2003). Human mitochondrial DNA is packaged with TFAM. Nucleic acids research *31*, 1640-1645.

Ambrus, A.M., Islam, A.B., Holmes, K.B., Moon, N.S., Lopez-Bigas, N., Benevolenskaya, E.V., and Frolov, M.V. (2013). Loss of dE2F compromises mitochondrial function. Developmental cell *27*, 438-451.

Ambrus, A.M., Rasheva, V.I., Nicolay, B.N., and Frolov, M.V. (2009). Mosaic genetic screen for suppressors of the de2f1 mutant phenotype in Drosophila. Genetics *183*, 79-92.

Amsterdam, A., Nissen, R.M., Sun, Z., Swindell, E.C., Farrington, S., and Hopkins, N. (2004). Identification of 315 genes essential for early zebrafish development. Proceedings of the National Academy of Sciences of the United States of America *101*, 12792-12797.

Bagga, S., and Bouchard, M.J. (2014). Cell cycle regulation during viral infection. Methods in molecular biology *1170*, 165-227.

Balakrishnan, L., and Bambara, R.A. (2013). Okazaki fragment metabolism. Cold Spring Harbor perspectives in biology *5*.

Bannai, H., Tamada, Y., Maruyama, O., Nakai, K., and Miyano, S. (2002). Extensive feature detection of N-terminal protein sorting signals. Bioinformatics *18*, 298-305.

Barshad, G., Marom, S., Cohen, T., and Mishmar, D. (2018). Mitochondrial DNA Transcription and Its Regulation: An Evolutionary Perspective. Trends in genetics : TIG *34*, 682-692.

Bartkova, J., Rezaei, N., Liontos, M., Karakaidos, P., Kletsas, D., Issaeva, N., Vassiliou, L.V., Kolettas, E., Niforou, K., Zoumpourlis, V.C.*, et al.* (2006). Oncogene-induced senescence is part of the tumorigenesis barrier imposed by DNA damage checkpoints. Nature *444*, 633-637.

Bauer, M.F., Hofmann, S., Neupert, W., and Brunner, M. (2000). Protein translocation into mitochondria: the role of TIM complexes. Trends in cell biology *10*, 25-31.

Belostotsky, R., Ben-Shalom, E., Rinat, C., Becker-Cohen, R., Feinstein, S., Zeligson, S., Segel, R., Elpeleg, O., Nassar, S., and Frishberg, Y. (2011). Mutations in the mitochondrial seryl-tRNA synthetase cause hyperuricemia, pulmonary hypertension, renal failure in infancy and alkalosis, HUPRA syndrome. American journal of human genetics *88*, 193-200.

Benda, C. (1898). Ueber die spermatogenese der vertebraten und höherer evertebraten, II. Theil: Die histiogenese der spermien. Arch Anat Physiol *73*, 393-398.

Benevolenskaya, E.V., and Frolov, M.V. (2015). Emerging links between E2F control and mitochondrial function. Cancer research *75*, 619-623.

Bertoli, C., Skotheim, J.M., and de Bruin, R.A. (2013). Control of cell cycle transcription during G1 and S phases. Nature reviews. Molecular cell biology *14*, 518-528.

Bezawork-Geleta, A., Brodie, E.J., Dougan, D.A., and Truscott, K.N. (2015). LON is the master protease that protects against protein aggregation in human mitochondria through direct degradation of misfolded proteins. Scientific reports *5*, 17397.

Blais, A., and Dynlacht, B.D. (2004). Hitting their targets: an emerging picture of E2F and cell cycle control. Current opinion in genetics & development *14*, 527-532.

Bleichert, F., Botchan, M.R., and Berger, J.M. (2017). Mechanisms for initiating cellular DNA replication. Science *355*.

Blobel, G., and Dobberstein, B. (1975). Transfer of proteins across membranes. I. Presence of proteolytically processed and unprocessed nascent immunoglobulin light chains on membrane-bound ribosomes of murine myeloma. The Journal of cell biology *67*, 835-851.

Bobrowicz, A.J., Lightowlers, R.N., and Chrzanowska-Lightowlers, Z. (2008). Polyadenylation and degradation of mRNA in mammalian mitochondria: a missing link? Biochemical Society transactions *36*, 517-519.

Bode, A.M., and Dong, Z. (2005). Inducible covalent posttranslational modification of histone H3. Science's STKE : signal transduction knowledge environment *2005*, re4.

Bogenhagen, D.F. (2012). Mitochondrial DNA nucleoid structure. Biochimica et biophysica acta *1819*, 914-920.

Bolstad, B.M., Collin, F., Simpson, K.M., Irizarry, R.A., and Speed, T.P. (2004). Experimental design and low-level analysis of microarray data. International review of neurobiology *60*, 25-58.

Bota, D.A., and Davies, K.J. (2002). Lon protease preferentially degrades oxidized mitochondrial aconitase by an ATP-stimulated mechanism. Nature cell biology *4*, 674-680.

Brand, M.D. (1990). The proton leak across the mitochondrial inner membrane. Biochimica et biophysica acta *1018*, 128-133.

Brand, M.D., and Nicholls, D.G. (2011). Assessing mitochondrial dysfunction in cells. The Biochemical journal *435*, 297-312.

Burnett, B.J., Altman, R.B., Ferguson, A., Wasserman, M.R., Zhou, Z., and Blanchard, S.C. (2014). Direct evidence of an elongation factor-Tu/Ts.GTP.Aminoacyl-tRNA quaternary complex. The Journal of biological chemistry *289*, 23917-23927.

Campbell, S.D., Sprenger, F., Edgar, B.A., and O'Farrell, P.H. (1995). Drosophila Wee1 kinase rescues fission yeast from mitotic catastrophe and phosphorylates Drosophila Cdc2 in vitro. Molecular biology of the cell *6*, 1333-1347.

Cardaioli, E., Da Pozzo, P., Cerase, A., Sicurelli, F., Malandrini, A., De Stefano, N., Stromillo, M.L., Battisti, C., Dotti, M.T., and Federico, A. (2006). Rapidly progressive neurodegeneration in a case with the 7472insC mutation and the A7472C polymorphism in the mtDNA tRNA ser(UCN) gene. Neuromuscular disorders : NMD *16*, 26-31.

Carter, C.W., Jr. (2017). Coding of Class I and II Aminoacyl-tRNA Synthetases. Advances in experimental medicine and biology *966*, 103-148.

Chandel, N.S. (2014). Mitochondria as signaling organelles. BMC biology *12*, 34.

Chimnaronk, S., Gravers Jeppesen, M., Suzuki, T., Nyborg, J., and Watanabe, K. (2005). Dual-mode recognition of noncanonical tRNAs(Ser) by seryl-tRNA synthetase in mammalian mitochondria. The EMBO journal *24*, 3369-3379.

Christian, B.E., and Spremulli, L.L. (2012). Mechanism of protein biosynthesis in mammalian mitochondria. Biochimica et biophysica acta *1819*, 1035-1054.

Chrzanowska-Lightowlers, Z.M., Pajak, A., and Lightowlers, R.N. (2011). Termination of protein synthesis in mammalian mitochondria. The Journal of biological chemistry *286*, 34479-34485.

Ciesielski, G.L., Oliveira, M.T., and Kaguni, L.S. (2016). Animal Mitochondrial DNA Replication. The Enzymes *39*, 255-292.

Clay-Farrace, L., Pelizon, C., Santamaria, D., Pines, J., and Laskey, R.A. (2003). Human replication protein Cdc6 prevents mitosis through a checkpoint mechanism that implicates Chk1. The EMBO journal *22*, 704-712.

Cook, J.G., Park, C.H., Burke, T.W., Leone, G., DeGregori, J., Engel, A., and Nevins, J.R. (2002). Analysis of Cdc6 function in the assembly of mammalian prereplication complexes. Proceedings of the National Academy of Sciences of the United States of America *99*, 1347-1352.

Cooper, G.M. (2018). The Cell: A Molecular Approach (Oxford University Press).

Couvillion, M.T., Soto, I.C., Shipkovenska, G., and Churchman, L.S. (2016). Synchronized mitochondrial and cytosolic translation programs. Nature *533*, 499-503.

Crevel, G., Mathe, E., and Cotterill, S. (2005). The Drosophila Cdc6/18 protein has functions in both early and late S phase in S2 cells. Journal of cell science *118*, 2451-2459.

Crick, F.H. (1958). On protein synthesis. Symposia of the Society for Experimental Biology *12*, 138-163.

Cusack, S., Berthet-Colominas, C., Hartlein, M., Nassar, N., and Leberman, R. (1990). A second class of synthetase structure revealed by X-ray analysis of Escherichia coli seryl-tRNA synthetase at 2.5 A. Nature *347*, 249-255.

Derive, N., Landmann, C., Montembault, E., Claverie, M.C., Pierre-Elies, P., Goutte-Gattat, D., Founounou, N., McCusker, D., and Royou, A. (2015). Bub3-BubR1-dependent sequestration of Cdc20Fizzy at DNA breaks facilitates the correct segregation of broken chromosomes. The Journal of cell biology *211*, 517-532.

Deshmukh, P., Unni, S., Krishnappa, G., and Padmanabhan, B. (2017). The Keap1-Nrf2 pathway: promising therapeutic target to counteract ROS-mediated damage in cancers and neurodegenerative diseases. Biophysical reviews *9*, 41-56.

Dever, T.E., and Green, R. (2012). The elongation, termination, and recycling phases of translation in eukaryotes. Cold Spring Harbor perspectives in biology *4*, a013706.

Dewar, J.M., Budzowska, M., and Walter, J.C. (2015). The mechanism of DNA replication termination in vertebrates. Nature *525*, 345-350.

Dewar, J.M., and Walter, J.C. (2017). Mechanisms of DNA replication termination. Nature reviews. Molecular cell biology *18*, 507-516.

Di Talia, S., and Wieschaus, E.F. (2012). Short-term integration of Cdc25 dynamics controls mitotic entry during Drosophila gastrulation. Developmental cell *22*, 763-774.

Dubrovsky, E.B., Dubrovskaya, V.A., Levinger, L., Schiffer, S., and Marchfelder, A. (2004). Drosophila RNase Z processes mitochondrial and nuclear pre-tRNA 3' ends in vivo. Nucleic acids research *32*, 255-262.

Edgar, B.A., and Lehner, C.F. (1996). Developmental control of cell cycle regulators: a fly's perspective. Science *274*, 1646-1652.

El-Gebali, S., Mistry, J., Bateman, A., Eddy, S.R., Luciani, A., Potter, S.C., Qureshi, M., Richardson, L.J., Salazar, G.A., Smart, A.*, et al.* (2018). The Pfam protein families database in 2019. Nucleic acids research.

Elsasser, S., Lou, F., Wang, B., Campbell, J.L., and Jong, A. (1996). Interaction between yeast Cdc6 protein and B-type cyclin/Cdc28 kinases. Molecular biology of the cell *7*, 1723-1735.

Fishovitz, J., Li, M., Frase, H., Hudak, J., Craig, S., Ko, K., Berdis, A.J., Suzuki, C.K., and Lee, I. (2011). Active-site-directed chemical tools for profiling mitochondrial Lon protease. ACS chemical biology *6*, 781-788.

Fragkos, M., Ganier, O., Coulombe, P., and Mechali, M. (2015). DNA replication origin activation in space and time. Nature reviews. Molecular cell biology *16*, 360-374.

Friguet, B., Bulteau, A.L., and Petropoulos, I. (2008). Mitochondrial protein quality control: implications in ageing. Biotechnology journal *3*, 757-764.

Fringer, J.M., Acker, M.G., Fekete, C.A., Lorsch, J.R., and Dever, T.E. (2007). Coupled release of eukaryotic translation initiation factors 5B and 1A from 80S ribosomes following subunit joining. Molecular and cellular biology *27*, 2384-2397.

Fukasawa, Y., Tsuji, J., Fu, S.C., Tomii, K., Horton, P., and Imai, K. (2015). MitoFates: improved prediction of mitochondrial targeting sequences and their cleavage sites. Molecular & cellular proteomics : MCP *14*, 1113-1126.

Fukui, H., Hanaoka, R., and Kawahara, A. (2009). Noncanonical activity of seryl-tRNA synthetase is involved in vascular development. Circulation research *104*, 1253-1259.

Fuse, Y., and Kobayashi, M. (2017). Conservation of the Keap1-Nrf2 System: An Evolutionary Journey through Stressful Space and Time. Molecules *22*.

Garesse, R., and Kaguni, L.S. (2005). A Drosophila model of mitochondrial DNA replication: proteins, genes and regulation. IUBMB life *57*, 555-561.

Gaspari, M., Falkenberg, M., Larsson, N.G., and Gustafsson, C.M. (2004). The mitochondrial RNA polymerase contributes critically to promoter specificity in mammalian cells. The EMBO journal *23*, 4606-4614.

Gaur, R., Grasso, D., Datta, P.P., Krishna, P.D., Das, G., Spencer, A., Agrawal, R.K., Spremulli, L., and Varshney, U. (2008). A single mammalian mitochondrial translation initiation factor functionally replaces two bacterial factors. Molecular cell *29*, 180-190.

Georgescu, R., Yuan, Z., Bai, L., de Luna Almeida Santos, R., Sun, J., Zhang, D., Yurieva, O., Li, H., and O'Donnell, M.E. (2017). Structure of eukaryotic CMG helicase at a replication fork and implications to replisome architecture and origin initiation. Proceedings of the National Academy of Sciences of the United States of America *114*, E697-E706.

Giege, R., Sissler, M., and Florentz, C. (1998). Universal rules and idiosyncratic features in tRNA identity. Nucleic acids research *26*, 5017-5035.

Gonzalez-Roca, E., Garcia-Albeniz, X., Rodriguez-Mulero, S., Gomis, R.R., Kornacker, K., and Auer, H. (2010). Accurate expression profiling of very small cell populations. PloS one *5*, e14418.

Goto, H., Tomono, Y., Ajiro, K., Kosako, H., Fujita, M., Sakurai, M., Okawa, K., Iwamatsu, A., Okigaki, T., Takahashi, T.*, et al.* (1999). Identification of a novel phosphorylation site on histone H3 coupled with mitotic chromosome condensation. The Journal of biological chemistry *274*, 25543-25549.

Green, B.M., Finn, K.J., and Li, J.J. (2010). Loss of DNA replication control is a potent inducer of gene amplification. Science *329*, 943-946.

Guitart, T., Leon Bernardo, T., Sagales, J., Stratmann, T., Bernues, J., and Ribas de Pouplana, L. (2010). New aminoacyl-tRNA synthetase-like protein in insecta with an essential mitochondrial function. The Journal of biological chemistry *285*, 38157-38166.

Guitart, T., Picchioni, D., Pineyro, D., and Ribas de Pouplana, L. (2013). Human mitochondrial disease-like symptoms caused by a reduced tRNA aminoacylation activity in flies. Nucleic acids research *41*, 6595-6608.

Guo, M., and Schimmel, P. (2013). Essential nontranslational functions of tRNA synthetases. Nature chemical biology *9*, 145-153.

Guo, M., Yang, X.L., and Schimmel, P. (2010). New functions of aminoacyl-tRNA synthetases beyond translation. Nature reviews. Molecular cell biology *11*, 668-674.

Guo, Y., Flegel, K., Kumar, J., McKay, D.J., and Buttitta, L.A. (2016). Ecdysone signaling induces two phases of cell cycle exit in Drosophila cells. Biology open *5*, 1648-1661.

Gustafsson, C.M., Falkenberg, M., and Larsson, N.G. (2016). Maintenance and Expression of Mammalian Mitochondrial DNA. Annual review of biochemistry *85*, 133-160.

Hallberg, B.M., and Larsson, N.G. (2014). Making proteins in the powerhouse. Cell metabolism *20*, 226-240.

Hanahan, D., and Weinberg, R.A. (2011). Hallmarks of cancer: the next generation. Cell *144*, 646-674.

Harashima, H., Dissmeyer, N., and Schnittger, A. (2013). Cell cycle control across the eukaryotic kingdom. Trends in cell biology *23*, 345-356.

Hartmann, R.K., Gossringer, M., Spath, B., Fischer, S., and Marchfelder, A. (2009). The making of tRNAs and more - RNase P and tRNase Z. Progress in molecular biology and translational science *85*, 319-368.

Hartwell, L.H., and Weinert, T.A. (1989). Checkpoints: controls that ensure the order of cell cycle events. Science *246*, 629-634.

Hatefi, Y. (1985). The mitochondrial electron transport and oxidative phosphorylation system. Annual review of biochemistry *54*, 1015-1069.

Hernández, G., and Jagus, R. (2016). Evolution of the protein synthesis machinery and its regulation.

Herzog, W., Muller, K., Huisken, J., and Stainier, D.Y. (2009). Genetic evidence for a noncanonical function of seryl-tRNA synthetase in vascular development. Circulation research *104*, 1260-1266.

Hillen, H.S., Parshin, A.V., Agaronyan, K., Morozov, Y.I., Graber, J.J., Chernev, A., Schwinghammer, K., Urlaub, H., Anikin, M., Cramer, P.*, et al.* (2017). Mechanism of Transcription Anti-termination in Human Mitochondria. Cell *171*, 1082-1093 e1013.

Hinnebusch, A.G. (2014). The scanning mechanism of eukaryotic translation initiation. Annual review of biochemistry *83*, 779-812.

Hutchin, T.P., Navarro-Coy, N.C., Van Camp, G., Tiranti, V., Zeviani, M., Schuelke, M., Jaksch, M., Newton, V., and Mueller, R.F. (2001). Multiple origins of the mtDNA 7472insC mutation associated with hearing loss and neurological dysfunction. European journal of human genetics : EJHG *9*, 385-387.

Ibba, M., and Soll, D. (2000). Aminoacyl-tRNA synthesis. Annual review of biochemistry *69*, 617-650.

Ilves, I., Petojevic, T., Pesavento, J.J., and Botchan, M.R. (2010). Activation of the MCM2-7 helicase by association with Cdc45 and GINS proteins. Molecular cell *37*, 247-258.

Irizarry, R.A., Bolstad, B.M., Collin, F., Cope, L.M., Hobbs, B., and Speed, T.P. (2003). Summaries of Affymetrix GeneChip probe level data. Nucleic acids research *31*, e15.

Ishimi, Y. (2018). Regulation of MCM2-7 function. Genes & genetic systems *93*, 125-133.

Itoh, K., Ye, P., Matsumiya, T., Tanji, K., and Ozaki, T. (2015). Emerging functional cross-talk between the Keap1-Nrf2 system and mitochondria. Journal of clinical biochemistry and nutrition *56*, 91-97.

Jackson, R.J., Hellen, C.U., and Pestova, T.V. (2010). The mechanism of eukaryotic translation initiation and principles of its regulation. Nature reviews. Molecular cell biology *11*, 113-127.

Jackson, R.J., Hellen, C.U., and Pestova, T.V. (2012). Termination and post-termination events in eukaryotic translation. Advances in protein chemistry and structural biology *86*, 45-93.

Joers, P., and Jacobs, H.T. (2013). Analysis of replication intermediates indicates that Drosophila melanogaster mitochondrial DNA replicates by a strand-coupled theta mechanism. PloS one *8*, e53249.

Jonsson, Z.O., and Hubscher, U. (1997). Proliferating cell nuclear antigen: more than a clamp for DNA polymerases. BioEssays : news and reviews in molecular, cellular and developmental biology *19*, 967-975.

Jukes, T.H., and Osawa, S. (1993). Evolutionary changes in the genetic code. Comparative biochemistry and physiology. B, Comparative biochemistry *106*, 489-494.

Jung, E.J., Liu, G., Zhou, W., and Chen, X. (2006). Myosin VI is a mediator of the p53-dependent cell survival pathway. Molecular and cellular biology *26*, 2175-2186.

Kelley, L.A., Mezulis, S., Yates, C.M., Wass, M.N., and Sternberg, M.J. (2015). The Phyre2 web portal for protein modeling, prediction and analysis. Nature protocols *10*, 845-858.

Kotiadis, V.N., Duchen, M.R., and Osellame, L.D. (2014). Mitochondrial quality control and communications with the nucleus are important in maintaining mitochondrial function and cell health. Biochimica et biophysica acta *1840*, 1254-1265.

Kozak, M. (1986). Point mutations define a sequence flanking the AUG initiator codon that modulates translation by eukaryotic ribosomes. Cell *44*, 283-292.

Kunz, B.A., Kohalmi, S.E., Kunkel, T.A., Mathews, C.K., McIntosh, E.M., and Reidy, J.A. (1994). International Commission for Protection Against Environmental Mutagens and Carcinogens. Deoxyribonucleoside triphosphate levels: a critical factor in the maintenance of genetic stability. Mutation research *318*, 1-64.

Landry, J.J., Pyl, P.T., Rausch, T., Zichner, T., Tekkedil, M.M., Stutz, A.M., Jauch, A., Aiyar, R.S., Pau, G., Delhomme, N.*, et al.* (2013). The genomic and transcriptomic landscape of a HeLa cell line. G3 *3*, 1213-1224.

Leadsham, J.E., Sanders, G., Giannaki, S., Bastow, E.L., Hutton, R., Naeimi, W.R., Breitenbach, M., and Gourlay, C.W. (2013). Loss of cytochrome c oxidase promotes RAS-dependent ROS production from the ER resident NADPH oxidase, Yno1p, in yeast. Cell metabolism *18*, 279-286.

Lee, Y.H., Campbell, H.D., and Stallcup, M.R. (2004). Developmentally essential protein flightless I is a nuclear receptor coactivator with actin binding activity. Molecular and cellular biology *24*, 2103-2117.

Liang, L., Haug, J.S., Seidel, C.W., and Gibson, M.C. (2014). Functional genomic analysis of the periodic transcriptome in the developing Drosophila wing. Developmental cell *29*, 112-127.

Lodish, H.F. (2000). Molecular cell biology, 4th edn (New York: W.H. Freeman).

Lopes, C.S., Sampaio, P., Williams, B., Goldberg, M., and Sunkel, C.E. (2005). The Drosophila Bub3 protein is required for the mitotic checkpoint and for normal

accumulation of cyclins during G2 and early stages of mitosis. Journal of cell science *118*, 187-198.

Lu, B., Lee, J., Nie, X., Li, M., Morozov, Y.I., Venkatesh, S., Bogenhagen, D.F., Temiakov, D., and Suzuki, C.K. (2013). Phosphorylation of human TFAM in mitochondria impairs DNA binding and promotes degradation by the AAA+ Lon protease. Molecular cell *49*, 121-132.

Lu, J., Marygold, S.J., Gharib, W.H., and Suter, B. (2015). The aminoacyl-tRNA synthetases of Drosophila melanogaster. Fly *9*, 53-61.

Lujan, S.A., Williams, J.S., and Kunkel, T.A. (2016). DNA Polymerases Divide the Labor of Genome Replication. Trends in cell biology *26*, 640-654.

Luse, D.S. (2014). The RNA polymerase II preinitiation complex. Through what pathway is the complex assembled? Transcription *5*, e27050.

Matsushima, Y., Adan, C., Garesse, R., and Kaguni, L.S. (2005). Drosophila mitochondrial transcription factor B1 modulates mitochondrial translation but not transcription or DNA copy number in Schneider cells. The Journal of biological chemistry *280*, 16815-16820.

Matsushima, Y., Garesse, R., and Kaguni, L.S. (2004). Drosophila mitochondrial transcription factor B2 regulates mitochondrial DNA copy number and transcription in schneider cells. The Journal of biological chemistry *279*, 26900-26905.

Matsushima, Y., Goto, Y., and Kaguni, L.S. (2010). Mitochondrial Lon protease regulates mitochondrial DNA copy number and transcription by selective degradation of mitochondrial transcription factor A (TFAM). Proceedings of the National Academy of Sciences of the United States of America *107*, 18410-18415.

Matsushima, Y., and Kaguni, L.S. (2012). Matrix proteases in mitochondrial DNA function. Biochimica et biophysica acta *1819*, 1080-1087.

McGuffin, L.J., Bryson, K., and Jones, D.T. (2000). The PSIPRED protein structure prediction server. Bioinformatics *16*, 404-405.

Meng, H., Yamashita, C., Hattori, N., and Imai, Y. (2017). Measurements of the mitochondrial respiration and glycolytic activity in Drosophila embryonic cells.

Minczuk, M., He, J., Duch, A.M., Ettema, T.J., Chlebowski, A., Dzionek, K., Nijtmans, L.G., Huynen, M.A., and Holt, I.J. (2011). TEFM (c17orf42) is necessary for transcription of human mtDNA. Nucleic acids research *39*, 4284-4299.

Monaghan, R.M., and Whitmarsh, A.J. (2015). Mitochondrial Proteins Moonlighting in the Nucleus. Trends in biochemical sciences *40*, 728-735.

Murphy, M.P. (2009). How mitochondria produce reactive oxygen species. The Biochemical journal *417*, 1-13.

Nargund, A.M., Pellegrino, M.W., Fiorese, C.J., Baker, B.M., and Haynes, C.M. (2012). Mitochondrial import efficiency of ATFS-1 regulates mitochondrial UPR activation. Science *337*, 587-590.

Neufeld, T.P., de la Cruz, A.F., Johnston, L.A., and Edgar, B.A. (1998). Coordination of growth and cell division in the Drosophila wing. Cell *93*, 1183-1193.

Ngo, H.B., Kaiser, J.T., and Chan, D.C. (2011). The mitochondrial transcription and packaging factor Tfam imposes a U-turn on mitochondrial DNA. Nature structural & molecular biology *18*, 1290-1296.

Nielsen, H., Engelbrecht, J., Brunak, S., and von Heijne, G. (1997). Identification of prokaryotic and eukaryotic signal peptides and prediction of their cleavage sites. Protein engineering *10*, 1-6.

Nikolov, D.B., and Burley, S.K. (1997). RNA polymerase II transcription initiation: a structural view. Proceedings of the National Academy of Sciences of the United States of America *94*, 15-22.

Ohta, S., Tatsumi, Y., Fujita, M., Tsurimoto, T., and Obuse, C. (2003). The ORC1 cycle in human cells: II. Dynamic changes in the human ORC complex during the cell cycle. The Journal of biological chemistry *278*, 41535-41540.

Ojala, D., Montoya, J., and Attardi, G. (1981). tRNA punctuation model of RNA processing in human mitochondria. Nature *290*, 470-474.

Pagliarini, D.J., and Rutter, J. (2013). Hallmarks of a new era in mitochondrial biochemistry. Genes & development *27*, 2615-2627.

Pai, C.C., and Kearsey, S.E. (2017). A Critical Balance: dNTPs and the Maintenance of Genome Stability. Genes *8*.

Palade, G.E. (1952). The fine structure of mitochondria. The Anatomical record *114*, 427-451.

Pareek, G., Thomas, R.E., Vincow, E.S., Morris, D.R., and Pallanck, L.J. (2018). Lon protease inactivation in Drosophila causes unfolded protein stress and inhibition of mitochondrial translation. Cell death discovery *5*, 51.

Park, S.C., Jia, B., Yang, J.K., Van, D.L., Shao, Y.G., Han, S.W., Jeon, Y.J., Chung, C.H., and Cheong, G.W. (2006). Oligomeric structure of the ATP-dependent protease La (Lon) of Escherichia coli. Molecules and cells *21*, 129-134.

Park, S.G., Schimmel, P., and Kim, S. (2008). Aminoacyl tRNA synthetases and their connections to disease. Proceedings of the National Academy of Sciences of the United States of America *105*, 11043-11049.

Parker, M.W., Botchan, M.R., and Berger, J.M. (2017). Mechanisms and regulation of DNA replication initiation in eukaryotes. Critical reviews in biochemistry and molecular biology *52*, 107-144.

Pearce, S.F., Rebelo-Guiomar, P., D'Souza, A.R., Powell, C.A., Van Haute, L., and Minczuk, M. (2017). Regulation of Mammalian Mitochondrial Gene Expression: Recent Advances. Trends in biochemical sciences *42*, 625-639.

Perez, Y., Shorer, Z., Liani-Leibson, K., Chabosseau, P., Kadir, R., Volodarsky, M., Halperin, D., Barber-Zucker, S., Shalev, H., Schreiber, R.*, et al.* (2017). SLC30A9 mutation affecting intracellular zinc homeostasis causes a novel cerebro-renal syndrome. Brain : a journal of neurology *140*, 928-939.

Perkins, G., and Diffley, J.F. (1998). Nucleotide-dependent prereplicative complex assembly by Cdc6p, a homolog of eukaryotic and prokaryotic clamp-loaders. Molecular cell *2*, 23-32.

Pestova, T.V., and Kolupaeva, V.G. (2002). The roles of individual eukaryotic translation initiation factors in ribosomal scanning and initiation codon selection. Genes & development *16*, 2906-2922.

Petersen, B.O., Wagener, C., Marinoni, F., Kramer, E.R., Melixetian, M., Lazzerini Denchi, E., Gieffers, C., Matteucci, C., Peters, J.M., and Helin, K. (2000). Cell cycle- and cell growth-regulated proteolysis of mammalian CDC6 is dependent on APC-CDH1. Genes & development *14*, 2330-2343.

Pietenpol, J.A., and Stewart, Z.A. (2002). Cell cycle checkpoint signaling: cell cycle arrest versus apoptosis. Toxicology *181-182*, 475-481.

Pietromonaco, S.F., Denslow, N.D., and O'Brien, T.W. (1991). Proteins of mammalian mitochondrial ribosomes. Biochimie *73*, 827-835.

Pinti, M., Gibellini, L., Liu, Y., Xu, S., Lu, B., and Cossarizza, A. (2015). Mitochondrial Lon protease at the crossroads of oxidative stress, ageing and cancer. Cellular and molecular life sciences : CMLS *72*, 4807-4824.

Pinti, M., Gibellini, L., Nasi, M., De Biasi, S., Bortolotti, C.A., Iannone, A., and Cossarizza, A. (2016). Emerging role of Lon protease as a master regulator of mitochondrial functions. Biochimica et biophysica acta *1857*, 1300-1306.

Pisarev, A.V., Hellen, C.U., and Pestova, T.V. (2007). Recycling of eukaryotic posttermination ribosomal complexes. Cell *131*, 286-299.

Pitoniak, A., and Bohmann, D. (2015). Mechanisms and functions of Nrf2 signaling in Drosophila. Free radical biology & medicine *88*, 302-313.

Porrua, O., and Libri, D. (2015). Transcription termination and the control of the transcriptome: why, where and how to stop. Nature reviews. Molecular cell biology *16*, 190-202.

Posse, V., Shahzad, S., Falkenberg, M., Hallberg, B.M., and Gustafsson, C.M. (2015). TEFM is a potent stimulator of mitochondrial transcription elongation in vitro. Nucleic acids research *43*, 2615-2624.

Postow, L., Crisona, N.J., Peter, B.J., Hardy, C.D., and Cozzarelli, N.R. (2001). Topological challenges to DNA replication: conformations at the fork. Proceedings of the National Academy of Sciences of the United States of America *98*, 8219-8226.

Preis, A., Heuer, A., Barrio-Garcia, C., Hauser, A., Eyler, D.E., Berninghausen, O., Green, R., Becker, T., and Beckmann, R. (2014). Cryoelectron microscopic structures of eukaryotic translation termination complexes containing eRF1-eRF3 or eRF1-ABCE1. Cell reports *8*, 59-65.

Quiros, P.M., Mottis, A., and Auwerx, J. (2016). Mitonuclear communication in homeostasis and stress. Nature reviews. Molecular cell biology *17*, 213-226.

R Development Core Team (2008). R: A language and enviornment for statistical computing. (R Foundation for Statistical Computing).

Ramakrishnan, V. (2002). Ribosome structure and the mechanism of translation. Cell *108*, 557-572.

Reichard, P. (1988). Interactions between deoxyribonucleotide and DNA synthesis. Annual review of biochemistry *57*, 349-374.

Reis, T., and Edgar, B.A. (2004). Negative regulation of dE2F1 by cyclin-dependent kinases controls cell cycle timing. Cell *117*, 253-264.

Ribas de Pouplana, L., and Schimmel, P. (2001). Two classes of tRNA synthetases suggested by sterically compatible dockings on tRNA acceptor stem. Cell *104*, 191-193.

Ritchie, M.E., Phipson, B., Wu, D., Hu, Y., Law, C.W., Shi, W., and Smyth, G.K. (2015). limma powers differential expression analyses for RNA-sequencing and microarray studies. Nucleic acids research *43*, e47.

Roberti, M., Bruni, F., Polosa, P.L., Gadaleta, M.N., and Cantatore, P. (2006). The Drosophila termination factor DmTTF regulates in vivo mitochondrial transcription. Nucleic acids research *34*, 2109-2116.

Rossetto, D., Avvakumov, N., and Cote, J. (2012). Histone phosphorylation: a chromatin modification involved in diverse nuclear events. Epigenetics *7*, 1098-1108.

Rubio-Cosials, A., Sidow, J.F., Jimenez-Menendez, N., Fernandez-Millan, P., Montoya, J., Jacobs, H.T., Coll, M., Bernado, P., and Sola, M. (2011). Human mitochondrial transcription factor A induces a U-turn structure in the light strand promoter. Nature structural & molecular biology *18*, 1281-1289.

Sainsbury, S., Bernecky, C., and Cramer, P. (2015). Structural basis of transcription initiation by RNA polymerase II. Nature reviews. Molecular cell biology *16*, 129-143.

Saisawang, C., Wongsantichon, J., and Ketterman, A.J. (2012). A preliminary characterization of the cytosolic glutathione transferase proteome from Drosophila melanogaster. The Biochemical journal *442*, 181-190.

Sanchez, M.I., Mercer, T.R., Davies, S.M., Shearwood, A.M., Nygard, K.K., Richman, T.R., Mattick, J.S., Rackham, O., and Filipovska, A. (2011). RNA processing in human mitochondria. Cell cycle *10*, 2904-2916.

Savojardo, C., Martelli, P.L., Fariselli, P., and Casadio, R. (2015). TPpred3 detects and discriminates mitochondrial and chloroplastic targeting peptides in eukaryotic proteins. Bioinformatics *31*, 3269-3275.

Shi, Y., Dierckx, A., Wanrooij, P.H., Wanrooij, S., Larsson, N.G., Wilhelmsson, L.M., Falkenberg, M., and Gustafsson, C.M. (2012). Mammalian transcription factor A is a core component of the mitochondrial transcription machinery. Proceedings of the National Academy of Sciences of the United States of America *109*, 16510-16515.

Shoemaker, C.B., and Chalkley, R. (1978). An H3 histone-specific kinase isolated from bovine thymus chromatin. The Journal of biological chemistry *253*, 5802-5807.

Siddiqui, K., On, K.F., and Diffley, J.F. (2013). Regulating DNA replication in eukarya. Cold Spring Harbor perspectives in biology *5*.

Siu, K.T., Rosner, M.R., and Minella, A.C. (2012). An integrated view of cyclin E function and regulation. Cell cycle *11*, 57-64.

Sjostrand, F.S. (1953). Electron microscopy of mitochondria and cytoplasmic double membranes. Nature *171*, 30-32.

Smits, P., Smeitink, J., and van den Heuvel, L. (2010). Mitochondrial translation and beyond: processes implicated in combined oxidative phosphorylation deficiencies. J Biomed Biotechnol *2010*, 737385.

Sokabe, M., and Fraser, C.S. (2014). Human eukaryotic initiation factor 2 (eIF2)-GTP-Met-tRNAi ternary complex and eIF3 stabilize the 43 S preinitiation complex. The Journal of biological chemistry *289*, 31827-31836.

Sologub, M., Litonin, D., Anikin, M., Mustaev, A., and Temiakov, D. (2009). TFB2 is a transient component of the catalytic site of the human mitochondrial RNA polymerase. Cell *139*, 934-944.

Sonenberg, N., and Hinnebusch, A.G. (2009). Regulation of translation initiation in eukaryotes: mechanisms and biological targets. Cell *136*, 731-745.

Stahlberg, H., Kutejova, E., Suda, K., Wolpensinger, B., Lustig, A., Schatz, G., Engel, A., and Suzuki, C.K. (1999). Mitochondrial Lon of Saccharomyces cerevisiae is a ring-shaped protease with seven flexible subunits. Proceedings of the National Academy of Sciences of the United States of America *96*, 6787-6790.

Steitz, T.A. (2008). A structural understanding of the dynamic ribosome machine. Nature reviews. Molecular cell biology *9*, 242-253.

Stumpff, J., Duncan, T., Homola, E., Campbell, S.D., and Su, T.T. (2004). Drosophila Wee1 kinase regulates Cdk1 and mitotic entry during embryogenesis. Current biology : CB *14*, 2143-2148.

Swalwell, H., Blakely, E.L., Sutton, R., Tonska, K., Elstner, M., He, L., Taivassalo, T., Burns, D.K., Turnbull, D.M., Haller, R.G*., et al.* (2008). A homoplasmic mtDNA variant can influence the phenotype of the pathogenic m.7472Cins MTTS1 mutation: are two mutations better than one? European journal of human genetics : EJHG *16*, 1265-1274.

Talbert, P.B., and Henikoff, S. (2010). Histone variants--ancient wrap artists of the epigenome. Nature reviews. Molecular cell biology *11*, 264-275.

Teng, H., Wu, B., Zhao, K., Yang, G., Wu, L., and Wang, R. (2013). Oxygen-sensitive mitochondrial accumulation of cystathionine beta-synthase mediated by

Lon protease. Proceedings of the National Academy of Sciences of the United States of America *110*, 12679-12684.

Teo, G., Liu, G., Zhang, J., Nesvizhskii, A.I., Gingras, A.C., and Choi, H. (2014). SAINTexpress: improvements and additional features in Significance Analysis of INTeractome software. Journal of proteomics *100*, 37-43.

Tiranti, V., Chariot, P., Carella, F., Toscano, A., Soliveri, P., Girlanda, P., Carrara, F., Fratta, G.M., Reid, F.M., Mariotti, C.*, et al.* (1995). Maternally inherited hearing loss, ataxia and myoclonus associated with a novel point mutation in mitochondrial tRNASer(UCN) gene. Human molecular genetics *4*, 1421-1427.

Toompuu, M., Yasukawa, T., Suzuki, T., Hakkinen, T., Spelbrink, J.N., Watanabe, K., and Jacobs, H.T. (2002). The 7472insC mitochondrial DNA mutation impairs the synthesis and extent of aminoacylation of tRNASer(UCN) but not its structure or rate of turnover. The Journal of biological chemistry *277*, 22240-22250.

van den Heuvel, S., and Dyson, N.J. (2008). Conserved functions of the pRB and E2F families. Nature reviews. Molecular cell biology *9*, 713-724.

Vaziri, C., Saxena, S., Jeon, Y., Lee, C., Murata, K., Machida, Y., Wagle, N., Hwang, D.S., and Dutta, A. (2003). A p53-dependent checkpoint pathway prevents rereplication. Molecular cell *11*, 997-1008.

Vreugde, S., Ferrai, C., Miluzio, A., Hauben, E., Marchisio, P.C., Crippa, M.P., Bussi, M., and Biffo, S. (2006). Nuclear myosin VI enhances RNA polymerase II-dependent transcription. Molecular cell *23*, 749-755.

Waga, S., and Stillman, B. (1998). The DNA replication fork in eukaryotic cells. Annual review of biochemistry *67*, 721-751.

Wallin, I.E. (1926). BACTERIA AND THE ORIGIN OF SPECIES. Science *64*, 173-175.

Wanrooij, P.H., Uhler, J.P., Simonsson, T., Falkenberg, M., and Gustafsson, C.M. (2010). G-quadruplex structures in RNA stimulate mitochondrial transcription termination and primer formation. Proceedings of the National Academy of Sciences of the United States of America *107*, 16072-16077.

Wasilewski, M., Chojnacka, K., and Chacinska, A. (2017). Protein trafficking at the crossroads to mitochondria. Biochimica et biophysica acta. Molecular cell research *1864*, 125-137.

Whitfield, W.G., Gonzalez, C., Maldonado-Codina, G., and Glover, D.M. (1990). The A- and B-type cyclins of Drosophila are accumulated and destroyed in

temporally distinct events that define separable phases of the G2-M transition. The EMBO journal *9*, 2563-2572.

Wydro, M., Bobrowicz, A., Temperley, R.J., Lightowlers, R.N., and Chrzanowska-Lightowlers, Z.M. (2010). Targeting of the cytosolic poly(A) binding protein PABPC1 to mitochondria causes mitochondrial translation inhibition. Nucleic acids research *38*, 3732-3742.

Xu, X., Shi, Y., Zhang, H.M., Swindell, E.C., Marshall, A.G., Guo, M., Kishi, S., and Yang, X.L. (2012). Unique domain appended to vertebrate tRNA synthetase is essential for vascular development. Nat Commun *3*, 681.

Yan, H., Merchant, A.M., and Tye, B.K. (1993). Cell cycle-regulated nuclear localization of MCM2 and MCM3, which are required for the initiation of DNA synthesis at chromosomal replication origins in yeast. Genes & development *7*, 2149-2160.

Yanow, S.K., Lygerou, Z., and Nurse, P. (2001). Expression of Cdc18/Cdc6 and Cdt1 during G2 phase induces initiation of DNA replication. The EMBO journal *20*, 4648-4656.

Yao, P., Poruri, K., Martinis, S.A., and Fox, P.L. (2014). Non-catalytic regulation of gene expression by aminoacyl-tRNA synthetases. Topics in current chemistry *344*, 167-187.

Zhang, H., Wang, P., Bisetto, S., Yoon, Y., Chen, Q., Sheu, S.S., and Wang, W. (2017). A novel fission-independent role of dynamin-related protein 1 in cardiac mitochondrial respiration. Cardiovascular research *113*, 160-170.

Zheng, J., Ji, Y., and Guan, M.X. (2012). Mitochondrial tRNA mutations associated with deafness. Mitochondrion *12*, 406-413.

ACKNOWLEDGMENTS

Voldria agrair a tothom que conscient o inconscientment m'han ajudat durant aquests quatre anys de doctorat, i és que força gent ha col·laborat en l'elaboració d'aquesta tesi, tant científicament com personalment.

En primer lloc vull agrair al meu director de tesi, el Lluis Ribas de Pouplana, per haver-me deixat realitzar la tesi al seu grup, per estar sempre "apretant-nos" i demanant més de nosaltres.

Voldria agrair també als membres del meu *Thesis Committee*, Juan Fernàndez Recio, Miquel Coll i en especial al Antonio Zorzano, també el meu tutor de tesi, per els seus comentaris i suggeriments durant aquest anys.

I would like to thank our collaboration with Laurie Kaguni Lab, for her input on the *Drosophila* LON protease and for the plasmids and antibodies. Also thank Sue Cotterill, for sending us antibody aliquots to detect MCM, Cdc6 and ORCs protein levels. I would like to acknowledge Travis Stracker for his close collaboration with many experiments and the discussion of the results, as well as the people from his lab, Joana Silva and Philip Knobel, for his help with the pulse-chase analysis and the BioID.

Al laboratori on vaig realitzar la *lab rotatio*n, amb el Marco Milan i la Lada Murcia, per tot el que em vau ensenyar del món *Drosophila*. Agrair també al laboratori del Jordi Bernués, a l'Olga i la Mònica, per les cèl·lules i tots els protocols o plasmidis que hem compartit.

Un agraïment especial a la Míriam Royo i el seu equip per la síntesi del pèptid per poder caracteritzar l'activitat de LON.

A la *facility* d'espectrometria de masses, a la Marta Vilaseca, la Marina Gay, la Laura Villareal i la Mar Vilanova, per tots els anàlisis i les estones revisant i discutint tots els resultats. També a la *facility* de genòmica, al Nacho i al David,

per l'anàlisi de microarray que hem realitzat. També agrair a la Camille Otto per el seu suport a l'hora d'analitzar les dades.

M'agradaria donar les gràcies al servei de citometria del Parc Científic, perquè és el segon lloc on més hores he passat després del laboratori. Gràcies Chari, Ricard, Sònia i Jaume per les hores i maldecaps compartits tot mirant cicles.

A tots els companys del IRB, que d'una manera o altra han contribuït en aquesta tesi, amb ajuda de materials, discussions i totes les bones estones durant aquests quatre anys. També al Juan Pablo Muñoz, per ser el meu postdoc durant aquest anys.

Als del Ribas Lab per tants i tants moments viscuts i per les vostres contribucions al projecte. A la Noelia, per les nostres converses de bon matí tot arreglant el món i per fer-nos veure sempre la part positiva de tot. A la Marta, per tantes i tantes coses i perquè ens hem tret un màster en teràpies psicològiques. Ara si, ja casi estem. A l'Alba, per compartir projecte i per els nostres debats eterns sobre la funció de SLIMP. A l'Enric, per les teves petites grans bromes i perquè sense tu no sabríem quan ve el Nadal. A l'Adrian, per els nostres cafès amb debats socials però també científics. A l'Helena i l'Àlbert, perquè entre un i l'altre fèieu del lab un lloc més alegre. A la Federica, la Daria i en David per les vostres contribucions al principi del projecte i per ajudar-me en els primers passos del doctorat.

Un agraïment especial a totes les estudiants que han passat pel laboratori, perquè espero que aprenguessin tot el que els podia ensenyar i per tots els bons moments que hem compartit. A la Maria Carretero, l'alegria personificada; a la Núria Bosch, o era Bàrbara?; a la July, because we had a really funny summer; a la Merve, a l'Antigoni, a la Maria Solé, la Maria Noguera, l'Alba Serrano i la Magalí Colomer per tots els bons moments viscuts.

A nivell més personal voldria agrair als de la uni, Aida, Alba, Carlos, Clara, Cris, Irene, Joan Pau, Joan, Laura, Marc, Marcel, Maria, Marta, Maura, Neus, Sergi i Ulises, per tots els moments viscuts i els que han de venir.

Als tapantonis i als del cole, Jon, Irene, Marta, Javi, Maria, Jordi i també Raquel i Meri, per els nostres sopars de desconnexió i per fer que sempre us expliqui la biologia de formes més planeres.

Oriol i Pol, gràcies per ser-hi sempre, per les nostres escapades i per els nostres grans àpats també amb la Mariona i la Sandra.

Als meus pares i a la meva família, perquè tot i no entendre mai gaire res del projecte, sempre esteu ajudant i animant. També a la Sole, l'Alejandro i el Xavi, per ser part de la família. Per acabar agrair-li en majúscules a la Laia, per tot, pel que hem passat junts, per ser-hi cada dia i perquè ets la millor.

Albert Antolin

Barcelona, Desembre 2018